

RETIRED A STARS REVISITED: AN UPDATED GIANT PLANET OCCURRENCE RATE AS A FUNCTION OF STELLAR METALLICITY AND MASS

LUAN GHEZZI,¹ BENJAMIN T. MONTEL,^{2,*} AND JOHN ASHER JOHNSON³

¹Observatório Nacional, Rua General José Cristino, 77, 20921-400, São Cristóvão, Rio de Janeiro, RJ, Brazil;
lghezzi@on.br

²Department of Astronomy and Astrophysics, University of Chicago, 5640 S. Ellis Ave, Chicago, IL 60637, USA

³Harvard-Smithsonian Center for Astrophysics, 60 Garden Street, Cambridge, MA 02138 USA

ABSTRACT

Exoplanet surveys of evolved stars have provided increasing evidence that the formation of giant planets depends not only on stellar metallicity ([Fe/H]), but also the mass (M_\star). However, measuring accurate masses for subgiants and giants is far more challenging than it is for their main-sequence counterparts, which has led to recent concerns regarding the veracity of the correlation between stellar mass and planet occurrence. In order to address these concerns we use HIRES spectra to perform a spectroscopic analysis on a sample of 245 subgiants and derive new atmospheric and physical parameters. We also calculate the space velocities of this sample in a homogeneous manner for the first time. When reddening corrections are considered in the calculations of stellar masses and a $-0.12 M_\odot$ offset is applied to the results, the masses of the subgiants are consistent with their space velocity distributions, contrary to claims in the literature. Similarly, our measurement of their rotational velocities provide additional confirmation that the masses of subgiants with $M_\star \geq 1.6 M_\odot$ (the “Retired A Stars”) have not been overestimated in previous analyses. Using these new results for our sample of evolved stars, together with an updated sample of FGKM dwarfs, we confirm that giant planet occurrence increases with both stellar mass and metallicity up to $2.0 M_\odot$. We show that the probability of formation of a giant planet is approximately a one-to-one function of the total amount of metals in the protoplanetary disk $M_\star 10^{[Fe/H]}$. This correlation provides additional support for the core accretion mechanism of planet formation.

Keywords: stars: fundamental parameters — stars: atmospheres — stars: evolution — planets: formation

1. INTRODUCTION

The ever increasing sample of exoplanets has facilitated many robust studies of how planet formation and evolution are affected by the physical properties of their host stars. One such result is the correlation between stellar metallicity and the occurrence rate of giant planets around FGK dwarf and subgiant stars (e.g., [Gonzalez 1997](#); [Fischer & Valenti 2005](#); [Ghezzi et al. 2010a](#); [Wang & Fischer 2015](#)). Similar analyses for the stellar masses, however, are much more scarce and controversial. The main limitation appears on the massive end ($\gtrsim 1.2 M_{\odot}$) of the planet search samples, since the detection or confirmation of exoplanets around main-sequence A and early F stars using radial velocities (RVs) is more difficult due to their higher effective temperatures and larger rotational velocities.

In order to overcome this issue, radial velocity surveys have focused on intermediate-mass stars. As stars evolve off of the main sequence towards the red giant branch (RGB), their effective temperatures decrease and their rotation velocities slow down, resulting in spectra from which precise Doppler shifts can be measured. To date, more than 100 exoplanets have been detected around more than 1000 evolved stars ([Jofré et al. 2015](#); [Niedzielski et al. 2015](#)). In one of these efforts, [Johnson et al. \(2010a\)](#) analyzed a sample of 246 subgiants from the SPOCS IV catalog, as well as 948 FGKM dwarfs and subgiants from the Keck M Dwarf Survey ([Butler et al. 2006](#)) and the original SPOCS catalog ([Valenti & Fischer 2005](#)). Using the complete sample of 1194 stars, with masses ranging from $0.2 M_{\odot}$ to $2.0 M_{\odot}$, [Johnson et al. \(2010a\)](#) determined that the occurrence rate of giant planets increases approximately linearly with stellar mass, from $\sim 3\%$ for M dwarfs, to $\sim 8\%$ for FGK dwarfs,

* Sagan Fellow

to $\sim 14\%$ for stars more massive than $1.5 M_{\odot}$, the so-called "Retired A stars." This correlation appears to be supported, at least for the FGKM dwarfs, by results from transit surveys (Fressin et al. 2013; Gaidos et al. 2013). Johnson et al. (2010a) also confirmed that the planet-metallicity correlation holds for both M dwarfs and the Retired A Stars. This suggests that planet formation is significantly affected by the stellar mass and chemical composition—two stellar properties that provide crucial links to the physical properties of stars' protoplanetary disks.

These findings were questioned by Lloyd (2011), who pointed out that some discrepancies between the rotational velocities distributions of evolved planet hosts and field stars could be traced back to erroneous mass determinations. Moreover, Lloyd found that the numbers of massive subgiants ($M_{\star} \gtrsim 1.5 M_{\odot}$) observed by Johnson et al. (2010a) seems inconsistent with the predictions from Galactic stellar population models. More massive stars are formed less frequently according to the initial mass function (IMF) and also have a relatively rapid evolution across the Hertzsprung Gap. Based on these arguments, Lloyd concludes that many of the Retired A Stars should in fact lie in the mass range $1.0\text{--}1.2 M_{\odot}$. The errors on the original masses could stem from systematic uncertainties on spectroscopically determined atmospheric parameters or ambiguities in the predictions from stellar evolution models.

Johnson et al. (2013) addressed the second concern by generating Galactic stellar population models with TRILEGAL (Girardi et al. 2005). Using a magnitude-limited sample (instead of the volume-limited sample used by Lloyd 2011), they produced a simulated distribution that allows for a larger number of massive stars than Lloyd found—an effect similar to the Malmquist bias—and is thus consistent with the masses determined by Johnson et al. (2010a). Lloyd (2013), on the other hand, argues that the mass distribution is not sensitive to the Malmquist bias, but instead to the usage of different Galactic models or input parameters within a given model. Using the Besançon model (Robin et al. 2003), Lloyd (2013) obtains a mass distribution with less massive subgiants that can not be reconciled with the observed data from Johnson et al. (2010a).

The fraction of massive subgiants within the Retired A Star sample was also questioned by Schlaufman & Winn (2013). Based on an analysis that is independent of stellar evolution mod-

els, they showed that the space velocity dispersion of the subgiants with planets were larger than those of a sample of main-sequence A5–F0 stars, but consistent with the that obtained for F5–G5 dwarfs. They thus conclude that the subgiants with planets are most likely the evolved counterparts of less massive main-sequence solar-type stars, instead of “Retired A Stars”. Their analysis also revealed that no more than 40% of the planet-hosting subgiants could have been A5–F0 stars more massive than $\sim 1.3 M_{\odot}$ while on the main sequence.

In another study, [Sousa et al. \(2015b\)](#) pointed out that, while the masses they determined for planet-host stars were in general good agreement with values from the literature, there were some notable exceptions. In particular, differences of up to 100% were found for a few evolved stars. Note, however, that some of these inconsistencies are explained by erroneous mass determinations in the original papers, as explained by ([Takeda & Tajitsu 2015](#), see Section 4.2).

More recent studies of the stellar mass dependence of planet occurrence have been performed by [Reffert et al. \(2015\)](#) and [Jones et al. \(2016\)](#). In the former study, the analysis of 373 G and K giants reveals that giant planet occurrence increases with stellar mass in the range $1.0 - 1.9 M_{\odot}$, consistent with the findings of [Johnson et al. \(2010a\)](#). Moreover, there seems to be a maximum for the occurrence rate as a function of stellar mass at $1.9_{-0.5}^{+0.1} M_{\odot}$ and a rapid decrease for more massive stars. The latter study uses a sample of 166 giant stars and finds a consistent result: occurrence rate increases with stellar mass, with the maximum at $2.1 M_{\odot}$.

In the previous works mentioned, masses for the evolved stars were estimated by comparing observed properties (effective temperature, metallicity, and luminosity or surface gravity) with grids of stellar evolution models (e.g., [Bressan et al. 2012](#)). Although the accuracy of this method has been thoroughly tested for main-sequence stars (e.g., [Torres et al. 2010](#)), results for subgiants and giants are still debated, as is clear from the above discussion. In an additional effort to test if stellar evolution models are also reliable for evolved stars, [Ghezzi & Johnson \(2015\)](#) showed that PARSEC evolutionary tracks ([Bressan et al. 2012](#)) coupled with the code PARAM ([da Silva et al. 2006](#)) can recover model-independent masses from eclipsing binaries and asteroseismology within $\sim 4\%$ for the interval $\sim 0.7 - 4.5 M_{\odot}$. Therefore, the method itself does not present any issues that would signif-

icantly overestimate the masses of subgiants and giants. Nevertheless, incorrect input parameters could still lead to erroneous mass determinations.

To avoid model-dependent issues, most recent efforts to solve the Retired A Stars controversy focused on the determination of empirical masses. [Johnson et al. \(2014\)](#) performed multiple mass measurements for the bright giant HD 185351 using spectroscopic, interferometric and asteroseismic data. Although discrepancies on the 2.6σ level were observed, all determined values confirm that HD 185351 is more massive than $1.5 M_{\odot}$. [Campante et al. \(2017\)](#) determined an asteroseismic mass for the planet-hosting subgiant HD 212771 that is consistent with recent spectroscopic estimates and also with its classification as a Retired A Star. [Stassun et al. \(2017\)](#) determined virtually model independent masses (from empirical radii and density or spectroscopic surface gravity) for 358 planet-hosting stars, achieving a precision better than 15% for 134 of them. Within this most accurate sample, 30 stars lie in the HR diagram region typically occupied by the Retired A Stars and $\sim 80\%$ of them have masses consistent with this classification.

[North et al. \(2017\)](#) and [Stello et al. \(2017\)](#) investigated the masses of evolved stars using asteroseismology. The former study show that five of the seven analyzed objects ($1.0 - 1.7 M_{\odot}$) have spectroscopic masses slightly larger than the corresponding asteroseismic value. However, the authors claim the offset is not significant and highly dependent on the adopted literature mass. In a similar comparison, the latter study reveals a 15-20% offset for six (out of seven) stars with masses larger than $1.6 M_{\odot}$. Both studies highlight a large scatter among literature masses and trace the differences back to the input parameters and their uncertainties used in the determination.

In this work, we revisit the Retired A Stars sample with the goal of checking if their original masses were in fact overestimated, thereby an artificial correlation between this physical parameter and the occurrence rate of giant planets. We also take the opportunity to investigate the concerns related to the kinematics of these stars. The paper is organized as follows. The sample is presented in Section 2 and new spectroscopic and kinematical analyzes are described in Section 3. Our results are validated in Section 4, including comparisons with the previous ones from [Johnson et al. \(2010a\)](#), other literature sources and other methods. In Section 5, we discuss the consistency between masses

and space and rotational velocities and obtain an updated relation for the occurrence rate of giant planets as a function of stellar metallicity and mass. Finally, our concluding remarks are presented in Section 6.

2. SAMPLE AND DATA

Our sample of subgiants consists of 245 stars that have been continuously monitored by the Lick and Keck subgiant planet surveys since 2004 and 2007, respectively (see Table 1). The details regarding the sample selection are described in Johnson et al. (2006, 2010b). In summary, targets were selected from the *Hipparcos* catalog (ESA 1997; van Leeuwen 2007)) according to the following criteria: $0.5 < M_V < 3.5$ and $0.55 < B - V < 1.10$ and $V \lesssim 8.5$. Stars lying less than 1 mag above the main sequence defined by Wright (2005) or in the clump ($B - V > 0.8$ and $M_V < 2.0$) region are excluded.

High-resolution spectra for stars in both the Lick and Keck surveys were obtained with the HIRES (High Resolution Echelle Spectrometer; Vogt et al. 1994) spectrograph on the Keck I 10-m telescope (Mauna Kea, Hawaii). Deckers B1, B2, B3, B5, C2 and E2 were used with a binning of 3x1. This instrumental setup produces resolutions $R \simeq 50,000 - 100,000$ ¹ and an almost complete spectral coverage from $\sim 3600 \text{ \AA}$ to $\sim 7990 \text{ \AA}$, except for an inter-detector gap from $\sim 6420 \text{ \AA}$ to $\sim 6543 \text{ \AA}$ and some inter-order spacings redward of 6600 \AA . We use the “template” spectra taken without the iodine cell. They were reduced with the Keck pipeline following standard procedures. We measured the signal-to-noise (S/N) values using 112 apparent continuum regions between 5220 \AA and 6860 \AA , carefully selected using the spectra of the Sun (reflected off Vesta) and HD 185351 as references. Our targets have S/N $\gtrsim 100$ and the typical value is ~ 220 (see Table 1).

3. ANALYSIS AND RESULTS

3.1. The Line List

We compiled the initial line list for Fe I and Fe II from multiple sources: Sousa et al. (2008), Ghezzi et al. (2010a), Schuler et al. (2011), Tsantaki et al. (2013), Sousa et al. (2014), Liu et al.

¹ <https://www2.keck.hawaii.edu/inst/hires/sltres.html>

(2014) and Bedell et al. (2014). Only spectral features with $\lambda > 5000 \text{ \AA}$ are selected because of line crowding for lower wavelengths. Lines in the intervals $6270 \text{ \AA} \leq \lambda \leq 6330 \text{ \AA}$ and $\lambda > 6865 \text{ \AA}$ are removed in order to avoid possible contamination by telluric lines. Using the HIRES solar spectrum as a reference, we selected only those Fe I lines that were relatively isolated and unblended. We were more flexible for the Fe II case due to the more limited number of lines available for this species. The HIRES solar spectrum was also used as a reference to exclude lines located in the inter-detector or inter-order gaps.

We retrieved all atomic parameters (wavelength λ , excitation potential χ , $\log gf$ and van der Waals damping factor) from the Vienna Atomic Line Database (VALD; Ryabchikova et al. 2015 and references therein) on January 2016. We measured equivalent widths (EWs) for all lines on the Solar Flux Atlas (Kurucz et al. 1984) with the updated version of ARES (Sousa et al. 2015a). We adopted the following parameters: *smoothder* = 4, *space* = 3.0, *rejt* = 0.999, *lineresol* = 0.1 and *miniline* = 5. A few lines presented clearly wrong EWs and these were replaced by manual measurements done using the task `splot` in IRAF².

Using the above list, a Kurucz ATLAS9 ODFNEW model atmosphere (Castelli & Kurucz 2004) for the Sun (effective temperature $T_{\text{eff}} = 5777 \text{ K}$, surface gravity $\log g = 4.44$, metallicity $[\text{Fe}/\text{H}]^3 = 0.00$ and microturbulence $\xi = 1.00 \text{ km s}^{-1}$) and the driver *abfind* of the July 2014 version of the Local Thermodynamic Equilibrium (LTE) line analysis code MOOG⁴ (Sneden 1973), we derived individual Fe abundances for all lines. Option 1 was used for the treatment of the damping in MOOG, i.e. tabulated van der Waals damping factors (Barklem et al. 2000; Barklem & Aspelund-Johansson 2005) are used when available within the code and values from VALD (see Table 2) are adopted otherwise. We removed the Fe I lines that returned absolute abundances $A(\text{Fe})^5$ lower than 7.20 or higher than 7.80. A similar cut was not applied to Fe II due to the more restricted number of lines for this species. We also excluded lines with reduced equivalent widths $\log(\text{RW}) \equiv \log(\text{EW}/\lambda)$

² Image Reduction and Analysis Facility (IRAF) is distributed by the National Optical Astronomy Observatory (NOAO), which is operated by the Association of Universities for Research in Astronomy, Inc. (AURA) under cooperative agreement with the National Science Foundation (NSF).

³ $[\text{Fe}/\text{H}] = \log(N_{\text{Fe}}/N_H)_* - \log(N_{\text{Fe}}/N_H)_\odot$

⁴ <http://www.as.utexas.edu/chris/moog.html>

⁵ $A(\text{Fe}) = \log(N_{\text{Fe}}/N_H) + 12$

lower than -6.0 and larger than -4.8 in order to avoid too weak or saturated lines, respectively. Finally, we derived solar log gf values by imposing that all remaining lines returned $A(\text{Fe}) = 7.50$ (Asplund et al. 2009) after running MOOG with the same model atmosphere as above. They were used in the analysis of our sample (see Section 3.2) in order to improve the precision of the results, since laboratory and theoretical log gf values for many iron lines still suffer from large uncertainties (e.g., Mashonkina et al. 2011).

The final line list contains 158 Fe I and 18 Fe II lines (see Table 2). Using the updated version of ARES (Sousa et al. 2015a), we automatically measured equivalent widths for the lines in this final list for all 245 target stars. The parameters were the same as those used for the Solar Atlas, except for $rejt$, which was chosen according to the S/N value of each individual spectrum.

3.2. Atmospheric Parameters

We determined a homogeneous set of atmospheric parameters (T_{eff} , $\log g$, [Fe/H] and ξ) for our target stars using the standard spectroscopic method, which is based on the excitation and ionization equilibria of Fe I and Fe II. As for the Solar Atlas, the analysis was performed in LTE using the July 2014 version of MOOG with option 1 for the damping parameter. We used the ATLAS9 ODFNEW grid from Castelli & Kurucz (2004) to obtain interpolated model atmospheres.

We obtained the final parameters for each star through an automated iterative process that has to simultaneously meet four criteria: zero slopes in the linear fits between $A(\text{Fe I})$ and χ (excitation equilibrium) and between $A(\text{Fe I})$ and $\log(\text{RW})$; same average values of $A(\text{Fe I})$ and $A(\text{Fe II})$ (ionization equilibrium); and same value for the metallicity in the input model atmosphere and the output result from MOOG. The convergence in each criterion is achieved by successive changes in T_{eff} , ξ , $\log g$ and [Fe/H], respectively. Note that $[\text{Fe}/\text{H}] = \langle A(\text{Fe I})_* \rangle - A(\text{Fe})_{\odot}$, where we adopted $A(\text{Fe})_{\odot} = 7.50$ (Asplund et al. 2009). The iterative process also included two rounds of 2σ clipping in order to remove lines that returned abundances too discrepant from the average values.

We calculated uncertainties in the atmospheric parameters in the following way. The microturbulence was changed until the linear fit between $A(\text{Fe I})$ and $\log(\text{RW})$ had a slope equal to the error of the zero slope from the converged solution. The difference between this new ξ and the best

value is adopted as the uncertainty in this parameter. A similar procedure was done for the effective temperature, but the linear fit between $A(\text{Fe I})$ and χ was used instead. Moreover, the contribution from the error in ξ is taken into account by varying this parameter by its uncertainty determined in the previous step and checking what is the slope produced in the linear fit between $A(\text{Fe I})$ and χ . Then, T_{eff} is varied until we recover a zero slope and the difference between this temperature and best one is taken as the contribution from the error in ξ . The uncertainty in the surface gravity is obtained by varying this parameter until the difference between $A(\text{Fe I})$ and $A(\text{Fe II})$ is equal to the standard deviation of the mean for the latter abundance, taken from the converged solution. The contribution of T_{eff} to the error on $\log g$ was also considered (in a procedure similar to the one used above to estimate contribution of ξ to the uncertainty on T_{eff}). Finally, the uncertainty in [Fe/H] takes into account the standard deviation of mean for $A(\text{Fe I})$ and the variations caused by the errors in T_{eff} , ξ and $\log g$, all added in quadrature.

As a first test for our method, we analyzed the HIRES spectrum of sunlight reflected off Vesta (S/N = 267) as if it was a regular target star. The only difference is that only one round of 2σ clipping was performed. Otherwise, many good lines would be excluded due to the low value of σ (as expected, since the $\log gf$ values were adjusted using the Sun as a reference). The determined atmospheric parameters are: $T_{\text{eff}} = 5778 \pm 20$ K, $\log g = 4.45 \pm 0.07$, $[\text{Fe}/\text{H}] = 0.01 \pm 0.01$ and $\xi = 1.009 \pm 0.030$ km s⁻¹. They are all in excellent agreement with the canonical solar values.

The final atmospheric parameters for our target stars are shown in Figure 1. The individual values as well as the associated uncertainties can be seen in Table 3. We should note that the relatively low errors presented on this table are the internal uncertainties of the spectroscopic analysis. More realistic external uncertainties for the standard spectroscopic method employed here (used in the discussion of Section 4.5.1) should be higher, with typical values of up to ~ 100 K for T_{eff} , ~ 0.2 dex for $\log g$, ~ 0.2 dex for [Fe/H] and ~ 0.2 km s⁻¹ for ξ (e.g., Ghezzi et al. 2010a; Hinkel et al. 2016). For completeness, we show in Table 4 the sensitivities of the atmospheric parameters to these larger uncertainties for HD 185351 (first spectrum), taken as a representative star in our sample.

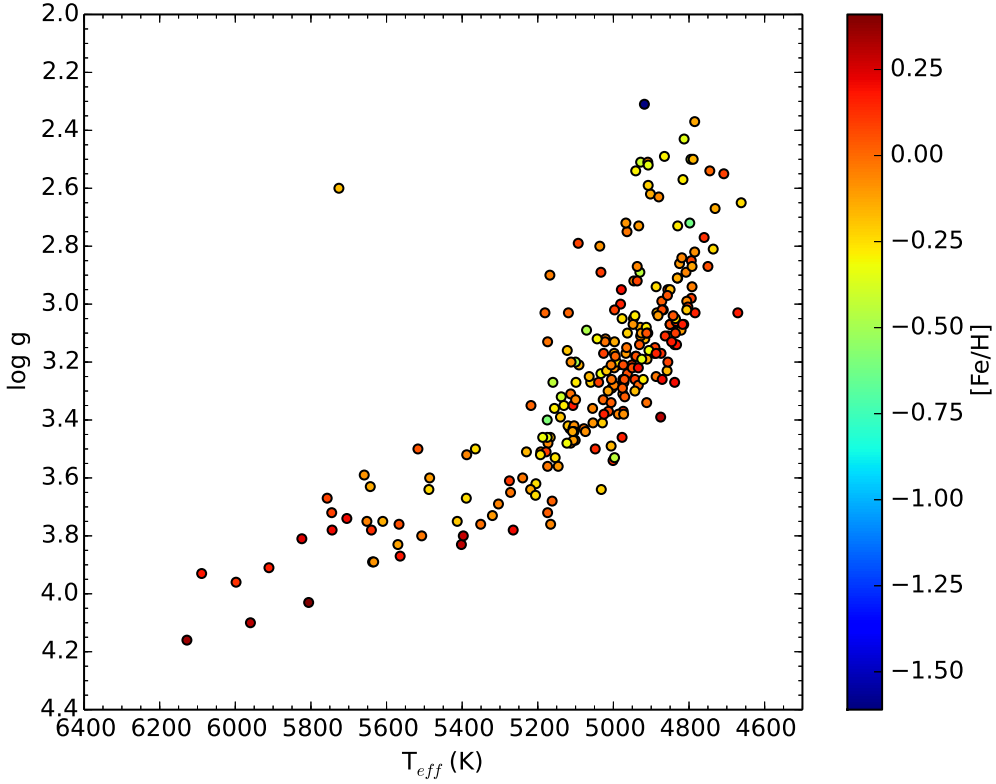


Figure 1. Atmospheric parameters (T_{eff} , $\log g$ and $[\text{Fe}/\text{H}]$) for our sample of 245 subgiants.

The three results for HD 185351 come from the independent analysis of three different spectra obtained during one observing night and reveal an excellent consistency between the derived parameters. For Figure 1 and the subsequent analyzes in this study, we adopted the arithmetic means as the final atmospheric parameters for HD 185351: $T_{\text{eff}} = 5039 \pm 16$ K, $\log g = 3.27 \pm 0.06$, $[\text{Fe}/\text{H}] = 0.09 \pm 0.01$ and $\xi = 1.110 \pm 0.020$ km s $^{-1}$. The uncertainties were calculated through simple error propagation. It is worth noting that the final $\log g$ value is in excellent agreement with the asteroseismic value (3.280 ± 0.011) presented by Johnson et al. (2014).

Two stars in Figure 1 clearly differ from the rest of the sample. The first is HD 150331, which apparently has a $\log g$ (2.60 ± 0.09) that is too low or a T_{eff} (5726 ± 35 K) that is too high relative to the region occupied by our sample. The Geneva-Copenhagen (GC) Catalog (Casagrande et al. 2011) reports an effective temperature similar to ours (5867 ± 93 K), but a discrepant surface gravity

(3.35). SIMBAD Astronomical Database shows it as a G0/2 bright giant, a classification that is more consistent with our parameters. The GC metallicity (0.42) is also very different from ours (-0.18). If we use a model atmosphere with the GC parameters and a microturbulence velocity $\xi = 1.000 \text{ km s}^{-1}$ as an input to the driver *ewfind* in MOOG, we do not obtain EWs consistent with those measured with ARES.

The second star is HD 21581 and it is significantly more metal-poor ($[\text{Fe}/\text{H}] = -1.61$) than all other stars in the sample. Nevertheless, this apparent discrepancy is not an issue since its metallicity, as well as T_{eff} and $\log g$ are consistent with other literature measurements (see the 2016 version of the PASTEL catalogue; [Soubiran et al. 2016](#)). Thus, we believe our parameters for these two stars are reliable and use them in the following analyzes.

3.3. Rotational Velocities

We determined the stellar projected rotational velocities $v \sin i$ for all our stars through spectral synthesis with MOOG. The driver *synth* was used with option 1 for the damping. The Fe I line at 6703.565 Å was chosen for the analysis because it is relatively isolated and unblended. The atomic parameters adopted for the line are the same as in Table 2. Model atmospheres for each star are also necessary as input and we used those obtained in Section 3.2 for the final atmospheric parameters.

The synthesis in MOOG was performed using the option *r* for the broadening of the spectral line. This means that separate values for the instrumental profile $\text{FWHM}_{\text{inst}}$, the macroturbulence velocity V_{macro} and the rotational velocity $v \sin i$ have to be provided. The values for $\text{FWHM}_{\text{inst}}$ were chosen according to the setup used for observing each star: 0.096 Å for deckers B1, B2 and B3; 0.112 Å for deckers B5 and C2; 0.065 Å for decker E2. These values correspond to resolutions of $\sim 70,000$, $\sim 60,000$ and $\sim 100,000$, respectively and can be seen in Table 5. We calculated the values of V_{macro} (see Table 5) using the relations presented by [Brewer et al. \(2016\)](#), using our values for T_{eff} and $\log g$ (the same as in the model atmospheres described above) in the equations. We should note that, although $[\text{Fe}/\text{H}]$ does not appear on the relations, HD 21581 has a significantly lower metallicity than the stars used to build the calibrations.

Small adjustments to the continuum level (typically 0.5%) and shifts to the central wavelength of the Fe line (typically 0.02 Å) were allowed in order to account for uncertainties in the normalization process and to properly match the observed feature, respectively. We also let the A(Fe) abundance vary within 0.06 dex (with steps of 0.02 dex) the [Fe/H] value determined for the star to account for intrinsic line-to-line scatter in the abundances. After these values were set, we computed a grid of synthetic spectra for $v \sin i$ values varying between 0.0 and 15.0 km s⁻¹ with steps of 0.2 km s⁻¹. The best match between the observed and synthetic spectra were found through the minimization of the reduced χ^2 :

$$\chi_r^2 = \frac{1}{(d - 1)} \sum_{i=1}^n \frac{(O_i - S_i)^2}{\sigma^2} \quad (1)$$

In the above equation, O_i and S_i correspond, respectively, to the observed and synthetic normalized fluxes at point i of the spectral line profile. The rms of the continuum is given by $\sigma = (\text{S/N})^{-1}$ (see Table 1 for S/N values) and $d = n - p$ represents the number of degrees of freedom in the fit, where n is the number of points in the observed spectra and $p = 1$ is the number of free parameters in the analysis (only $v \sin i$). We calculated the uncertainties on $v \sin i$ by varying this parameter until $\Delta\chi_r^2 = \chi_r^2 - \chi_{r,\min}^2 = 1$. The values of the rotational velocities and its associated errors are shown in Table 5. As an example, we show the best fit for the second spectrum of HD 185351 in Figure 2. For this star, we can see a very good consistency between the three sets of results. As for the atmospheric parameters, we decided to adopt the arithmetic mean and the propagated error as the final value $v \sin i = 1.7 \pm 0.4$ km s⁻¹.

As an initial test for our method, we once again analyzed the HIRES spectrum of sunlight reflected off Vesta (S/N = 267) as if it was a regular target star. Using $\text{FHWM}_{inst} = 0.096$ Å (decker B2) and the calculated $V_{macro} = 3.57$ km s⁻¹, we obtained 1.4 ± 0.8 km s⁻¹, which is in very good agreement with the typical solar value (≈ 1.6 km s⁻¹; e.g., Valenti & Fischer 2005; Pavlenko et al. 2012; Brewer et al. 2016). In a more general test, we computed synthetic spectra for the Fe I 6703.565 Å line using a model atmosphere calculated for the typical atmospheric parameters in our sample ($T_{\text{eff}} = 5050$ K, $\log g = 3.30$, $[\text{Fe}/\text{H}] = 0.00$ and $\xi = 1.000$ km s⁻¹), the corresponding V_{macro} (3.45

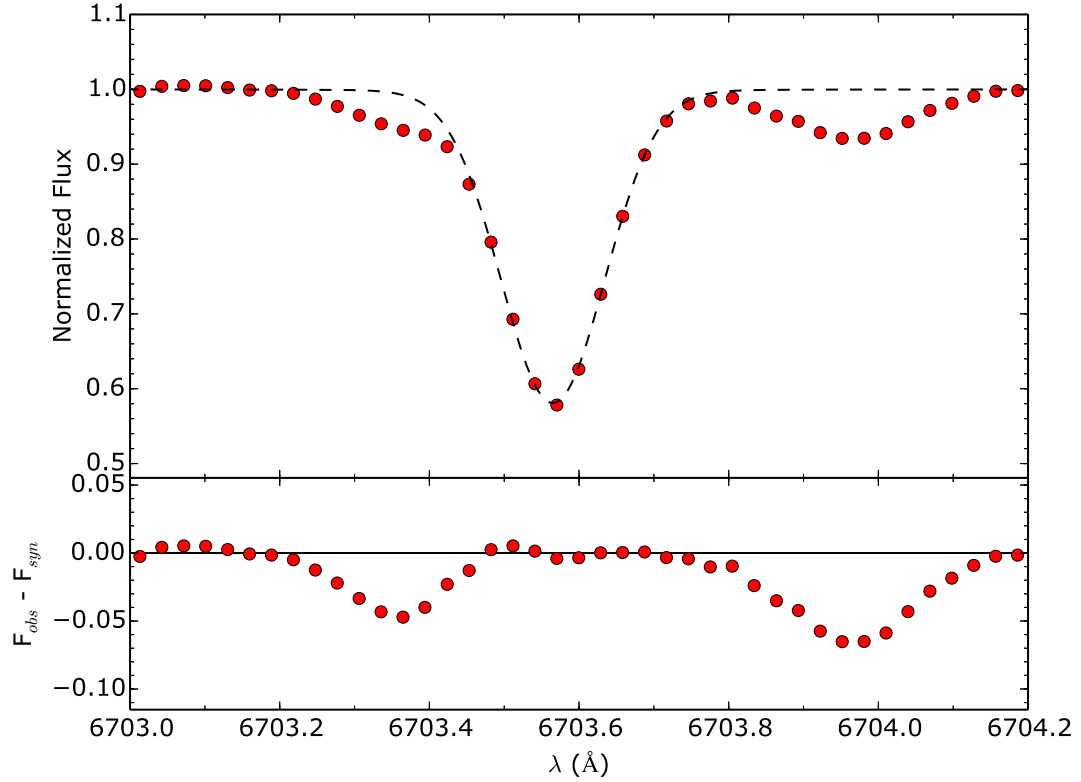


Figure 2. *Upper panel:* Observed (red circles) and best fit synthetic spectrum (black dashed line) for the second spectrum of HD 185351. Only the Fe I line at 6703.565 Å was considered in the fit. *Lower panel:* Differences between the observed and synthetic spectrum (red circles). The black solid line represents a null difference.

km s⁻¹), $\text{FHWM}_{\text{inst}} = 0.112 \text{ \AA}$ (the lower resolution) and $v \sin i$ values ranging from 0.0 to 10.0 km s⁻¹, with steps of 0.5 km s⁻¹. Then, we used the method described above to analyze these spectra as if they belonged to real stars and were able to recover all rotational velocities within 0.5 km s⁻¹.

3.4. Evolutionary Parameters

We determined the evolutionary parameters of our target stars (mass, radius, $\log g$ and age) through the comparison of observational parameters with grids of evolutionary tracks. We performed this analysis using the version 1.3 of the PARAM code, kindly provided by Leo Girardi⁶. The code

⁶ For the web interface maintained by Leo Girardi at the Osservatorio Astronomico di Padova, visit <http://stev.oapd.inaf.it/cgi-bin/param>.

adopts a Bayesian statistical framework in order to determine masses, radii, surface gravities and ages from given sets of priors and input parameters (da Silva et al. 2006). We used version 1.1 of the PARSEC evolutionary tracks (Bressan et al. 2012) as well as the default options for the Bayesian priors: lognormal Initial Mass Function (IMF) from Chabrier (2001), constant Stellar Formation Rate (SFR), and the age interval from 0.1 to 12.0 Gyr. We also chose to provide the input parameters T_{eff} , [Fe/H], V magnitude and parallax π because asteroseismic information is not available for most of our targets.

The effective temperatures and metallicities were homogeneously and spectroscopically determined on this study (see Section 3.2). The adopted parallaxes and associated uncertainties (see Table 1) are the revised values from van Leeuwen (2007). The only exception was the star HD 33298, which had the negative parallax replaced by the original value from the *The Hipparcos and Tycho Catalogues* (ESA 1997). We calculated the V magnitudes from the formula $V = V_T - [0.090 \times (B_T - V_T)]$, with values of B_T and V_T taken from the *Tycho-2* catalog (Høg et al. 2000). Uncertainties were determined through simple error propagation.

We corrected all V magnitudes for extinction using A_V values calculated with an adapted version of the code `extinct.for` (Hakkila et al. 1997), which uses the tables from Arenou et al. (1992) (see Table 1). These tables remain among the most reliable sources for estimating reddening for nearby stars within 280 pc (e.g., Gontcharov & Mosenkov 2017). Uncertainties on the corrected magnitudes V_0 were obtained through simple error propagation, where A_V uncertainties were estimated using the relative errors σ_{A_V}/A_V given in the tables from Arenou et al. (1992).

The distributions for the evolutionary parameters are shown in Figure 3. The individual values for each star are presented on Table 6 along with their uncertainties. The histograms confirm that our stars are mostly more massive, evolved and younger than the Sun, as expected from the target selection. It should also be noted that the mass distribution is consistent with the simulation presented in Figure 3 of Johnson et al. (2013).

3.5. Kinematics

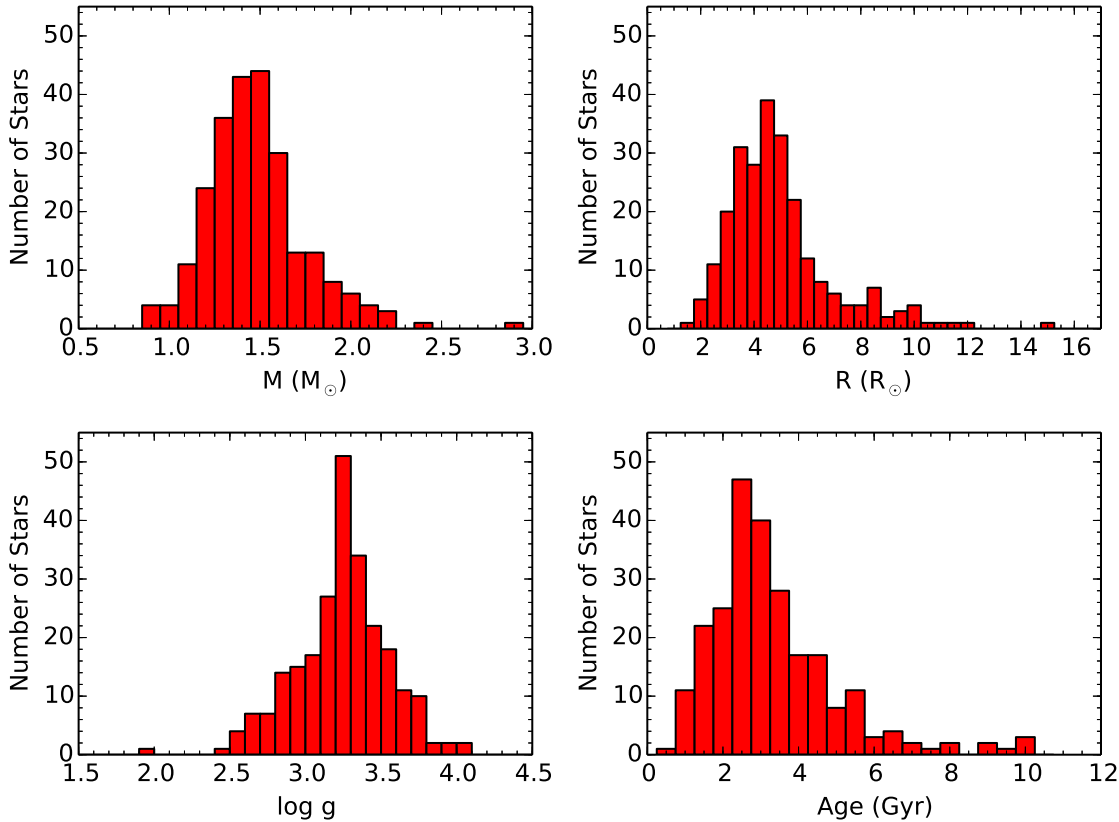


Figure 3. Distributions for the evolutionary parameters for our sample of 245 subgiants. Masses, radii, surface gravities and ages are shown in the upper left, upper right, lower left and lower right panels, respectively.

We calculated galactic UVW space velocities for our target stars using an adapted version of the code `gal_uvw.py`⁷. Equatorial coordinates (right ascension α and declination δ), parallaxes and proper motions were taken from [van Leeuwen \(2007\)](#) (see Table 1). The California Planet Survey uses the iodine cell technique of [Butler et al. \(1996\)](#) to compute highly precise RVs relative to each star's own spectrum, and therefore produces relative RV measurements. We use absolute RVs, where available, for our kinematics study from the following references, in order of preference: [Chubak et al. \(2012\)](#), [Anderson & Francis \(2012\)](#), [Gontcharov \(2006\)](#), [Massarotti et al. \(2008\)](#) and [Brewer et al. \(2016\)](#) (see Table 1). The star HD 10245 did not have a RV available in any of these references and

⁷ Originally written by W. Landsman and made available by Sergey Koposov on astrolibpy at GitHub.

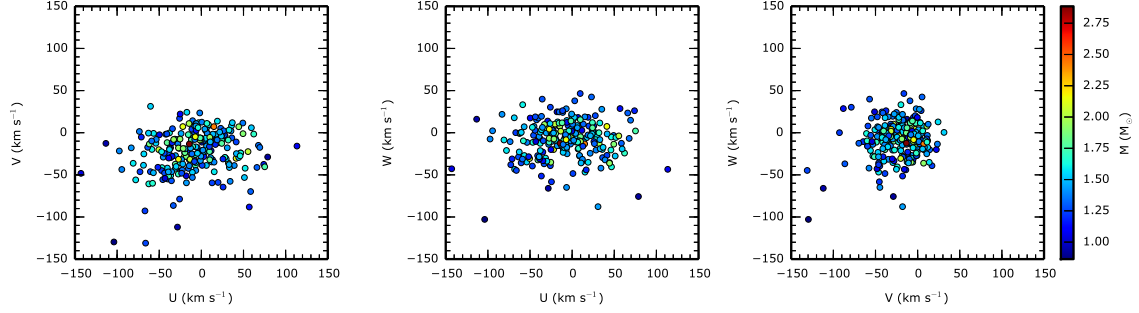


Figure 4. Galactic UVW space velocities for 244 of the subgiants (HD 10425 did not have an available radial velocity). Masses are represented by the color scale.

therefore its space velocities were not calculated. The resulting UVW velocities can be seen on Table 7 and their distributions are presented in Figure 4. Note that U , V and W are positive towards the Galactic center, in the direction of Galactic rotation and in the direction towards the North Galactic pole, respectively. We have not applied corrections for the solar motion in order to compare our results to those presented by Schlaufman & Winn (2013).

4. VALIDATION OF THE RESULTS

As discussed in Section 1, possibly overestimated masses in Johnson et al. (2010a) could have been produced by systematic uncertainties on the input atmospheric parameters. Although the results derived in our study are homogeneous and precise, their accuracy has yet to be tested. We do this by comparing our spectroscopic parameters with those derived by independent methods or studies.

4.1. Validation of the Spectroscopic Temperatures

As a first check, we calculated photometric effective temperatures for our sample using the T_{eff} versus $V - K_S$ calibrations from González Hernández & Bonifacio (2009). We calculated the V magnitudes from B_T and V_T taken from the *Tycho-2* catalog (Høg et al. 2000), as explained in Section 3.4. We adopted K_S magnitudes from the Two Micron All Sky Survey (2MASS) All-Sky Catalog of Point Sources (Cutri et al. 2003) (see Table 8). We removed 15 stars with flags D, E or F for the K_S magnitude. Moreover, we could not find a reasonable match for the star HD 136418 (i.e., with a K_S value that would provide a reasonable T_{eff}) within the 2MASS catalog.

We corrected the $V - K_S$ colors for the reddening in the following way. First, we converted A_V values derived in Section 3.4 to $E(B - V)$ using the formula $A_V = 3.1 \times E(B - V)$. Then, we calculated $E(V - K_S)$ values from $E(B - V)$ using the relation $E(V - K_S) = 2.70 \times E(B - V)$, where the coefficient was taken from [Ramírez & Meléndez \(2005\)](#). The final dereddened color $(V - K_S)_0$ was obtained with the formula $(V - K_S)_0 = (V - K_S) - E(V - K_S)$.

The calculated sets of photometric effective temperatures and its errors are presented in Table 8. It should be noted that [González Hernández & Bonifacio \(2009\)](#) derive different polynomials for dwarfs/subgiants and giants, with the limit placed at $\log g = 3.00$ (González Hernández, private communication). We followed this separation when choosing which calibration would be applied to each star, using the spectroscopic $\log g$ values as the reference. We calculated the uncertainties in the photometric effective temperatures by adding two contributions in quadrature: the errors propagated from $(V - K_S)_0$ and [Fe/H] and the standard deviation of the final calibration (32 K for the dwarfs/subgiants and 23 K for the giants).

The photometric temperatures are compared with the spectroscopic values in Figure 5. We can observe a general good agreement over the whole T_{eff} interval. Most stars present offsets lower than ± 200 K, and the average difference (in the sense spectroscopic - photometric) is -27 ± 111 K. If we do not consider the six stars with differences larger than ± 300 K, the mean difference is -16 ± 87 K. These values validate our spectroscopic temperature scale and are consistent with the typical external uncertainty (~ 100 K) mentioned in Section 3.2. Moreover, both the differences and the scatters are similar to those obtained by [González Hernández & Bonifacio \(2009\)](#) when their results are compared with spectroscopic temperatures (see their Section 8.4).

4.2. Validation of the Spectroscopic Gravities

The second test consisted in the comparison of the spectroscopic surface gravities with the trigonometric values returned by PARAM in Section 3.4 (see Table 6). We can see in Figure 6 that the global agreement is good and most stars have offsets smaller than ± 0.4 dex, considered as a 2σ limit, where σ is taken as, e.g., the value of the external uncertainty for $\log g$ quoted in Section 3.2 or the systematic offset between spectroscopic and trigonometric surface gravities discussed by

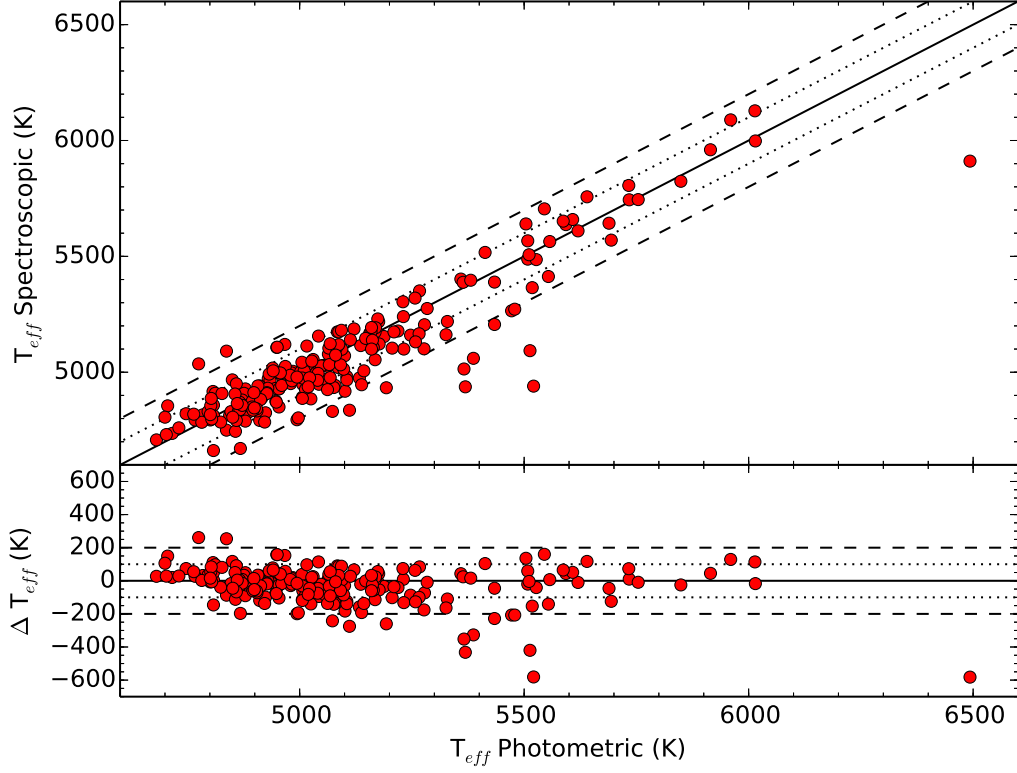


Figure 5. Comparison between spectroscopic and photometric effective temperatures for 229 out of 245 target stars (see text for the reasons why some stars were removed). The upper panel shows the direct comparison between the two sets of temperatures. The lower panel presents the difference $\Delta T_{\text{eff}} = T_{\text{eff}}^{\text{Spec}} - T_{\text{eff}}^{\text{Phot}}$ as a function of the photometric T_{eff} . In both panels, solid lines represent a perfect agreement, while dotted and dashed lines correspond to ± 100 K and ± 200 K, respectively.

da Silva et al. (2006). The mean difference (in the sense spectroscopic - trigonometric) is -0.008 ± 0.163 dex. If the ten stars with differences larger than ± 0.4 are not taken into account, the average difference becomes 0.012 ± 0.131 dex. We should note that the outliers in this case are note the same as the ones found in the comparison of the temperatures. As for T_{eff} , the above differences are consistent with the typical external uncertainty (~ 0.2 dex) mentioned in Section 3.2.

We also checked if there was any correlation between the differences in T_{eff} and $\log g$ because systematically incorrect effective temperatures could cause systematic offsets in the surface gravities in the spectroscopic method. We can see there is no such correlation in Figure 7. A linear fit to

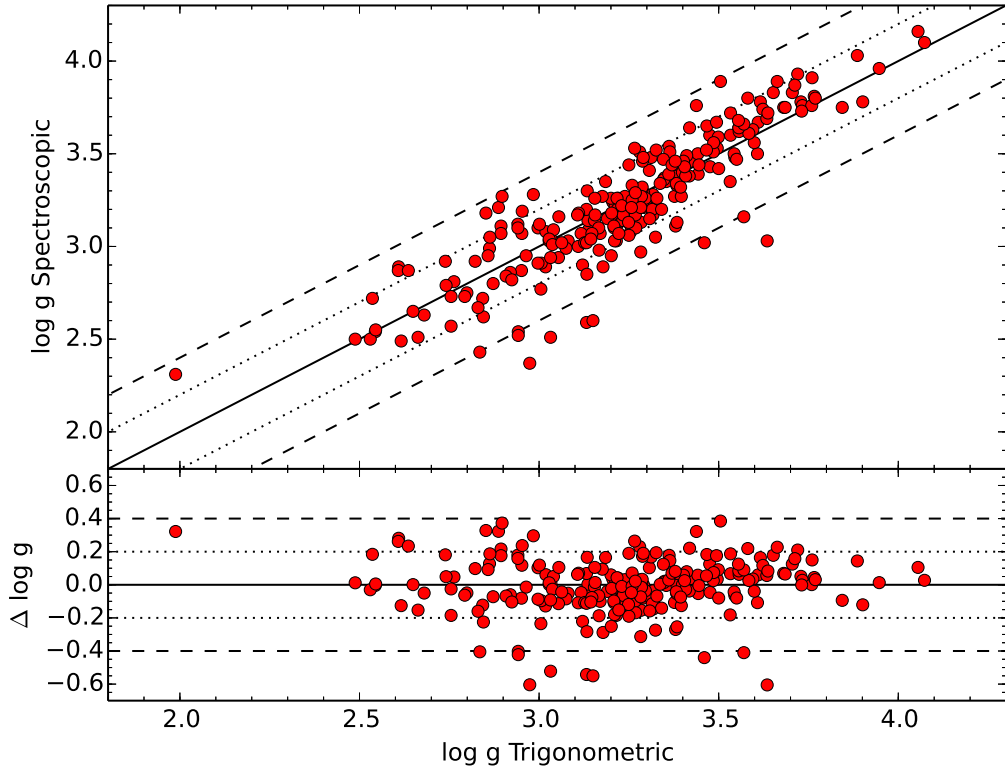


Figure 6. Comparison between spectroscopic and trigonometric surface gravities for our 245 target stars. The upper panel shows the direct comparison between the two sets of gravities. The lower panel presents the difference $\Delta \log g = \log g^{Spec} - \log g^{Trig}$ as a function of the trigonometric $\log g$. In both panels, solid lines represent a perfect agreement, while dotted and dashed lines correspond to ± 0.2 dex and ± 0.4 dex, respectively.

the data returns a correlation coefficient $R^2 = 0.06$. Another evidence that our surface gravities are reliable is the excellent agreement between the spectroscopic values obtained for the star HD 185351 and the asteroseismic measurement presented by Johnson et al. (2014), as discussed in Section 3.2.

4.3. Validation of the Metallicities

Photometric metallicities are not as precise as the spectroscopic ones, so they do not provide a good reference to validate our results. In order to do that, we decided to perform an analysis of the Hyades stars studied by Dutra-Ferreira et al. (2016). The reduced spectra were kindly made available

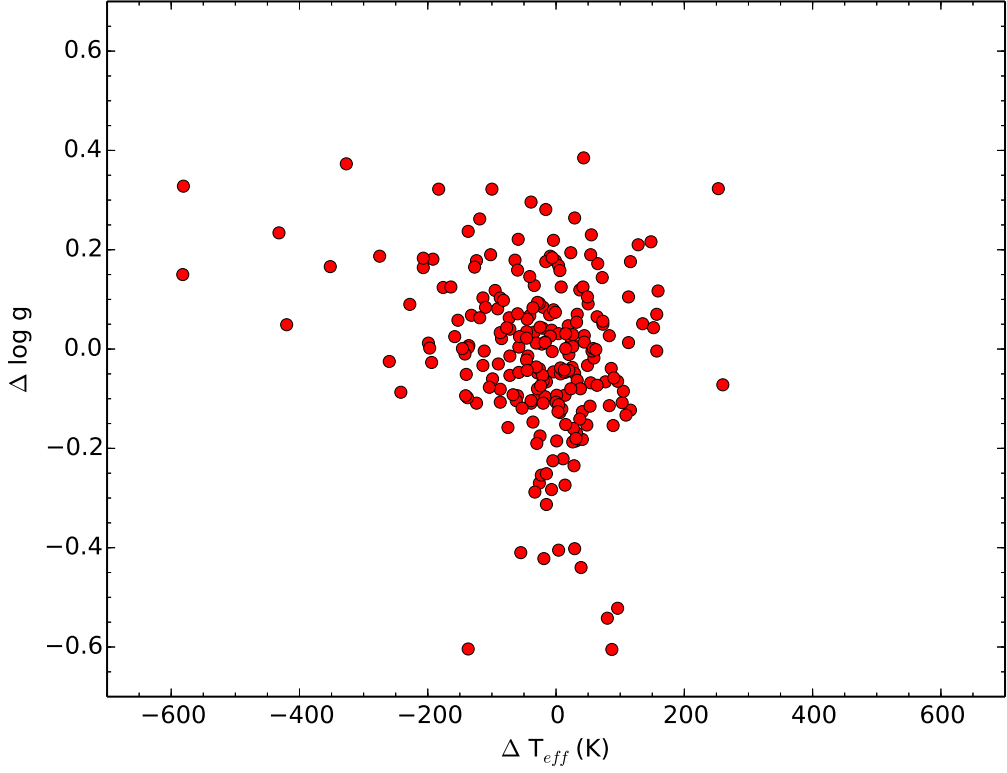


Figure 7. Differences between spectroscopic and trigonometric surface gravities as a function of the differences between spectroscopic and photometric effective temperatures.

by Letícia Dutra-Ferreira and the S/N values were taken from Table 1 of the corresponding paper. We analyzed all 17 stars (14 dwarfs and 3 giants) in the same way as our targets (see Section 3.2).

The average metallicity found for the cluster was $\langle \text{[Fe/H]} \rangle = 0.16 \pm 0.04$, which is in very good agreement with the value recommended by Dutra-Ferreira et al. (2016) (0.18 ± 0.03). The mean metallicities for the dwarfs (0.16 ± 0.04) and the giants (0.15 ± 0.02) are in excellent agreement, which shows that our line list is capable of providing a consistent metallicity scale for stars in a wide range of effective temperatures and in different evolutionary stages. Moreover, we do not find any trends in [Fe/H] as a function of T_{eff} , which is an additional evidence that our metallicity scale is consistent. Finally, the average metallicity obtained for the giants is consistent with the value obtained by Dutra-Ferreira et al. (2016) (0.14 ± 0.03) when using an optimized line list in a classical

spectroscopic analysis. This result supports the fact that the metallicity scale for the subgiants is reliable.

4.4. Comparison with the SPOCS Catalogues

The parameters used by [Johnson et al. \(2010a\)](#) were obtained from the Spectroscopic Properties of Cool Stars (SPOCS) catalog and derived through spectral synthesis using the Spectroscopy Made Easy (SME) software ([Valenti & Fischer 2005](#)). They thus provide an additional independent check for the results derived in this work. All stars in our sample have SME parameters and the average differences (in the sense this work - SPOCS) are: $\Delta T_{\text{eff}} = -8 \pm 165$ K, $\Delta [\text{Fe}/\text{H}] = -0.04 \pm 0.14$ dex and $\Delta \log g = -0.08 \pm 0.34$ dex. Although the mean differences are reasonable, the dispersions are larger than the typical external uncertainties. This is also clear from Figure 8, where we can also see some trends in the residuals, especially as a function of $[\text{Fe}/\text{H}]$ ($R^2 = 0.50, 0.41$ and 0.42 for ΔT_{eff} , $\Delta [\text{Fe}/\text{H}]$ and $\Delta \log g$, respectively).

A similar comparison for the masses yields an average difference (in the sense this work - SPOCS) of $\Delta M_{\star} = 0.05 \pm 0.28 M_{\odot}$. Again, the mean difference is good, but the dispersion too large. As clearly seen in Figure 9, a significant trend is present in the residuals ($R^2 = 0.43$), probably a consequence of the trends observed for the atmospheric parameters.

The most recent version of the SPOCS catalog ([Brewer et al. 2016](#)) contains atmospheric parameters and chemical abundances for 1626 FGK stars. For the 204 stars in common with our data set, the average differences (in the sense this work - SPOCS) are: $\Delta T_{\text{eff}} = 48 \pm 38$ K, $\Delta [\text{Fe}/\text{H}] = -0.04 \pm 0.05$ dex and $\Delta \log g = -0.01 \pm 0.09$ dex. Note that [Brewer et al. \(2016\)](#) adopted a lower reference solar iron abundance ($A(\text{Fe}) = 7.45$), so we applied a correction of -0.05 dex for all SPOCS $[\text{Fe}/\text{H}]$ values in order to put their metallicities into our scale. There is a considerable improvement in the dispersions, however a few trends in the residuals are still present, in particular for $\Delta [\text{Fe}/\text{H}]$ versus $\log g$ ($R^2 = 0.58$), getting stronger for the more evolved stars ($\log g \lesssim 3.5$).

Similar trends are found by [Brewer et al. \(2016\)](#) when comparing their results with other spectroscopic analyzes, but their origin remain unclear. Possible explanations could be the strong correlations observed between T_{eff} , $[\text{Fe}/\text{H}]$ and $\log g$ when spectral synthesis is used (e.g., [Torres et al. 2012](#)) or

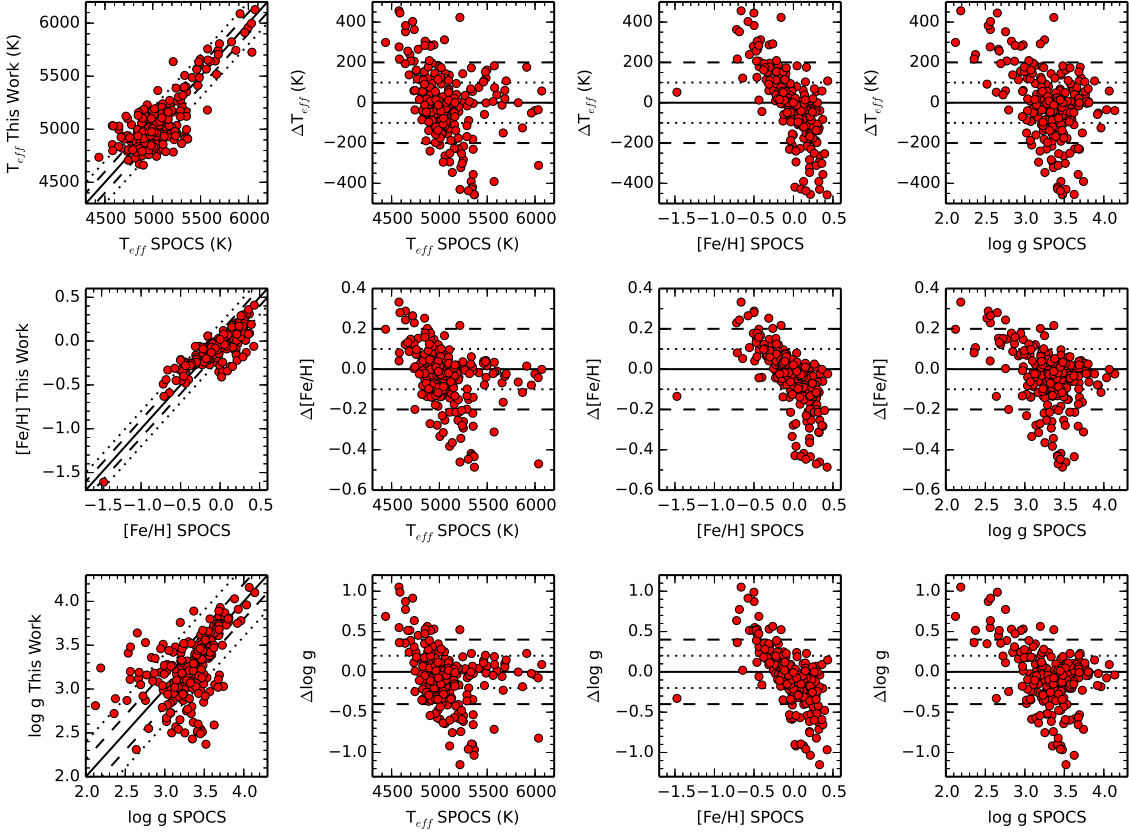


Figure 8. Comparison between the atmospheric parameters derived in this work (see Section 3.2) and those used by Johnson et al. (2010a). The left column of panels shows the direct comparisons between the two sets of parameters. The other three columns present the differences between the two sets of parameters (in the sense this work - SPOCS) as a function of, from left to right, T_{eff} , $[\text{Fe}/\text{H}]$ and $\log g$ from the SPOCS catalog. In all panels, solid lines represent a perfect agreement. Dotted and dashed lines correspond, respectively, to $\Delta T_{\text{eff}} = \pm 100$ K and ± 200 K, $\Delta [\text{Fe}/\text{H}] = \pm 0.1$ dex and ± 0.2 dex or $\Delta \log g = \pm 0.2$ dex and ± 0.4 dex.

the fixed value for the microturbulence (0.85 km s^{-1}) adopted in SME. We stress that the standard spectroscopic analysis employed in this work shows no such correlations (Torres et al. 2012) and our results are in good agreement with those obtained from independent methods.

Brewer et al. (2016) also determined rotational velocities and we compare our values with theirs in Figure 10. For the 204 stars in common, the average difference (in the sense this work - SPOCS) is $\Delta v \sin i = -0.25 \pm 0.73 \text{ km s}^{-1}$. The stars with differences larger than 2.0 km s^{-1} are HD 31543 (-5.4

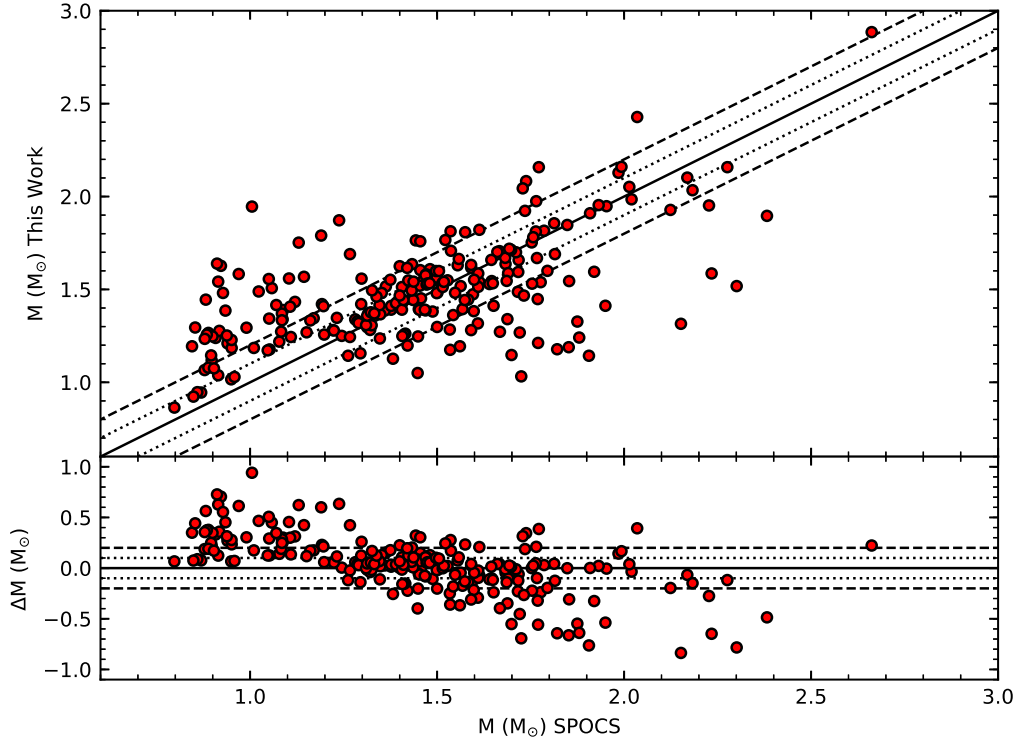


Figure 9. Comparison between the masses derived in this work (see Section 3.4) and those used by Johnson et al. (2010a). The upper panel shows the direct comparison between the two sets of parameters. The lower panel presents the difference $\Delta M_\star = M_\star(\text{This Work}) - M_\star(\text{SPOCS})$ as a function of the latter. In both panels, solid lines represent a perfect agreement, while dotted and dashed lines correspond to $\pm 0.1 M_\odot$ and $\pm 0.2 M_\odot$, respectively.

km s⁻¹), a possible single-lined spectroscopic binary (SB1; Chubak et al. 2012), and HD 103616 (-2.8 km s⁻¹), a suspected binary (Nordström et al. 2004).

4.5. Possible Systematic Offsets on the Masses

4.5.1. Possible Offsets in the Atmospheric Parameters

In the previous sections, we showed that the spectroscopic atmospheric parameters of the subgiants are accurate. Ghezzi & Johnson (2015) showed that PARSEC evolutionary tracks (da Silva et al. 2006) and the PARAM code are able to provide reliable masses for a sample of 59 benchmark subgiants and giants. Nevertheless, we decided to test if the masses of subgiants could be significantly

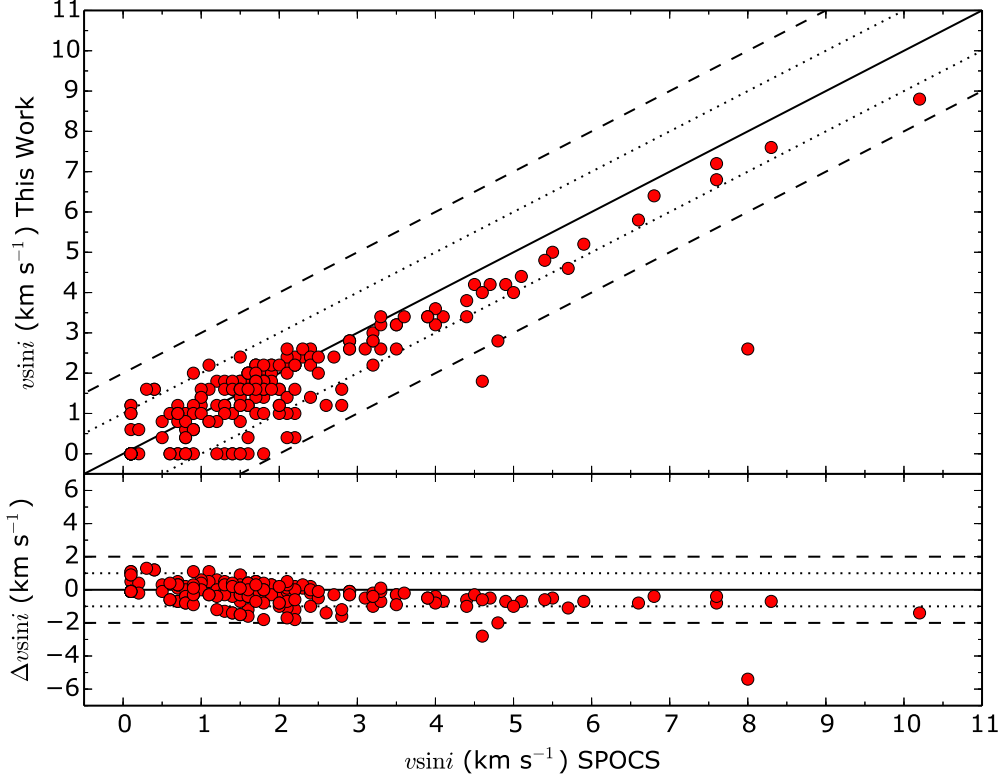


Figure 10. Comparison between the rotational velocities derived in this work (see Section 3.3) and those determined by Brewer et al. (2016). The upper panel shows the direct comparison between the two sets of parameters. The lower panel presents the difference $\Delta v \sin i = v \sin i$ (This Work) - $v \sin i$ (SPOCS) as a function of the latter. In both panels, solid lines represent a perfect agreement, while dotted and dashed lines correspond to ± 1.0 km s⁻¹ and ± 2.0 km s⁻¹, respectively.

overestimated if systematic offsets were present in the input atmospheric parameters derived in this work (T_{eff} and [Fe/H]). In order to do this, we decreased all our effective temperatures and metallicities by 100 K and 0.10 dex, respectively. The offset in T_{eff} was chosen so that we would have a decrease in the stellar masses and is consistent with typical external uncertainties (see Section 3.2) found in the literature when different studies are compared (but higher than the internal errors derived here). We should also note that the offsets are consistent, in the sense that such a decrease of ~ 100 K in the T_{eff} for a typical Retired A Star ($T_{\text{eff}} \sim 5000$ K) would cause a decrease in the iron abundance of about ~ 0.1 dex (see Table 4).

Using these new parameters, we repeated the analysis done in Section 3.4. The comparison of the new set of masses with the original ones can be seen in Figure 11. As expected, the new masses are smaller than the original ones. The average difference (in the sense no offset - with offset in the atmospheric parameters) is $0.20 \pm 0.14 M_{\odot}$. Considering the typical uncertainty of the original masses is $0.11 M_{\odot}$, this difference is consistent with a 2σ offset and much smaller than the possible overestimation of up to 50% suggested by Lloyd (2011). We should also highlight that the T_{eff} and [Fe/H] offsets used in this test are much larger than the average difference between our spectroscopic and photometric temperatures (-27 K) and the offsets in the metallicities scales obtained for the Hyades stars (-0.02, with our values being smaller), respectively. Therefore, we feel confident that possible offsets in the atmospheric parameters are small (if present) and do not significantly overestimate the masses of the subgiants.

4.5.2. Effect of the Reddening

Another input parameter that can affect the determination of the masses is the reddening. In order to test how much the reddening corrections could overestimate our masses, we decide to repeat the analysis done in Section 3.4 considering $A_V = 0$ for all stars in our sample. The comparison of these new results with the original ones is shown in Figure 12. As expected, masses obtained without correcting the V magnitudes for the reddening are smaller, however the difference is not significant. The mean difference (in the sense with reddening - without reddening) is $0.05 \pm 0.05 M_{\odot}$, a value that is smaller than the typical uncertainty of $0.11 M_{\odot}$. Therefore, we see that the reddening correction does not significantly increase the masses of the subgiants.

4.5.3. Gaia's Parallaxes

Gaia's first data release⁸ (DR1; Gaia Collaboration 2016) presents trigonometric parallaxes for ~ 2 million stars in common with *Hipparcos* (ESA 1997) and *Tycho-2* Catalogues (Høg et al. 2000). We found 208 stars from our sample in DR1 and decided to compare Gaia's new parallaxes with the *Hipparcos* revised values adopted in this work (van Leeuwen 2007) (see Figure 13). The average

⁸ <http://www.cosmos.esa.int/web/gaia/dr1>

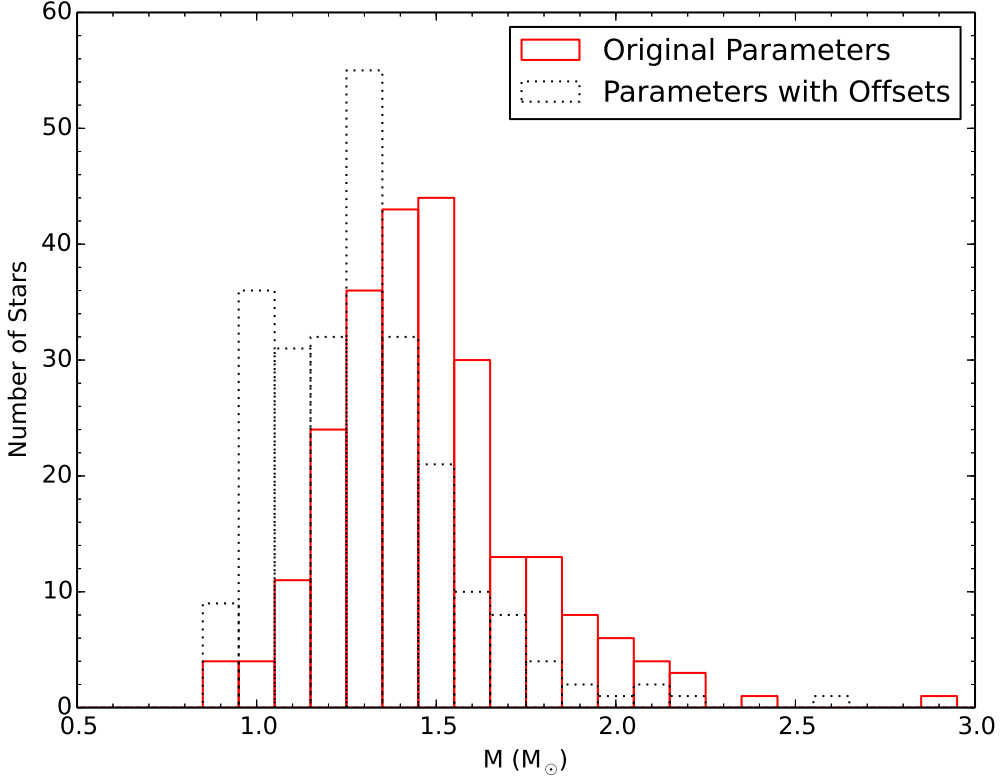


Figure 11. Comparison between the mass distributions obtained with the original atmospheric parameters derived in this work (solid red histogram) and the ones obtained with the offsets of -100 K in T_{eff} and -0.1 dex in [Fe/H] (black dotted histogram).

difference (in the sense Hipparcos - Gaia) is 0.25 ± 1.30 mas or $3 \pm 20\%$. We should highlight that Stassun & Torres (2016) found the exact same systematic offset for a sample of eclipsing binaries with accurate empirical distances.

Although the average difference is small, there are a few stars with discrepancies between 50% and 100%. Thus, we decided to test if the masses of the subgiants are affected by the parallax choice. When using Gaia's parallaxes for the 208 stars in common (and not considering the remaining 37 stars), we obtain masses that are on average higher than those derived with *Hipparcos* parallaxes by $0.08 \pm 0.21 M_{\odot}$ or $6 \pm 14\%$. We see that the choice of *Hipparcos* parallaxes provides slightly lower masses, so they are not causing any systematic effects that would overestimate the masses of the subgiants. We decided not to use Gaia's parallaxes for now because the astrometric results from

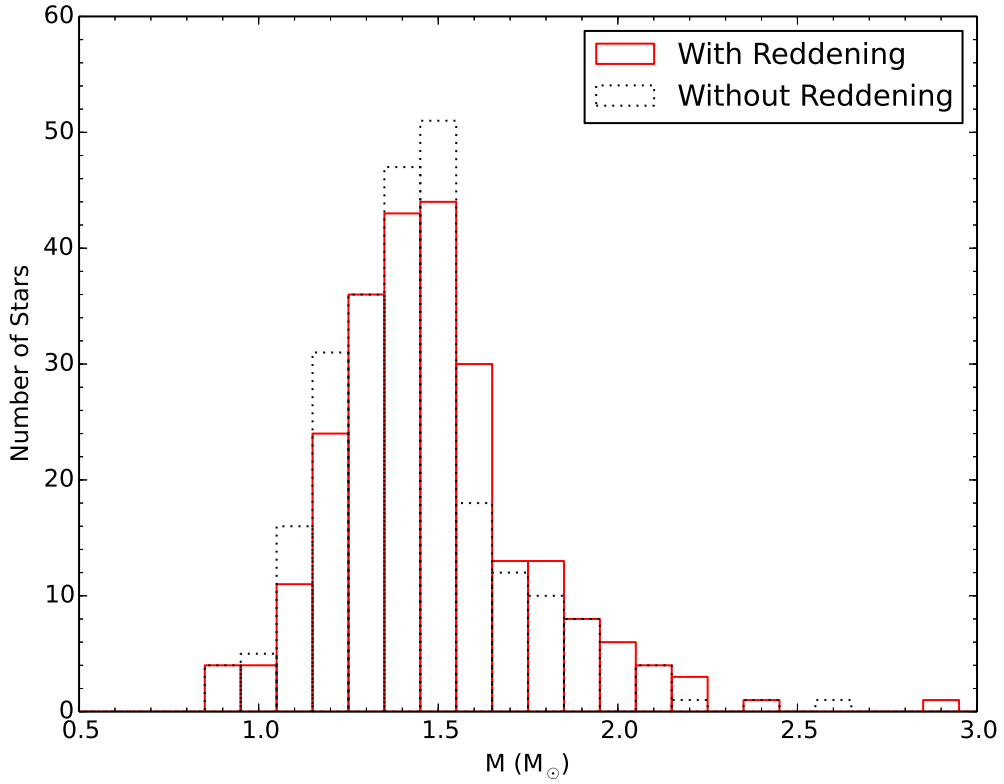


Figure 12. Comparison between the mass distributions obtained with (solid red histogram) and without (black dotted histogram) correcting the V magnitudes for the reddening.

DR1 are still preliminary. However, we anticipate that this particular choice does not affect the conclusions drawn from this study.

4.6. Validation of Space Velocities

Space velocities calculated in Section 3.5 can also be compared with values from the literature. Our sample has 114 stars that were also analyzed by Schlaufman & Winn (2013). As can be seen in Figure 14, there is a very good agreement between the two sets, with the following average differences (in the sense this work - SW): $\Delta U = -0.01 \pm 1.08 \text{ km s}^{-1}$, $\Delta V = -0.15 \pm 1.73 \text{ km s}^{-1}$ and $\Delta W = -0.28 \pm 1.42 \text{ km s}^{-1}$. Six stars (HD 11970, HD 126991, HD 158038, HD 180053, HD 193342 and HD 203471) present higher than average differences, which are related to different values adopted for the radial velocities.

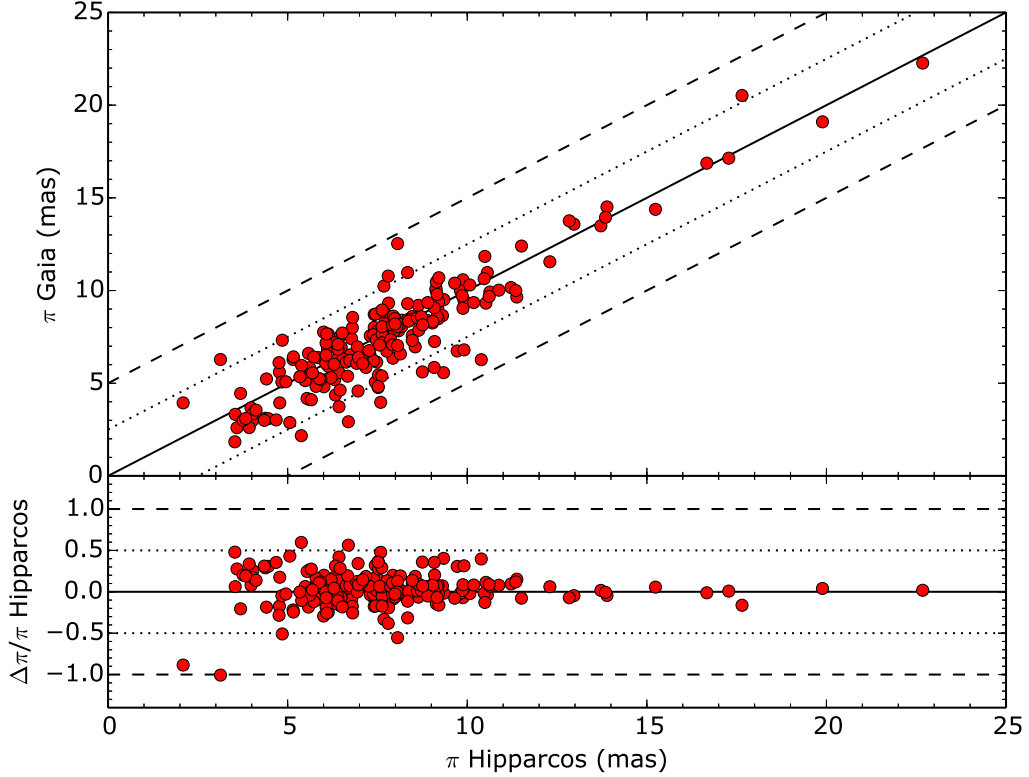


Figure 13. *Upper panel:* Comparison between Gaia’s new parallaxes and the Hipparcos revised values adopted in this work. The black solid line represents a perfect agreement, while dotted and dashed lines show ± 2.5 mas and ± 5 mas offsets, respectively. *Lower panel:* Percentual differences (in the sense Hipparcos - Gaia) between the two sets of parallaxes. The black solid line shows a null difference. Dotted and dashed lines represent 50% and 100% differences.

Our sample also has 28 stars in common with the Geneva Copenhagen Catalog (Casagrande et al. 2011). The agreement between the two sets of values is good and the average differences (in the sense this work - GC) are: $\Delta U = 0.95 \pm 2.81 \text{ km s}^{-1}$, $\Delta V = 1.39 \pm 6.17 \text{ km s}^{-1}$ and $\Delta W = -0.97 \pm 4.98 \text{ km s}^{-1}$. Three stars (HD 11970, HD 31543 and HD 64730) present large differences in the space velocities and are basically responsible for the relatively high dispersions around the averages. These differences can be traced back to distinct values adopted for the radial velocities. These two comparisons confirm that our UVW velocities are consistent with previous values from the literature, and thus are reliable for being used in the following discussions.

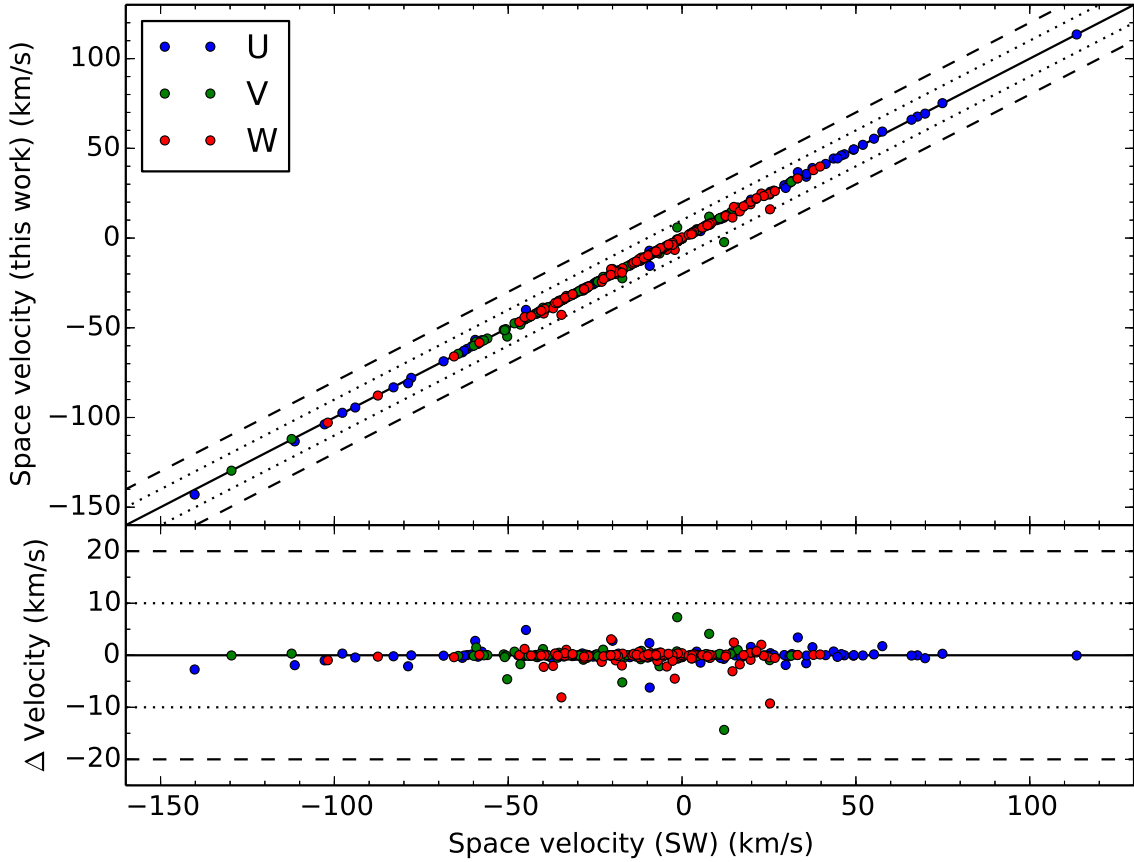


Figure 14. Comparison between UVW velocities (blue, green and red points, respectively) derived in this work and those from Schlaufman & Winn (2013). The black solid line represents a perfect agreement. Dotted and dashed lines show, respectively, $\pm 10 \text{ km s}^{-1}$ and $\pm 20 \text{ km s}^{-1}$ offsets, arbitrarily chosen for reference. *Lower panel:* Absolute differences (in the sense this work - SW) between the two sets of space velocities. The lines are the same as in the upper panel.

5. DISCUSSION

5.1. Consistency between Masses and Kinematics

One of the main concerns regarding the Retired A Stars is that their masses may not be consistent with their space velocities (Schlaufman & Winn 2013). If these stars are indeed the evolved counterparts of A dwarfs, we would expect their velocity dispersions to be smaller than those that would be observed if they were actually F and G stars while on the main sequence. Using solar neighborhood samples defined within the *Hipparcos* catalog, Schlaufman & Winn (2013) showed that subgiant

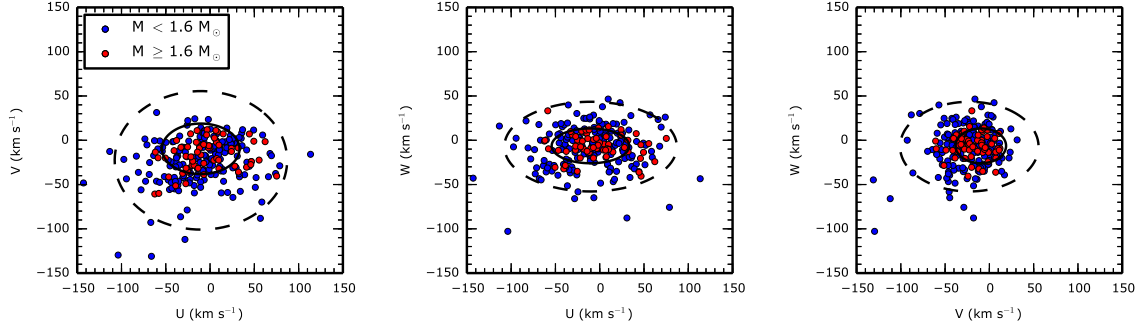


Figure 15. Galactic UVW space velocities for 244 of our subgiants (HD 10245 did not have an available radial velocity). Stars with masses $M_\star < 1.6 \text{ M}_\odot$ and $M_\star \geq 1.6 \text{ M}_\odot$ are represented by blue and red points, respectively. The black solid and dashed lines show the 95% velocity ellipsoids for, respectively, the samples of main-sequence A5-F0 and F5-G5 *Hipparcos* stars, as defined in Schlaufman & Winn (2013).

planet-hosting stars⁹ are more likely to have evolved from main-sequence F5-G5 rather than A5-F0 stars.

In Figure 15, we compare the space velocities derived in this work for the subgiants with the 95% velocity ellipsoids for the samples of main-sequence A5-F0 and F5-G5 *Hipparcos* stars, taken from Schlaufman & Winn (2013). It should be noted that these stars have mean distances of 100 ± 44 pc and 62 ± 23 pc, thus sampling the solar neighborhood. With an average distance of 141 ± 54 pc, our targets sample a very similar volume. If we consider our targets with fractional uncertainties in the parallax lower than 20% (following Schlaufman & Winn 2013), the fractions of subgiants within the A5-F0 95% velocity ellipsoids are: 54% for UV, 48% for UW and 47% for VW. However, if we restrict our sample to $M_\star \geq 1.6 \text{ M}_\odot$, these fractions increase to 67%, 63% and 71%, respectively.

Following equation 1 from Schlaufman & Winn (2013), we calculated δ_i values for each star in their A5-F0 and F5-G5 samples, as well as for our sample of subgiants. We compare these distributions using a Kolmogorov-Smirnov test and again considering only stars with fractional uncertainties in the parallax lower than 20%. The probability that the subgiants and the A5-F0 stars are drawn from the same parent population is $\sim 10^{-38}$, but much higher (≈ 0.06) when compared to the F5-G5 stars.

⁹ Their sample is different from the ones analyzed here and in Johnson et al. (2010a).

If we now use only Retired A Stars (i.e., stars with $M_* \geq 1.6 M_\odot$), the former probability increases to $\sim 10^{-6}$ and the latter decreases to ≈ 0.05 . Although the agreement is much better, this result still supports the idea that the kinematics of the Retired A Stars would imply they were in fact FG dwarfs while on the main sequence.

[Schlaufman & Winn \(2013\)](#) apparently did not use any reddening corrections before selecting the sample of A5-F0 stars. Using a similar procedure as the one described in Section 3.4, we derived A_V and $E(B - V) \approx A_V/3.1$ values for all stars in their sample. Applying these corrections, respectively, to their absolute magnitudes M_V and colors $B - V$, we obtain a new group of main-sequence A5-F0 stars following the selection criteria in [Schlaufman & Winn \(2013\)](#): $0.15 < B - V < 0.30$, $1.9 < M_V < 2.7$ and $\sigma_\pi/\pi < 0.20$. Defining the new corresponding 95% velocity ellipsoids, the fractions of Retired A Stars $\sigma_\pi/\pi < 0.20$ within them are: 77% for UV, 79% for UW and 85% for VW. These numbers are significantly higher than those obtained for the original ellipsoids from [Schlaufman & Winn \(2013\)](#). Because reddening was not accounted for, the M_V and $B - V$ intervals were including brighter and hotter stars, which naturally define smaller ellipsoids.

As this effect could explain the apparent inconsistency between kinematics and mass, we applied reddening corrections to the selection of A5-F0 and F5-G5 stars and performed new KS tests. The probabilities that these samples and the Retired A Stars are drawn from the same parent population are ≈ 0.0003 and ≈ 0.02 , respectively. Although reddening corrections make the A5-F0 sample more consistent with the Retired A Stars, it is not able to explain the apparent inconsistency between their kinematics and masses.

The last test was to check if the uncertainties on the masses contributed to this inconsistency. Using steps of $0.01 M_\odot$ for offsets in the masses of the Retired A Stars, we discovered that, for a decrease of only $0.12 M_\odot$, we can no longer reject the null hypothesis that they are drawn from the same parent population as the A5-F0 stars ($p \approx 0.03$), as defined by [Schlaufman & Winn \(2013\)](#). At this point, the probability that our stars and their F5-G5 sample are drawn from the same distribution is $p \approx 0.009$. If reddening corrections are considered in the selection of the A5-F0 and F5-G5 samples (see discussion above), the transition occurs for an even smaller decrease in mass: $0.04 M_\odot$. For this

offset, the probabilities that the Retired A Stars and A5-F0 and F5-G5 stars are drawn from the same parent population are $p \approx 0.02$ and $p \approx 0.008$, respectively. Therefore, we can conclude that masses derived from evolutionary tracks and the kinematics of the Retired A Stars are consistent within the expected uncertainties of these two different approaches, especially if reddening is considered.

5.2. Consistency between Masses and Rotational Velocities

Another concern regarding the Retired A Stars is that their masses may not be consistent with their rotational velocities (Lloyd 2011). Stellar rotation is a strong function of both mass and evolutionary stage. Stars born with masses above the Kraft break ($\sim 1.3 M_{\odot}$; Kraft 1967) have progressively thinner convective envelopes, or no surface convection at all. Therefore, angular momentum loss through magnetic winds is negligible or absent during the main sequence and they remain as rapid rotators until the end of this evolutionary stage. As these stars evolve across the subgiant branch however, a convective zone develops in the expanding and cooling envelope and magnetic winds are also produced. These effects combined decrease the stellar rotation rate. Therefore, the analysis of the rotation of subgiants provides a powerful diagnostics for stellar mass (e.g., van Saders & Pinsonneault 2013).

Lloyd (2011) noted that three of the evolved planet hosts with $1.6 M_{\odot} < M_{\star} < 2.0 M_{\odot}$ had lower than expected rotational velocities when compared to field stars in the same mass range and in similar evolutionary stages. This discrepancy suggested that they were in fact the evolved counterparts of less massive stars and, mass determinations for two of them were shown to be erroneous. We should note that, besides the studies quoted by Lloyd (2011), Ghezzi et al. (2010b) also showed that HD 154857 has $M_{\star} = 1.21 M_{\odot}$ using a similar method as the one described in this work. HD 102956, on the other hand, was analyzed here and it is indeed massive ($1.67 \pm 0.10 M_{\odot}$). It has $\log g = 3.38 \pm 0.16$ and $v \sin i = 1.6 \pm 0.6 \text{ km s}^{-1}$, thus being consistent with both planet hosting and field stars in the lower panel of Figure 1 from Lloyd (2011). Unfortunately, HD 190228 was not analyzed in our study, but recent determinations confirm its a lower mass star with $1.18 M_{\odot}$ (Jofré et al. 2015).

In order to address this concern regarding the actual sample of Retired A Stars (note that Lloyd 2011 did not use the sample from Johnson et al. 2010a), we analyzed their rotational velocities (see

Section 3.3) as a function of their masses (see Section 3.4) and evolutionary stages (represented by $\log g$; see Section 3.2) in Figure 16. We can observe a very good agreement with the field stars shown in Figure 1 of Lloyd (2011). In the lower panel of this figure, no stars with $\log g \gtrsim 3.6$ have $v \sin i \lesssim 2.5 \text{ km s}^{-1}$. In our sample, only one star is found in this region: HD 171264. It has $\log g = 3.65 \pm 0.04$, $M_\star = 1.64 \pm 0.08 M_\odot$ and $v \sin i = 1.4 \pm 0.8 \text{ km s}^{-1}$. Thus, it is consistent with the field stars from Lloyd (2011) within the uncertainties. We should also note that the value of $v \sin i = 2.4 \text{ km s}^{-1}$ from Brewer et al. (2016) is consistent with the lower limit determined by the field stars. This sample also seems to have an upper limit of $\approx 5 \text{ km s}^{-1}$ for stars with $\log g \lesssim 3.4$. One star in our sample appears above this limit: HD 150331. It is a G0/2 bright giant (see Section 3.2) with a mass of $2.05 M_\odot$ and an age of 1 Gyr (see Table 3.4). In conclusion, the rotational velocities provide another confirmation that masses of the Retired A Stars were not overestimated.

5.3. Giant Planet-Metallicity-Mass Correlation

In the previous sections, we showed that the atmospheric and evolutionary parameters derived for the subgiants are reliable. We now use these results to investigate how the formation of giant planets is influenced by stellar mass and metallicity. We follow the method described in Johnson et al. (2010a) or Montet et al. (2014) and adopt a similar function to describe the fraction of stars with giant planets:

$$f(M_\star, F) = CM_\star^\alpha 10^{\beta F} \quad (2)$$

In the above equation, M_\star is the stellar mass in M_\odot and $F \equiv [\text{Fe}/\text{H}]$ is the stellar metallicity. The free parameters α , β and C are determined so the likelihood conditioned on the data is maximized. We decided to use uniform priors within the following intervals: $\alpha = (0.00, 3.00)$ with 0.05 steps, $\beta = (0.00, 3.00)$ with 0.05 steps and $C = (0.005, 0.150)$ with 0.005 steps.

The first test consists in our best effort to mimic as closely as possible the analysis done by Johnson et al. (2010a) and check if we are able to recover their results: $\alpha = 1.00$, $\beta = 1.20$ and $C = 0.07$. The respective confidence intervals are: $(0.70, 1.30)$, $(1.00, 1.40)$ and $(0.06, 0.08)$. As we

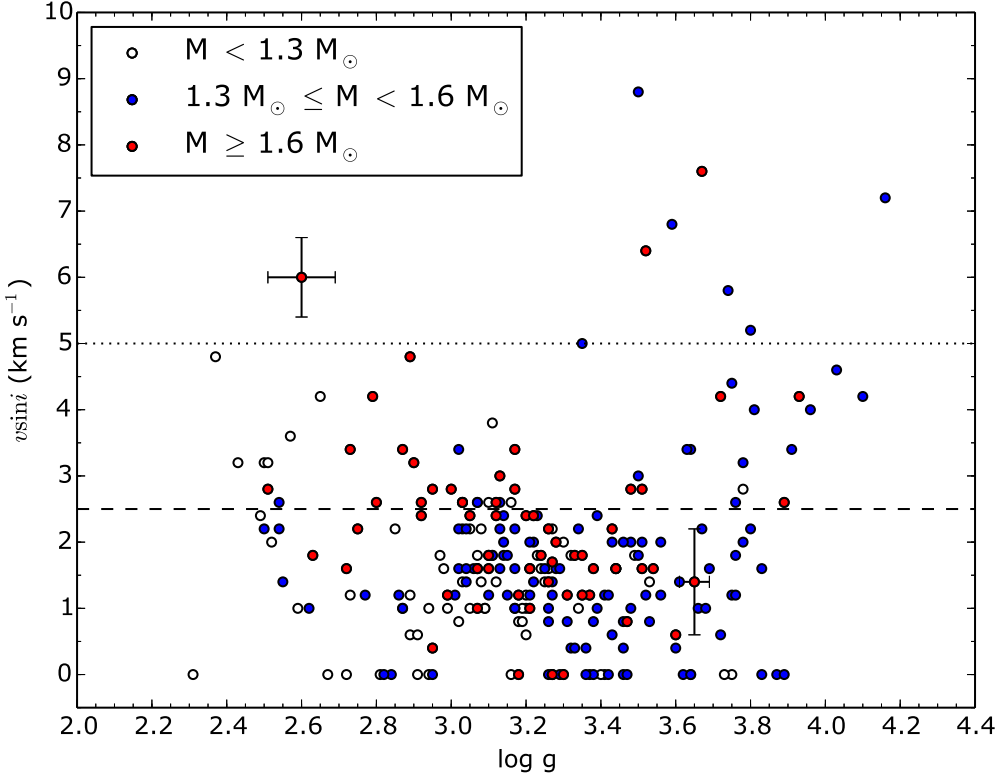


Figure 16. Rotational velocities $v \sin i$ for the subgiants as a function of $\log g$. Stars with masses $M_* < 1.3 M_\odot$, $1.3 M_\odot \leq M_* < 1.6 M_\odot$ and $M_* \geq 1.6 M_\odot$ (i.e., Retired A Stars) are represented by open, blue and red circles, respectively. The black dashed and dotted lines show the limits $v \sin i = 3$ and 5 km s^{-1} discussed in the text. Stars with error bars are discussed in the text.

can see in the first line of Table 9, our results are consistent with these values within the confidence intervals.

We then used the sample of FGKM dwarfs of Johnson et al. (2010a), but replaced their subgiants with our own sample. It should be noted that this was not just an update of the parameters. The sample of subgiants in this work is not the same as the one from Johnson et al. (2010a), there are 56 different objects. Some stars were included because they now fulfill the requirement of at least nine observations, while others were removed due to scientific reasons (e.g., confirmation that they are binaries or poor RV measurements due to enhanced activity or variability).

Since we are only interested in the giant planets in this work, we considered stars that have detected planets with real or minimum masses larger than $0.50 M_{Jup}$. This is almost twice Saturn’s mass and close to the detection limit of $0.44 M_{Jup}$ for a $0.4 M_\odot$ star described in Johnson et al. (2010a). If a star only has planets less massive than this limit, we treat it as if it does not have planets in the following analyses. We also used this lower limit to update the list of planet hosts in the FGKM sample.

With these constraints, we obtain a new giant planet occurrence relation and see that our overall occurrence parameter, C , increases, which is expected since, as our mass threshold is lower and time baseline longer than Johnson et al. (2010a), there are more detected planets in our revised sample. The values of α and β change by the same amount, in opposite directions, but within the errors in both cases (see the second line of Table 9).

Still using our results for the subgiants, we replaced the parameters and uncertainties of the M stars by those from Montet et al. (2014). Whenever available, we also adopted parameters and errors from Brewer et al. (2016) for the FGK dwarfs, keeping the results from Johnson et al. (2010a) otherwise. This is our complete and updated sample of 1225 stars and it is depicted in Figure 17. Although there are some stars with very low metallicities, we highlight that there are no selection biases that cause a correlation between these quantity and the stellar masses. A linear fit to the entire set of stars returns a correlation coefficient $R^2 = 0.08$. When this complete sample is used, we notice slight changes in both α and β , but again the results are consistent with the previous values within the uncertainties (see the third line of Table 9 and Eq. 3).

Schlaufman & Winn (2013) mention that a systematic offset as small as $\approx +0.05$ in the metallicities of the Retired A Stars could explain the larger occurrence rate of giant planets around them. In fact, our metallicities are, on average, 0.04 dex smaller than those of Johnson et al. (2010a) and Brewer et al. (2016) (see Section 4.4). Despite this, we can still see an increased occurrence rate of giant planets around more massive stars.

We saw in Section 4.3 that there is no reason to believe that our [Fe/H] values would be systematically higher for evolved stars relative to dwarfs. However, for completeness, we decided to test

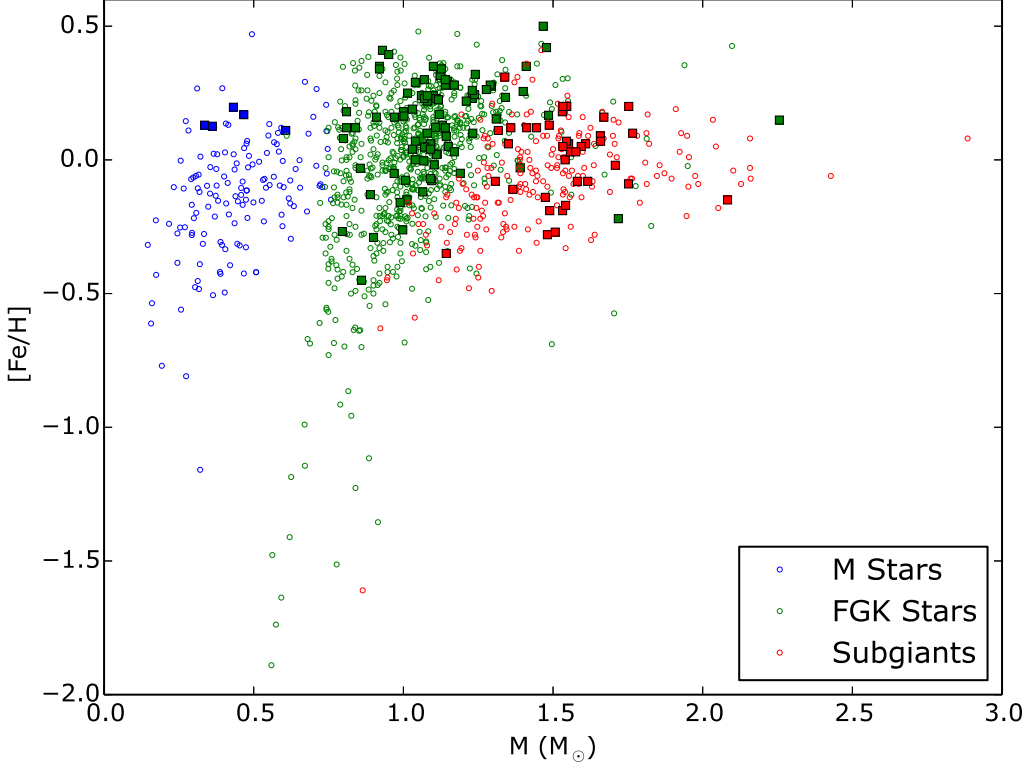


Figure 17. Masses and metallicities for our complete sample of 1225 M (blue), FGK (green) and subgiants (red). Filled squares and open circles represent stars with and without planets, respectively.

whether corrections to the metallicity scale (-0.05 and -0.10 dex) would change our results. We can see in Table 9 that the dependence of the occurrence rate of giant planets on metallicity decreases. As a consequence, the dependence on mass becomes increasingly stronger. Thus, if the Retired A Stars were more metal-poor, then planet formation would be a steeper function of stellar mass in order to explain the giant planets detected at the high-mass end of our sample.

We saw in Section 5.1 that a decrease of only $0.12 M_{\odot}$ in the masses of the Retired A Stars is sufficient to reconcile their kinematics with the velocity dispersions of a sample of A5-F0 dwarfs. As this offset is almost equal to the typical uncertainties in our mass determinations, we tested how it affects the occurrence rate. Table 9 shows that the effect of this mass offset is negligible. Therefore, the correlation between giant planets, metallicity and mass is robust against the typical errors in the latter.

As discussed in Section 4.5.1, a decrease in [Fe/H] will cause a decrease in mass, so these parameters are not independent. In order to account for this, we tested how giant planet occurrence is affected by simultaneous offsets in the metallicities (-0.05 and -0.10 dex) and masses (-0.12 M_⊕) of the subgiants. The results in Table 9 reveal a significant decrease in β and an increase in α , in a similar manner as observed when only [Fe/H] is altered.

These results confirm that giant planet occurrence is a clear function of both metallicity and mass and was not artificially produced by uncertainties or systematic offsets in any or both of these parameters. The best functional form to describe this dependence is (see also Figure 18):

$$f(M_*, F) = 0.085_{-0.010}^{+0.008} M_*^{1.05_{-0.24}^{+0.28}} 10^{1.05_{-0.17}^{+0.21} F} \quad (3)$$

It is interesting to note that, in the previous tests, both α and β always change in opposite directions, meaning that lower metallicities can be compensated by larger masses and vice-versa (as already suggested in Ghezzi et al. 2010b). Therefore, it seems that the formation of giant planets depends on the quantity $M_* \times 10^{[Fe/H]}$. In order to test this, we now describe planet occurrence in the following way:

$$f(M_*, F) = C(M_* \times 10^F)^\gamma \quad (4)$$

As before, the free parameters γ and C are determined so the likelihood conditioned on the data is maximized. We decided to use uniform priors within the following intervals: $\gamma = (0.00, 2.30)$ with 0.02 steps and $C = (0.002, 0.150)$ with 0.002 steps. Using the most updated results for all stars, we obtain the following best functional form to describe this dependence (see also Figure 19):

$$f(M_*, F) = 0.086_{-0.010}^{+0.008} (M_* \times 10^F)^{1.04_{-0.16}^{+0.12}} \quad (5)$$

We note that the best value for γ is very close to 1.00. Offsets applied to the metallicities and/or masses of the subgiants did not change the results significantly (see Table 10). If we remember that $M_d \propto M_*$, where M_d and M_* are the masses of the protoplanetary disk and stellar host, respectively

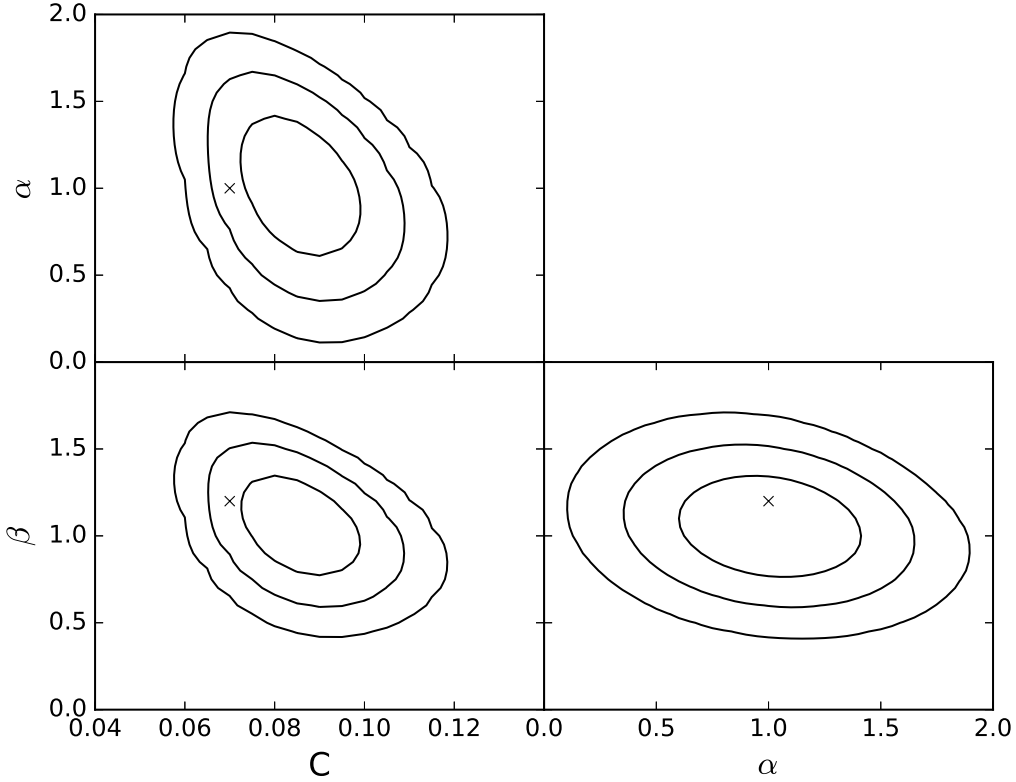


Figure 18. Marginal posterior probability density functions for the parameters α , β and C conditioned on the data. Lines represent the 68%, 95% and 99.7% contours (from smaller to larger). The crosses represent the best-fitting values from Johnson et al. (2010a): $\alpha = 1.00$, $\beta = 1.20$ and $C = 0.07$.

(Andrews et al. 2013), the quantity $M_{\star} \times 10^{[Fe/H]}$ can be considered as proxy for the amount of metals in the disk from which planets formed. In this scenario, our results reveal that the formation of giant planets is an almost linear function of the amount of metals in the protoplanetary disk, going from $\approx 2\%$ in the interval $0.0 - 0.5 M_{\odot}$ to $\approx 24\%$ between $2.0 - 2.5 M_{\odot}$ (see Figure 20). The behavior beyond this interval is too uncertain due to low number statistics. Independently of the functional form chosen, our results provide a strong support for the core accretion hypothesis (Ida & Lin 2004).

6. CONCLUSIONS

We determined atmospheric (effective temperature, metallicity and surface gravity), rotational ($v \sin i$), evolutionary (mass, radius and age) and kinematical (UVW space velocities) parameters for a sample of 245 subgiants. Thorough tests and comparisons showed that our results agree well

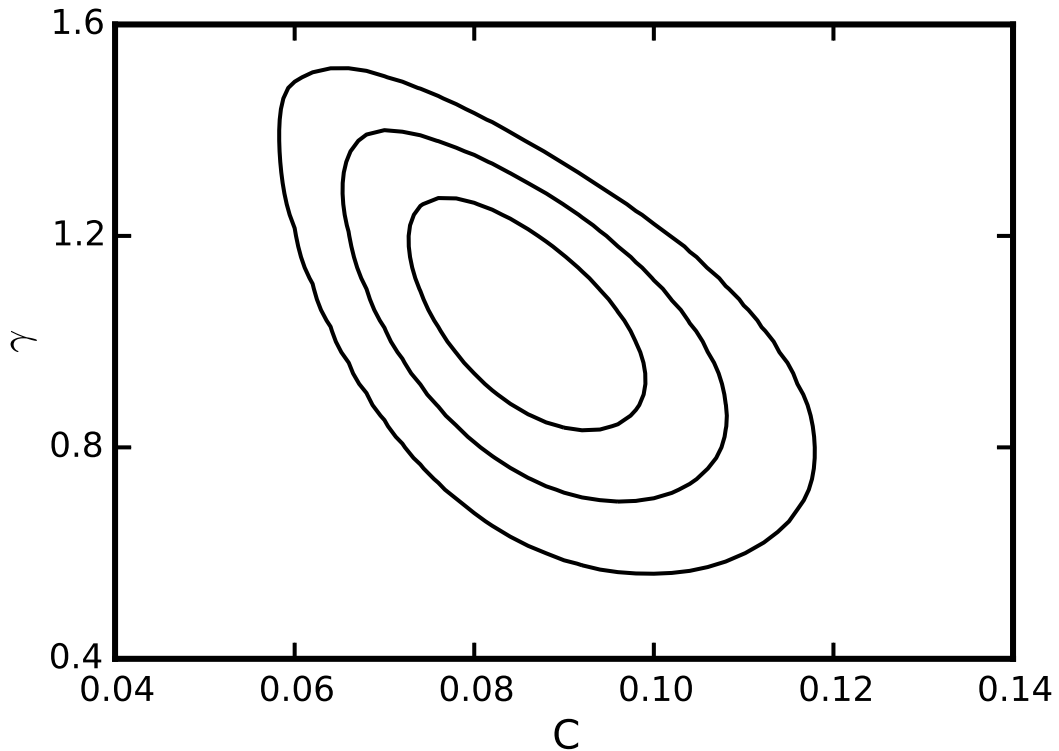


Figure 19. Same as Figure 18, but now for parameters γ and C .

with those determined using other methods and exhibit acceptable offsets when systematic errors are applied to the input data. In particular, we estimate the typical uncertainties on the masses to be $0.11 M_{\odot}$, while a maximum offset of $0.20 M_{\odot}$ could be present if the input parameters were simultaneously affected by systematic errors. This larger value would correspond to an error of $\lesssim 13\%$, much lower than the 50% overestimate suggested by [Lloyd \(2011, 2013\)](#).

We also presented a simple explanation to the apparent inconsistency between their masses and kinematics observed by [Schlaufman & Winn \(2013\)](#). By restricting our sample to Retired A Stars (i.e., stars with $M_{\star} \geq 1.6 M_{\odot}$) and applying an offset of just $-0.12 M_{\odot}$, the velocity dispersions become consistent with the main-sequence A5-F0 stars from [Schlaufman & Winn \(2013\)](#). If reddening is considered for the latter sample, this offset decreases to $0.04 M_{\odot}$. The rotational velocities derived for our targets corroborated that the Retired A Stars are indeed massive, contrary to the concerns

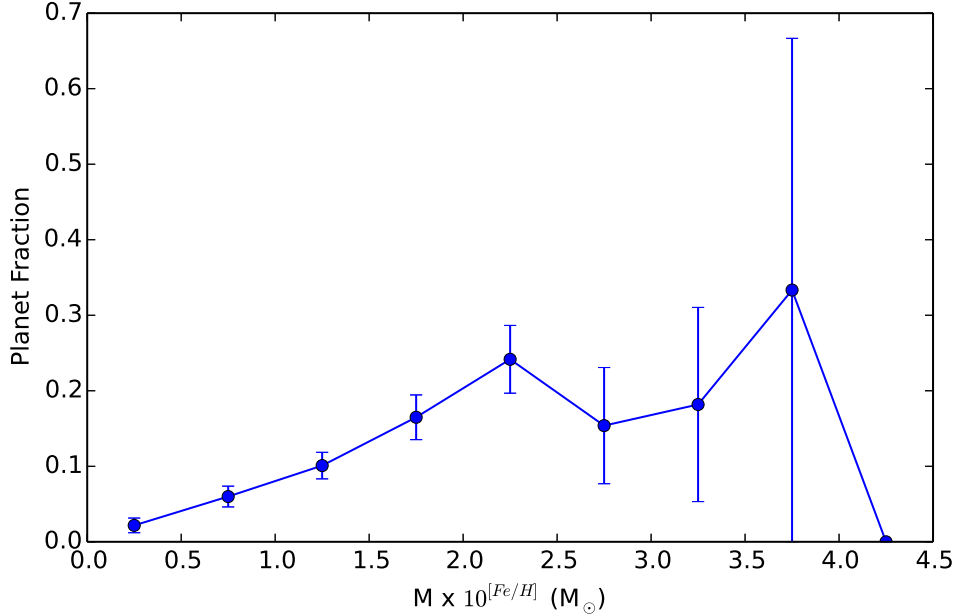


Figure 20. Fraction of stars with planets as a function of the amount of metals in the protoplanetary disk.

raised by [Lloyd \(2011\)](#). Therefore, a thorough and simultaneous analysis of kinematics, rotation and masses confirm that the latter were not significantly overestimated within the expected errors for the Retired A Stars.

Having confirmed the masses and metallicities derived in this study are reliable, we extended our sample with main-sequence FGKM stars from [Johnson et al. \(2010a\)](#), but adopted updated parameters from [Montet et al. \(2014\)](#) and [Brewer et al. \(2016\)](#) (whenever available) and accounted for the most recent giant planet detections. This sample of 1225 stars was used to study the correlation between giant planet occurrence and both stellar mass and metallicity. We confirm recent results (e.g. [Johnson et al. 2010a; Reffert et al. 2015; Jones et al. 2016](#)) that show there is a higher probability of forming giant planets around more massive and metal-rich stars up to $\sim 2.0 - 2.5 M_{\odot}$. Tests with offsets in metallicity, mass or both confirm that this correlation is real, and not artificially produced by systematic uncertainties.

Since mass and metallicity seem to be equally important for the formation of giant planets, we also studied planet occurrence as a function of $(M_* \times 10^{[Fe/H]})^{\gamma}$. This quantity can be thought as the

total amount of metals in the protoplanetary disk, assuming that $M_d \propto M_*$ (Andrews et al. 2013). We observed that the formation of giant planets is an almost linear function of the total amount of metals in the protoplanetary disk ($\gamma \approx 1$). This result agrees with the suggestion given by Ghezzi et al. (2010b) and provides another strong evidence that most (if not all) giant planets form through the core accretion mechanism (e.g., Ida & Lin 2004).

This study also highlights the crucial role detailed stellar characterization plays on a complete understanding of planet formation. In this sense, our team continues to follow-up and analyze samples of evolved stars with the goal of obtaining more accurate and precise models for the giant planet-mass-metallicity correlations. New planet detections and updated stellar parameters will be presented in future contributions.

This work has made use of: SIMBAD database, operated at CDS, Strasbourg, France; VALD database, operated at Uppsala University, the Institute of Astronomy RAS in Moscow, and the University of Vienna; NASA’s Astrophysics Data System (ADS) and Exoplanet Archive.

The authors would like to thank Leo Girardi for kindly sharing the PARAM code, Kevian Schlaufman for providing data for the discussion regarding the kinematics and Letícia Dutra-Ferreira for making the reduced spectra of the Hyades stars available. We also thank the referee for their insightful comments, which led to a much improved manuscript. LG would like to thank the financial support from Coordenação de Aperfeiçoamento de Pessoal de Nível Superior (CAPES), Ciência sem Fronteiras, Harvard College Observatory, and Fundação Lemann. JAJ is grateful for the generous grant support provided by the Alfred P. Sloan and David & Lucile Packard foundations. Work by B.T.M. was performed in part under contract with the California Institute of Technology (Caltech)/Jet Propulsion Laboratory (JPL) funded by NASA through the Sagan Fellowship Program executed by the NASA Exoplanet Science Institute.

Facility: Keck (HIRES)

Software: numpy (Van Der Walt et al. 2011), matplotlib (Hunter et al. 2007), MOOG (Sneden 1973) IRAF, PARAM, astrolibpy

REFERENCES

- Anderson, E., & Francis, C. 2012, *Astronomy Letters*, 38, 331
- Andrews, S. M., Rosenfeld, K. A., Kraus, A. L., & Wilner, D. J. 2013, *ApJ*, 771, 129
- Arenou, F., Grenon, M., & Gomez, A. 1992, *A&A*, 258, 104
- Asplund, M., Grevesse, N., Sauval, A. J., & Scott, P. 2009, *ARA&A*, 47, 481
- Barklem, P. S., & Aspelund-Johansson, J. 2005, *A&A*, 435, 373
- Barklem, P. S., Piskunov, N., & O’Mara, B. J. 2000, *A&AS*, 142, 467
- Bedell, M., Meléndez, J., Bean, J. L., et al. 2014, *ApJ*, 795, 23
- Bressan, A., Marigo, P., Girardi, L., et al. 2012, *MNRAS*, 427, 127
- Brewer, J. M., Fischer, D. A., Valenti, J. A., & Piskunov, N. 2016, *ApJS*, 225, 32
- Butler, R. P., Johnson, J. A., Marcy, G. W., et al. 2006, *PASP*, 118, 1685

- Butler, R. P., Marcy, G. W., Williams, E., et al. 1996, PASP, 108, 500
- Campante, T. L., Veras, D., North, T. S. H., et al. 2017, MNRAS, 469, 1360
- Carroll, B. W., & Ostlie, D. A. 2006, An Introduction to Modern Astrophysics, 2nd edition. (San Francisco, CA: Pearson, Addison-Wesley)
- Casagrande, L., Ramírez, I., Meléndez, J., Bessell, M., & Asplund, M. 2010, A&A, 512, A54
- Casagrande, L., Schönrich, R., Asplund, M., et al. 2011, A&A, 530, A138
- Castelli, F., & Kurucz, R. L. 2004, in IAU Symp. 210, Modelling of Stellar Atmospheres, ed. N. Piskunov, et al. (Dordrecht: Kluwer), poster A20 (arXiv:astro-ph/0405087)
- Chabrier, G. 2001, ApJ, 554, 1274
- Chubak, C., Marcy, G., Fischer, D. A., et al. 2012, arXiv:1207.6212
- Cutri, R. M., et al. 2003, The IRSA 2MASS All-Sky Point Source Catalog, NASA/IPAC Infrared Science Archive
- da Silva, L., Girardi, L., Pasquini, L., et al. 2006, A&A, 458, 609
- Demarque, P., Woo, J.-H., Kim, Y.-C., & Yi, S. K. 2004, ApJS, 155, 667
- Dutra-Ferreira, L., Pasquini, L., Smiljanic, R., Porto de Mello, G. F., & Steffen, M. 2016, A&A, 585, A75
- ESA 1997, The Hipparcos and Tycho Catalogues, ESA Special Publication, 1200 (Noordwijk: ESA)
- Fischer, D. A., & Valenti, J. A. 2005, ApJ, 622, 1102
- Fressin, F., Torres, G., Charbonneau, D., et al. 2013, ApJ, 766, 81
- Gaidos, E., Fischer, D. A., Mann, A. W., & Howard, A. W. 2013, ApJ, 771, 18
- Ghezzi, L., Cunha, K., Smith, V. V., de Araújo, F. X., Schuler, S., & de la Reza, R. 2010, ApJ, 720, 1290
- Ghezzi, L., Cunha, K., Schuler, S. C., & Smith, V. V. 2010, ApJ, 725, 721
- Ghezzi, L., & Johnson, J. A. 2015, ApJ, 812, 96
- Girardi, L., Groenewegen, M. A. T., Hatziminaoglou, E., & da Costa, L. 2005, A&A, 436, 895
- Gontcharov, G. A. 2006, Astronomy Letters, 32, 759
- Gontcharov, G. A., & Mosenkov, A. V. 2017, MNRAS, 472, 3805
- Gonzalez, G. 1997, MNRAS, 285, 403
- González Hernández, J. I., & Bonifacio, P. 2009, A&A, 497, 497
- Hakkila, J., Myers, J. M., Stidham, B. J., & Hartmann, D. H. 1997, AJ, 114, 2043
- Hinkel, N. R., Young, P. A., Pagano, M. D., et al. 2016, ApJS, 226, 4
- Høg, E., Fabricius, C., Makarov, V. V., et al. 2000, A&A, 355, L27
- Hunter, J. D., et al. 2007, Computing in science and engineering, 9, 90
- Ida, S., & Lin, D. N. C. 2004, ApJ, 616, 567

- Jofré, E., Petrucci, R., Saffe, C., et al. 2015, *A&A*, 574, A50
- Johnson, J. A., Marcy, G. W., Fischer, D. A., et al. 2006, *ApJ*, 652, 1724
- Johnson, J. A., Aller, K. M., Howard, A. W., & Crepp, J. R. 2010, *PASP*, 122, 905
- Johnson, J. A., Howard, A. W., Bowler, B. P., et al. 2010, *PASP*, 122, 701
- Johnson, J. A., Huber, D., Boyajian, T., et al. 2014, *ApJ*, 794, 15
- Johnson & Wright, J. T. 2013, arXiv:1306.6627v1
- Johnson, J. A., Morton, T. D., & Wright, J. T. 2013, *ApJ*, 763, 53
- Jones, M. I., Jenkins, J. S., Brahm, R., et al. 2016, *A&A*, 590, A38
- Kraft, R. P. 1967, *ApJ*, 150, 551
- Kurucz, R. L., Furenlid, I., Brault, J., & Testerman, L. 1984, Solar Flux Atlas from 296 to 1300 nm (Cambridge: Harvard Univ. Press)
- Liu, F., Asplund, M., Ramírez, I., Yong, D., & Meléndez, J. 2014, *MNRAS*, 442, L51
- Lloyd, J. P. 2011, *ApJL*, 739, L49
- Lloyd, J. P. 2013, *ApJL*, 774, L2
- Mashonkina, L., Gehren, T., Shi, J.-R., Korn, A. J., & Grupp, F. 2011, *A&A*, 528, A87
- Massarotti, A., Latham, D. W., Stefanik, R. P., & Fogel, J. 2008, *AJ*, 135, 209
- Montet, B. T., Crepp, J. R., Johnson, J. A., Howard, A. W., & Marcy, G. W. 2014, *ApJ*, 781, 28
- Niedzielski, A., Villaver, E., Wolszczan, A., et al. 2015, *A&A*, 573, A36
- Nordström, B., Mayor, M., Andersen, J., et al. 2004, *A&A*, 418, 989
- North, T. S. H., Campante, T. L., Miglio, A., et al. 2017, *MNRAS*, 472, 1866
- Pavlenko, Y. V., Jenkins, J. S., Jones, H. R. A., Ivanyuk, O., & Pinfield, D. J. 2012, *MNRAS*, 422, 542
- Ramírez, I., & Meléndez, J. 2005, *ApJ*, 626, 465
- Reffert, S., Bergmann, C., Quirrenbach, A., Trifonov, T., & Künstler, A. 2015, *A&A*, 574, A116
- Robin, A. C., Reylé, C., Derrière, S., & Picaud, S. 2003, *A&A*, 409, 523
- Ryabchikova, T., Piskunov, N., Kurucz, R. L., et al. 2015, *PhyS*, 90, 054005
- Schlafman, K. C., & Winn, J. N. 2013, *ApJ*, 772, 143
- Schuler, S. C., Flateau, D., Cunha, K., et al. 2011, *ApJ*, 732, 55
- Sneden, C. 1973, PhD thesis, Univ. Texas, Austin
- Soubiran, C., Le Campion, J.-F., Brouillet, N., & Chemin, L. 2016, *A&A*, 591, A118
- Sousa, S. G., Santos, N. C., Adibekyan, V., Delgado-Mena, E., & Israelian, G. 2015, *A&A*, 577, A67
- Sousa, S. G., Santos, N. C., Adibekyan, V., et al. 2014, *A&A*, 561, A21
- Sousa, S. G., Santos, N. C., Mayor, M., et al. 2008, *A&A*, 487, 373
- Sousa, S. G., Santos, N. C., Mortier, A., et al. 2015, *A&A*, 576, A94
- Stassun, K. G., & Torres, G. 2016, *ApJL*, 831, L6

- Stassun, K. G., Collins, K. A., & Gaudi, B. S.
2017, AJ, 153, 136
- Stello, D., Huber, D., Grundahl, F., et al. 2017,
MNRAS, 472, 4110
- Takeda, Y., & Tajitsu, A. 2015, MNRAS, 450, 397
- Torres, G., Andersen, J., & Giménez, A. 2010,
A&A Rv, 18, 67
- Torres, G., Fischer, D. A., Sozzetti, A., et al.
2012, ApJ, 757, 161
- Tsantaki, M., Sousa, S. G., Adibekyan, V. Z., et
al. 2013, A&A, 555, A150
- Valenti, J. A., & Fischer, D. A. 2005, ApJS, 159,
141
- Van Der Walt, S., Colbert, S. C., & Varoquaux,
G. 2011, Computing in Science & Engineering,
13, 22
- van Leeuwen, F. 2007, A&A, 474, 653
- van Saders, J. L., & Pinsonneault, M. H. 2013,
ApJ, 776, 67
- Vogt, S. S., Allen, S. L., Bigelow, B. C., et al.
1994, Proc. SPIE, 2198, 362
- Wang, J., & Fischer, D. A. 2015, AJ, 149, 14
- Wright, J. T. 2005, PASP, 117, 657

Table 1. Sample of Subgiants.

Star	α (J2000.0)	δ (J2000.0)	V	A_V	π (mas)	μ_α (mas yr $^{-1}$)	μ_δ (mas yr $^{-1}$)	RV (km s $^{-1}$)	S/N
HD 1100	003.81777959	-06.13821196	7.762 \pm 0.013	0.099 \pm 0.035	7.12 \pm 0.92	-36.51	-49.99	22.749	199
HD 1293	004.27312298	-01.65301289	8.376 \pm 0.016	0.099 \pm 0.035	6.31 \pm 1.05	25.88	11.56	45.140	241
HD 1384	004.55058081	+52.41254980	8.097 \pm 0.013	0.110 \pm 0.015	9.34 \pm 1.14	-14.90	-56.14	-35.185	144
HD 1502	004.82110857	+14.05475398	8.349 \pm 0.015	0.108 \pm 0.080	6.28 \pm 0.75	74.64	-18.15	-10.024	170
HD 2946	008.14629082	-18.10912237	8.080 \pm 0.013	0.099 \pm 0.035	7.41 \pm 0.94	34.13	15.59	10.460	254
HD 3458	009.34561534	-19.56502439	8.257 \pm 0.013	0.099 \pm 0.035	3.53 \pm 0.80	-3.82	-3.96	-4.607	223
HD 4313	011.41815996	+07.84502103	7.829 \pm 0.014	0.100 \pm 0.074	7.30 \pm 0.76	-5.14	6.69	14.482	181
HD 4395	011.55728796	-11.45237787	7.689 \pm 0.013	0.099 \pm 0.028	10.56 \pm 0.68	-106.18	-38.11	-0.439	249
HD 4917	012.77614783	-12.92760455	8.051 \pm 0.015	0.099 \pm 0.028	7.44 \pm 0.84	21.61	-15.20	-11.482	180
HD 5891	015.13830018	+20.29248280	8.121 \pm 0.015	0.396 \pm 0.396	3.98 \pm 1.21	2.64	-41.89	-96.564	239
HD 6019	015.41505988	+07.30529335	7.732 \pm 0.013	0.099 \pm 0.073	7.46 \pm 0.84	-19.10	-2.42	-23.812	252
HD 6030	015.42870486	+09.74602251	7.863 \pm 0.014	0.087 \pm 0.065	9.08 \pm 1.03	15.12	36.19	-21.000	211
HD 7530	018.78347930	-22.89946990	8.316 \pm 0.013	0.098 \pm 0.037	6.38 \pm 1.32	47.37	3.43	55.245	257
HD 7931	019.63437081	-28.73295461	7.926 \pm 0.012	0.100 \pm 0.038	8.06 \pm 0.76	75.50	5.23	11.248	191
HD 7980	019.85056751	+18.13777069	7.640 \pm 0.012	0.141 \pm 0.141	7.51 \pm 0.68	-73.34	-59.79	-35.830	174
HD 8375	020.90615147	+34.24588758	6.286 \pm 0.011	0.060 \pm 0.021	17.65 \pm 0.39	233.10	117.80	4.600	256
HD 8407	020.76089051	-16.56031152	7.764 \pm 0.012	0.098 \pm 0.037	10.39 \pm 0.94	94.71	64.70	-6.833	233
HD 8508	021.17891865	+36.06390331	7.872 \pm 0.012	0.161 \pm 0.055	5.61 \pm 0.66	46.13	-79.00	9.086	225
HD 9156	022.57801433	+11.09089735	8.428 \pm 0.017	0.117 \pm 0.087	4.03 \pm 0.95	8.41	1.21	28.918	229
HD 9218	022.55779613	-28.86543582	7.956 \pm 0.012	0.100 \pm 0.038	6.74 \pm 0.65	40.96	-9.27	11.171	224
HD 9313	022.97857228	+16.04695686	7.817 \pm 0.012	0.088 \pm 0.065	9.03 \pm 0.74	2.75	-148.06	-14.840	189
HD 9554	023.31615748	-25.66720006	8.355 \pm 0.014	0.100 \pm 0.036	5.38 \pm 0.78	55.53	-32.75	-18.085	221
HD 9625	023.56810341	-06.27259106	8.389 \pm 0.015	0.098 \pm 0.037	3.13 \pm 1.07	-8.21	-28.02	-26.883	212
HD 10011	024.35865432	-15.99768292	7.996 \pm 0.013	0.098 \pm 0.037	7.68 \pm 0.87	69.89	23.34	47.000	225
HD 10212	025.20706456	+45.01895994	8.136 \pm 0.014	0.126 \pm 0.043	7.70 \pm 0.88	-48.86	-50.01	-26.400	233
HD 10245	025.09814690	+07.08658407	8.228 \pm 0.015	0.104 \pm 0.077	6.84 \pm 1.11	2.52	-32.18	...	96

Table 1 continued on next page

Table 1 (*continued*)

Star	α (J2000.0)	δ (J2000.0)	V	A_V	π (mas)	μ_α (mas yr $^{-1}$)	μ_δ (mas yr $^{-1}$)	RV	S/N
HD 10383	025.28736342	-09.96857564	8.287 \pm 0.017	0.098 \pm 0.037	5.86 \pm 0.84	-0.89	-34.01	20.676	152
HD 10479	025.51431837	-04.94447815	8.767 \pm 0.018	0.098 \pm 0.037	3.59 \pm 1.06	27.53	19.95	2.045	235
HD 10823	026.49043992	-04.22867213	8.105 \pm 0.015	0.098 \pm 0.037	7.55 \pm 0.76	-19.66	-38.06	25.650	226
HD 10909	026.67353205	-24.01397533	8.099 \pm 0.013	0.100 \pm 0.036	7.41 \pm 0.87	151.45	96.25	8.760	210
HD 11288	027.58461085	-23.77186757	8.467 \pm 0.014	0.100 \pm 0.036	5.52 \pm 1.23	57.78	-15.66	9.400	225
HD 11970	029.60127276	+40.91366703	8.233 \pm 0.014	0.125 \pm 0.043	7.71 \pm 0.96	111.26	-9.28	-14.377	260
HD 12137	030.08946630	+44.10270698	7.668 \pm 0.012	0.131 \pm 0.045	7.29 \pm 0.73	33.63	-14.64	-12.799	223
HD 12164	029.94415781	+15.95788312	8.036 \pm 0.013	0.142 \pm 0.142	7.48 \pm 0.88	-28.83	-18.70	-18.252	253
HD 13167	032.05742471	-24.69540754	8.325 \pm 0.016	0.100 \pm 0.036	8.55 \pm 1.21	43.00	-37.02	15.780	228
HD 14787	035.80855513	+10.83674593	7.646 \pm 0.013	0.093 \pm 0.069	8.19 \pm 1.11	-12.11	11.90	-8.220	218
HD 15336	036.93718826	-11.97902798	8.930 \pm 0.021	0.100 \pm 0.036	5.06 \pm 1.43	-9.73	-13.59	-30.453	241
HD 15391	037.07944711	-11.71634666	8.628 \pm 0.020	0.100 \pm 0.036	3.69 \pm 0.97	-3.97	20.23	28.682	222
HD 15928	038.31417251	-14.36275033	7.815 \pm 0.014	0.100 \pm 0.036	9.88 \pm 0.82	-40.19	32.42	11.064	247
HD 16175	039.25796235	+42.06263206	7.291 \pm 0.011	0.051 \pm 0.031	17.28 \pm 0.67	-38.90	-40.37	21.949	231
HD 16178	039.04983969	+15.14870116	8.410 \pm 0.015	0.396 \pm 0.396	4.38 \pm 0.74	-1.98	-40.02	-24.585	209
HD 16984	040.95084647	+12.02971930	8.227 \pm 0.019	0.067 \pm 0.016	7.58 \pm 0.89	55.72	3.11	69.677	223
HD 17311	041.63264789	-08.02807911	8.212 \pm 0.014	0.177 \pm 0.018	6.78 \pm 0.70	-51.26	-17.81	18.516	222
HD 17620	042.23242819	-24.60979917	8.202 \pm 0.012	0.100 \pm 0.038	4.85 \pm 0.91	-6.73	-2.11	1.340	233
HD 18015	043.36336189	-08.84802119	7.913 \pm 0.013	0.148 \pm 0.015	8.34 \pm 0.79	63.70	-4.73	19.008	232
HD 18645	044.97154200	-00.67971900	7.862 \pm 0.015	0.090 \pm 0.066	8.75 \pm 0.83	-6.99	-24.77	-2.656	226
HD 18667	045.03415287	+00.23542665	8.311 \pm 0.020	0.095 \pm 0.071	7.93 \pm 1.53	45.66	-6.50	3.660	207
HD 18742	045.04440167	-20.80260631	7.822 \pm 0.013	0.100 \pm 0.036	7.39 \pm 0.78	-19.81	-23.37	-13.831	223
HD 19522	047.00532690	-12.04132568	8.122 \pm 0.013	0.153 \pm 0.015	8.06 \pm 1.00	140.42	45.41	57.359	228
HD 19659	047.17702968	-35.43289844	7.114 \pm 0.011	0.154 \pm 0.012	10.47 \pm 0.52	-27.22	-112.76	1.974	262
HD 21340	051.40204264	-27.27248989	7.397 \pm 0.011	0.160 \pm 0.013	7.39 \pm 0.68	68.17	-0.15	21.900	241
HD 21449	052.23845417	+40.18646846	7.327 \pm 0.012	0.252 \pm 0.008	6.15 \pm 0.72	29.18	1.00	-5.328	215
HD 21581	052.22702500	-00.41753100	8.718 \pm 0.015	0.271 \pm 0.065	4.03 \pm 1.00	67.09	-78.56	152.943	259
HD 22233	053.58382361	-14.71044808	7.937 \pm 0.014	0.195 \pm 0.020	6.01 \pm 1.00	3.28	-1.80	19.434	227
HD 22657	054.58527200	-11.20146171	7.830 \pm 0.014	0.152 \pm 0.015	8.09 \pm 0.87	40.54	30.44	65.610	203

Table 1 continued on next page

Table 1 (*continued*)

Star	α	δ	V	A_V	π	μ_α	μ_δ	RV	S/N
	(J2000.0)	(J2000.0)			(mas)	(mas yr $^{-1}$)	(mas yr $^{-1}$)	(km s $^{-1}$)	
HD 22682	054.82105522	+13.89149080	6.677 \pm 0.012	0.015 \pm 0.004	13.89 \pm 0.57	12.66	-100.91	-25.500	246
HD 22844	055.72831810	+56.40515710	8.125 \pm 0.014	0.306 \pm 0.070	9.81 \pm 0.72	58.13	-20.70	-26.972	217
HD 23134	055.50814950	-21.23725321	8.318 \pm 0.014	0.160 \pm 0.013	6.00 \pm 1.14	-19.55	-20.54	18.831	200
HD 23825	057.09140366	+10.79306356	7.929 \pm 0.014	0.043 \pm 0.010	9.18 \pm 0.81	-21.68	-117.36	-16.793	222
HD 24148	057.54322170	-16.77526339	8.140 \pm 0.015	0.208 \pm 0.021	5.57 \pm 0.91	46.66	0.90	49.483	223
HD 24316	057.88586416	-17.16648839	7.712 \pm 0.014	0.207 \pm 0.021	5.58 \pm 0.78	-66.35	-65.08	52.272	205
HD 24365	058.40726726	+28.14811281	7.879 \pm 0.013	0.174 \pm 0.073	10.07 \pm 0.97	99.01	-11.31	19.276	229
HD 25622	060.81571891	-21.41743214	7.626 \pm 0.013	0.160 \pm 0.013	6.54 \pm 0.93	4.87	26.77	-1.817	216
HD 25975	062.06411652	+37.72749471	6.071 \pm 0.011	0.292 \pm 0.146	22.68 \pm 0.34	-100.02	-196.30	-44.350	224
HD 26007	061.54759581	-23.27981685	8.397 \pm 0.012	0.160 \pm 0.013	4.78 \pm 0.90	25.36	19.73	9.167	224
HD 26634	063.04665317	-13.63717234	7.998 \pm 0.014	0.242 \pm 0.022	6.13 \pm 0.76	63.88	-14.55	8.476	216
HD 27297	064.68402808	+03.14904452	8.247 \pm 0.019	0.069 \pm 0.017	7.47 \pm 1.30	63.18	-33.34	42.493	218
HD 27956	066.04206235	-16.04184962	8.080 \pm 0.013	0.242 \pm 0.022	6.90 \pm 0.90	-14.97	-58.75	45.984	227
HD 28678	067.85606392	+04.57529762	8.447 \pm 0.020	0.391 \pm 0.164	4.41 \pm 0.93	4.03	-8.82	61.465	225
HD 28737	067.93599227	-01.35259495	8.241 \pm 0.017	0.122 \pm 0.029	5.80 \pm 1.11	14.85	-25.03	-5.702	196
HD 30090	071.61217190	+42.34856041	6.541 \pm 0.011	0.141 \pm 0.052	14.91 \pm 0.61	-3.68	70.45	23.377	303
HD 30128	071.01308253	-21.10693387	8.266 \pm 0.014	0.242 \pm 0.022	4.12 \pm 0.92	25.98	0.72	20.863	201
HD 30166	072.16017092	+58.38973250	7.673 \pm 0.011	0.341 \pm 0.130	7.27 \pm 0.62	-8.77	-54.66	-32.300	205
HD 30856	072.57442501	-24.36884155	7.918 \pm 0.011	0.230 \pm 0.021	8.47 \pm 0.71	18.91	-18.93	35.457	230
HD 30882	073.45986898	+47.95627712	8.353 \pm 0.014	0.515 \pm 0.206	6.43 \pm 0.87	51.07	-41.90	-39.511	220
HD 31018	073.34185318	+24.17736470	7.633 \pm 0.013	0.563 \pm 0.281	11.38 \pm 0.97	12.61	-22.73	-4.147	291
HD 31451	074.46083941	+39.63237281	8.078 \pm 0.016	0.268 \pm 0.099	7.69 \pm 0.87	-5.94	-17.92	0.644	251
HD 31543	074.10330715	-07.02319711	8.163 \pm 0.015	0.162 \pm 0.073	5.57 \pm 1.05	6.88	-47.31	-6.940	229
HD 31693	074.45159576	-04.65495354	7.675 \pm 0.013	0.138 \pm 0.062	6.80 \pm 0.95	17.44	-20.85	29.318	180
HD 33142	076.89808933	-13.98647842	7.963 \pm 0.013	0.121 \pm 0.054	7.94 \pm 0.72	-7.49	35.37	33.525	210
HD 33240	076.91066506	-28.97745375	8.234 \pm 0.013	0.242 \pm 0.022	6.43 \pm 1.03	1.98	-9.92	10.465	209
HD 33298	077.75964660	+39.28205809	8.288 \pm 0.015	0.253 \pm 0.094	8.18 \pm 3.13	23.92	20.17	-6.983	270
HD 33844	078.15042069	-14.95111346	7.293 \pm 0.011	0.099 \pm 0.045	9.91 \pm 0.64	33.84	29.99	36.307	162
HD 34538	079.41767383	-13.51982741	5.495 \pm 0.010	0.051 \pm 0.023	20.40 \pm 0.39	-7.63	-49.16	75.300	251

Table 1 continued on next page

Table 1 (*continued*)

Star	α (J2000.0)	δ (J2000.0)	V	A_V	π (mas)	μ_α (mas yr $^{-1}$)	μ_δ (mas yr $^{-1}$)	RV	S/N
HD 34909	080.15615519	-05.82264099	8.002 \pm 0.014	0.126 \pm 0.057	7.53 \pm 1.13	-7.78	-29.24	-0.426	219
HD 37445	084.52265654	-14.75615341	8.323 \pm 0.014	0.192 \pm 0.087	4.46 \pm 1.03	-19.24	5.59	38.804	212
HD 37601	085.75697376	+56.58152362	6.052 \pm 0.011	0.148 \pm 0.056	16.90 \pm 0.38	15.29	29.20	-31.690	229
HD 38505	086.68560645	+11.05041615	7.634 \pm 0.013	0.084 \pm 0.003	8.94 \pm 1.16	57.41	-57.77	75.613	182
HD 39142	087.65994927	+01.69967404	7.950 \pm 0.014	0.192 \pm 0.033	4.69 \pm 1.00	-6.74	1.85	8.977	205
HD 39731	088.64927517	+05.35368987	8.265 \pm 0.015	0.122 \pm 0.021	7.24 \pm 1.65	-9.47	-8.65	32.695	216
HD 39828	088.91266366	+13.00188362	7.698 \pm 0.013	0.095 \pm 0.004	7.85 \pm 1.29	29.30	-4.69	28.802	195
HD 40537	089.64767208	-21.54389390	7.314 \pm 0.011	0.078 \pm 0.005	12.97 \pm 0.66	103.76	40.49	53.783	241
HD 45210	096.72929876	+17.45157707	7.721 \pm 0.014	0.137 \pm 0.066	7.63 \pm 0.81	-52.33	-2.67	53.781	269
HD 45410	097.69628320	+58.16263358	5.862 \pm 0.011	0.030 \pm 0.012	17.92 \pm 0.47	-30.14	-338.67	39.477	259
HD 45506	097.11688662	+16.23838604	6.241 \pm 0.011	0.072 \pm 0.035	14.51 \pm 0.47	-92.18	-48.73	40.900	235
HD 47562	099.56743229	-22.76755707	8.254 \pm 0.011	0.077 \pm 0.020	4.77 \pm 0.73	0.41	-18.91	17.309	271
HD 48122	100.56665962	+12.00793095	8.003 \pm 0.018	0.188 \pm 0.107	6.25 \pm 0.74	50.10	11.37	2.698	272
HD 50275	103.35922801	+21.71822350	8.291 \pm 0.015	0.150 \pm 0.043	6.21 \pm 1.01	-19.14	-32.53	84.308	190
HD 51272	104.59510314	+37.98798053	7.794 \pm 0.014	0.083 \pm 0.034	5.73 \pm 0.77	-42.72	-27.01	13.400	213
HD 64413	118.46576774	+00.33145681	8.247 \pm 0.019	0.061 \pm 0.010	4.35 \pm 1.27	8.45	-20.02	15.856	243
HD 64730	118.93927791	+13.33187742	7.981 \pm 0.016	0.011 \pm 0.000	5.79 \pm 0.96	-14.74	-48.21	15.976	236
HD 72003	128.27220420	+55.35475652	7.670 \pm 0.012	0.066 \pm 0.066	7.20 \pm 1.25	-23.57	-61.87	-6.950	221
HD 72440	128.75450407	+50.47200396	8.293 \pm 0.014	0.066 \pm 0.066	6.49 \pm 1.10	-7.72	-9.95	-33.261	268
HD 72490	128.40271687	+13.55078801	7.836 \pm 0.014	0.000 \pm 0.000	7.63 \pm 0.92	25.04	-16.18	31.512	254
HD 74390	131.33920039	+42.40384013	8.199 \pm 0.014	0.066 \pm 0.066	6.08 \pm 0.86	18.02	-65.79	-58.086	203
HD 76445	134.19162325	+17.48135033	7.647 \pm 0.013	0.000 \pm 0.000	11.22 \pm 0.70	32.18	-20.33	-16.402	233
HD 77172	135.71582235	+52.28582611	8.086 \pm 0.014	0.066 \pm 0.066	7.59 \pm 1.01	-75.85	-138.08	-15.808	211
HD 77818	136.85891294	+58.87505348	7.635 \pm 0.012	0.000 \pm 0.000	7.98 \pm 0.70	17.63	-90.52	-44.051	212
HD 80811	140.55399843	+12.54910041	8.357 \pm 0.016	0.006 \pm 0.005	8.47 \pm 1.15	-124.85	-195.01	30.014	204
HD 82074	142.38506562	-04.24663549	6.265 \pm 0.011	0.031 \pm 0.022	17.97 \pm 0.50	-31.03	-52.33	-12.800	253
HD 82886	143.93826142	+34.78074254	7.633 \pm 0.012	0.125 \pm 0.124	7.97 \pm 0.74	14.33	-34.78	12.554	229
HD 83024	143.91858782	+02.63742541	7.911 \pm 0.014	0.031 \pm 0.022	8.21 \pm 0.61	-84.14	10.63	4.556	186
HD 83394	144.99621282	+53.49696317	7.448 \pm 0.011	0.001 \pm 0.000	9.35 \pm 0.66	-9.53	-131.53	40.345	250

Table 1 continued on next page

Table 1 (*continued*)

Star	α (J2000.0)	δ (J2000.0)	V	A_V	π (mas)	μ_α (mas yr $^{-1}$)	μ_δ (mas yr $^{-1}$)	RV	S/N
HD 83752	145.13246924	-01.73009336	7.554 \pm 0.012	0.031 \pm 0.022	8.64 \pm 0.53	-45.53	-27.39	31.200	165
HD 85440	148.11955363	+27.77405677	7.821 \pm 0.012	0.067 \pm 0.009	8.86 \pm 0.84	1.36	-14.80	-4.184	256
HD 85472	148.49148324	+57.68370349	7.459 \pm 0.011	0.001 \pm 0.000	13.72 \pm 0.70	36.85	-93.52	-9.954	267
HD 87230	150.80226430	-20.93086250	7.794 \pm 0.014	0.145 \pm 0.009	8.14 \pm 0.64	-61.00	-24.39	42.625	232
HD 87669	151.65651379	+06.90554668	8.195 \pm 0.014	0.019 \pm 0.002	6.43 \pm 0.90	92.55	-72.35	8.257	198
HD 88134	152.53131437	+16.51662479	8.316 \pm 0.015	0.112 \pm 0.016	6.63 \pm 0.78	23.90	-45.13	21.617	212
HD 88654	153.318444818	-08.44555205	7.688 \pm 0.012	0.112 \pm 0.011	10.63 \pm 0.76	22.99	-30.30	-6.933	226
HD 89391	154.60461607	-26.50034192	7.946 \pm 0.013	0.156 \pm 0.056	9.31 \pm 0.81	37.99	-41.36	29.603	226
HD 90043	155.86820800	-00.90224700	6.448 \pm 0.011	0.031 \pm 0.022	12.91 \pm 0.38	66.21	-34.92	7.088	207
HD 90792	157.19297727	-14.46565080	8.179 \pm 0.014	0.156 \pm 0.016	5.54 \pm 0.78	-33.28	-7.73	32.556	220
HD 93396	161.70725271	-09.39902416	8.045 \pm 0.014	0.119 \pm 0.012	9.76 \pm 0.85	-78.30	-77.61	34.959	226
HD 93461	161.83994926	-01.72491378	8.271 \pm 0.015	0.019 \pm 0.002	7.62 \pm 0.96	5.95	-18.66	13.093	245
HD 93864	162.49379759	-07.48241297	8.010 \pm 0.013	0.123 \pm 0.012	9.20 \pm 0.75	-155.71	-38.17	15.935	236
HD 94834	164.31297046	+24.14278282	7.616 \pm 0.013	0.048 \pm 0.046	10.88 \pm 0.64	-73.37	36.90	2.813	195
HD 95089	164.69890121	+01.72921549	7.953 \pm 0.014	0.019 \pm 0.002	7.19 \pm 0.83	-35.31	-47.27	8.081	231
HD 95526	165.53574128	+43.72111110	8.328 \pm 0.015	0.082 \pm 0.059	6.73 \pm 0.97	-122.11	-102.40	22.059	214
HD 96063	166.18522764	-02.51321852	8.261 \pm 0.018	0.019 \pm 0.002	6.33 \pm 0.82	27.69	-17.60	-1.373	246
HD 96683	166.99633928	-23.85846670	8.211 \pm 0.012	0.152 \pm 0.015	6.11 \pm 0.86	-32.03	-1.92	17.922	199
HD 97601	168.63913911	+52.94690305	7.454 \pm 0.011	0.001 \pm 0.000	8.90 \pm 0.75	32.88	-29.95	-62.000	231
HD 98219	169.44813718	-23.97541613	8.040 \pm 0.012	0.139 \pm 0.014	7.45 \pm 0.67	-131.02	-16.91	-10.458	220
HD 99706	172.12589042	+43.96658060	7.644 \pm 0.013	0.082 \pm 0.059	7.76 \pm 0.68	45.57	-86.89	-30.256	210
HD 100337	173.26720547	+39.32167273	7.937 \pm 0.013	0.082 \pm 0.059	6.40 \pm 0.76	38.42	-1.58	-30.480	217
HD 102329	176.69435490	+03.47429342	7.893 \pm 0.015	0.065 \pm 0.023	6.33 \pm 0.83	-45.38	-18.46	14.580	197
HD 102444	176.88109122	-05.26361962	7.960 \pm 0.012	0.019 \pm 0.002	9.19 \pm 0.90	-26.41	-38.70	23.056	243
HD 102956	177.84380061	+57.64073508	7.858 \pm 0.011	0.001 \pm 0.000	7.92 \pm 0.83	-10.82	-17.14	-26.025	205
HD 103616	178.96409204	-21.65943614	7.681 \pm 0.013	0.201 \pm 0.010	9.72 \pm 0.77	-34.55	-133.19	8.000	226
HD 104017	179.68829140	+37.87721968	7.843 \pm 0.012	0.080 \pm 0.057	9.16 \pm 0.87	-4.92	26.10	-4.577	156
HD 106270	183.40535538	-09.51338029	7.586 \pm 0.012	0.019 \pm 0.002	11.78 \pm 0.79	-99.69	-41.86	24.331	244
HD 106279	183.39435584	+30.56245543	8.366 \pm 0.014	0.054 \pm 0.027	4.68 \pm 0.84	1.42	-17.58	-45.801	228

Table 1 continued on next page

Table 1 (*continued*)

Star	α (J2000.0)	δ (J2000.0)	V	A_V	π (mas)	μ_α (mas yr $^{-1}$)	μ_δ (mas yr $^{-1}$)	RV (km s $^{-1}$)	S/N
HD 107990	186.13579644	+04.33117025	7.955 \pm 0.013	0.099 \pm 0.039	3.54 \pm 0.85	30.37	-22.81	-6.554	230
HD 108189	186.41909600	-00.28217500	7.729 \pm 0.013	0.099 \pm 0.039	6.46 \pm 0.66	-81.65	26.97	-3.686	247
HD 108863	187.58296070	+21.94824495	7.746 \pm 0.013	0.059 \pm 0.021	7.18 \pm 0.78	-73.83	-33.29	-27.984	202
HD 109159	188.17178904	-17.22067971	7.975 \pm 0.013	0.174 \pm 0.009	9.86 \pm 0.66	-110.26	13.97	9.348	242
HD 109218	188.28502907	+01.04399524	8.109 \pm 0.016	0.037 \pm 0.014	10.52 \pm 0.67	-98.57	-52.35	18.423	239
HD 109929	189.60618423	+14.87241216	7.654 \pm 0.013	0.013 \pm 0.005	12.84 \pm 0.56	-38.91	-7.44	-10.706	275
HD 112115	193.48092215	+24.63589363	8.143 \pm 0.014	0.094 \pm 0.009	3.08 \pm 0.80	-37.87	-14.53	3.973	142
HD 112973	195.03118430	+34.91935057	7.626 \pm 0.012	0.024 \pm 0.003	8.44 \pm 0.74	-77.00	1.51	-34.986	219
HD 112988	195.04286438	+34.99841754	7.772 \pm 0.012	0.032 \pm 0.004	7.80 \pm 0.75	-78.70	1.88	-32.842	228
HD 114161	197.24014828	-13.44118482	8.047 \pm 0.015	0.174 \pm 0.009	5.49 \pm 0.82	-37.20	-5.96	-7.180	192
HD 114659	197.95297265	+12.73043994	8.306 \pm 0.016	0.094 \pm 0.009	4.84 \pm 0.95	-5.20	-7.89	-1.322	179
HD 116029	200.16476095	+24.64869668	7.878 \pm 0.011	0.081 \pm 0.081	8.12 \pm 0.65	-13.30	-52.49	-6.923	172
HD 117623	202.47027856	+64.18050702	7.046 \pm 0.011	0.001 \pm 0.000	4.95 \pm 0.53	-42.67	-6.00	-6.631	240
HD 117762	203.07305100	+06.35363375	7.920 \pm 0.013	0.079 \pm 0.008	6.81 \pm 0.69	-40.76	80.45	-26.104	256
HD 118082	203.67496352	-09.10676347	8.038 \pm 0.014	0.174 \pm 0.009	6.94 \pm 0.72	8.91	-6.93	-26.805	207
HD 118744	204.68050952	+09.98081992	7.859 \pm 0.013	0.034 \pm 0.005	5.52 \pm 0.72	7.03	1.11	-0.025	203
HD 120531	207.37374736	+30.72079905	7.967 \pm 0.012	0.100 \pm 0.073	7.81 \pm 0.64	-19.33	15.17	24.663	247
HD 122253	209.92300367	+42.04980641	7.801 \pm 0.012	0.087 \pm 0.087	9.88 \pm 0.56	5.55	28.67	-9.990	241
HD 123239	211.68781193	-14.09526636	8.407 \pm 0.017	0.339 \pm 0.034	5.15 \pm 0.83	8.23	25.08	41.990	227
HD 124641	213.44852868	+41.18759190	8.049 \pm 0.012	0.100 \pm 0.100	5.92 \pm 0.76	-8.13	4.63	11.842	201
HD 125217	214.60943928	-19.56242033	8.314 \pm 0.015	0.312 \pm 0.031	6.13 \pm 0.93	-18.93	-18.78	-6.304	193
HD 125390	214.53883030	+38.96697805	8.213 \pm 0.012	0.100 \pm 0.100	5.15 \pm 0.82	-13.22	-16.17	-76.758	225
HD 125607	214.86337106	+37.60996555	8.100 \pm 0.012	0.100 \pm 0.100	7.52 \pm 0.87	-47.62	-33.70	-39.000	222
HD 126991	217.06688240	+24.51754394	7.938 \pm 0.013	0.100 \pm 0.073	9.91 \pm 0.71	-231.51	121.48	-94.578	239
HD 127374	217.82732826	-11.87017594	8.397 \pm 0.015	0.297 \pm 0.030	6.69 \pm 0.92	-30.91	-14.22	-35.966	226
HD 128095	218.57238375	+28.48599918	8.139 \pm 0.012	0.100 \pm 0.073	8.37 \pm 0.83	49.09	-107.70	28.952	215
HD 128720	219.52401938	+12.80361485	8.317 \pm 0.019	0.087 \pm 0.087	7.56 \pm 1.28	17.22	-70.33	16.832	199
HD 131496	223.34595295	+18.23540451	7.806 \pm 0.012	0.073 \pm 0.073	9.09 \pm 0.78	44.46	-35.08	1.146	196
HD 136418	229.77575899	+41.73320606	7.886 \pm 0.012	0.129 \pm 0.004	10.18 \pm 0.58	-19.66	-181.92	-34.407	208

Table 1 continued on next page

Table 1 (*continued*)

Star	α (J2000.0)	δ (J2000.0)	V	A_V	π (mas)	μ_α (mas yr $^{-1}$)	μ_δ (mas yr $^{-1}$)	RV	S/N
HD 136513	230.21645277	+07.68271400	8.252 \pm 0.014	0.053 \pm 0.002	5.88 \pm 0.85	-47.81	-13.38	-59.606	222
HD 140025	234.93843043	+44.31118878	8.231 \pm 0.013	0.132 \pm 0.004	8.61 \pm 0.57	1.56	-60.42	30.158	223
HD 141712	237.05581068	+50.95455308	8.378 \pm 0.014	0.132 \pm 0.004	5.61 \pm 0.66	-16.45	-24.21	-23.235	228
HD 142091	237.80804694	+35.65737975	4.803 \pm 0.010	0.034 \pm 0.001	32.79 \pm 0.21	-8.55	-348.44	-25.107	194
HD 142245	238.23450511	+15.43070731	7.458 \pm 0.013	0.053 \pm 0.002	9.13 \pm 0.62	-55.58	-20.82	6.708	168
HD 144363	241.43641272	-07.08485533	8.248 \pm 0.013	0.286 \pm 0.220	7.07 \pm 0.99	2.35	21.79	6.500	221
HD 145428	242.96355647	-25.88357239	7.754 \pm 0.012	0.568 \pm 0.210	7.62 \pm 0.81	-128.94	-58.98	-1.100	235
HD 146278	243.46435843	+40.34880889	7.987 \pm 0.013	0.132 \pm 0.004	6.06 \pm 0.57	-25.59	-99.56	11.352	199
HD 150331	250.43939338	-33.14576125	5.846 \pm 0.011	0.276 \pm 0.105	11.51 \pm 0.42	-58.47	-57.57	-6.637	284
HD 152581	253.43159405	+11.97374506	8.354 \pm 0.013	0.069 \pm 0.069	5.39 \pm 0.96	11.49	-15.79	3.739	246
HD 152733	253.23839725	+44.40240031	8.105 \pm 0.014	0.102 \pm 0.028	6.92 \pm 0.49	-9.53	69.38	-27.517	191
HD 155413	257.99431423	-14.62037900	7.267 \pm 0.012	0.225 \pm 0.092	12.30 \pm 0.69	-16.13	-39.92	-23.274	281
HD 158038	261.43928820	+27.30334069	7.471 \pm 0.011	0.115 \pm 0.006	9.65 \pm 0.74	48.35	-59.04	19.632	139
HD 158449	262.28977625	+06.14846658	8.035 \pm 0.013	0.527 \pm 0.153	6.31 \pm 0.81	-19.52	23.16	-26.926	215
HD 160215	264.13206977	+44.72336309	8.160 \pm 0.013	0.101 \pm 0.028	9.08 \pm 0.60	-55.37	56.25	-59.230	201
HD 163528	268.50302932	+49.79514098	8.353 \pm 0.015	0.102 \pm 0.004	5.34 \pm 0.57	-0.19	30.06	-65.155	203
HD 166494	271.87260166	+56.80190136	7.686 \pm 0.012	0.028 \pm 0.009	8.72 \pm 0.45	22.36	64.09	-30.304	220
HD 167042	272.63183367	+54.28655340	5.977 \pm 0.010	0.012 \pm 0.004	19.91 \pm 0.26	107.94	247.35	-18.181	235
HD 171264	278.41951987	+04.59237354	8.106 \pm 0.013	0.397 \pm 0.167	8.34 \pm 0.75	19.27	-3.97	11.300	246
HD 175541	283.92035082	+04.26532615	8.013 \pm 0.014	0.321 \pm 0.096	7.87 \pm 0.95	-6.82	-89.23	19.674	282
HD 178251	287.23442012	-28.74104258	8.001 \pm 0.013	0.316 \pm 0.101	6.67 \pm 0.96	46.27	-80.26	91.769	259
HD 180053	288.40089062	+34.91454362	7.942 \pm 0.013	0.116 \pm 0.002	7.92 \pm 0.54	-9.65	29.34	-5.874	207
HD 180902	289.82378283	-23.55815627	7.786 \pm 0.014	0.252 \pm 0.081	9.13 \pm 0.86	33.18	-20.50	-4.651	218
HD 181342	290.26762895	-23.61957022	7.557 \pm 0.013	0.254 \pm 0.081	9.04 \pm 0.61	-45.87	-30.58	-0.837	194
HD 183473	291.98849995	+42.77663779	7.887 \pm 0.012	0.050 \pm 0.047	9.14 \pm 0.51	71.49	155.17	-46.421	239
HD 185269	294.29892048	+28.49986264	6.679 \pm 0.011	0.088 \pm 0.033	19.89 \pm 0.56	-32.03	-81.18	0.620	233
HD 185351	294.15823711	+44.69493494	5.176 \pm 0.010	0.019 \pm 0.018	24.49 \pm 0.22	-94.81	-104.25	-5.900	250
HD 185351	294.15823711	+44.69493494	5.176 \pm 0.010	0.019 \pm 0.018	24.49 \pm 0.22	-94.81	-104.25	-5.900	243
HD 185351	294.15823711	+44.69493494	5.176 \pm 0.010	0.019 \pm 0.018	24.49 \pm 0.22	-94.81	-104.25	-5.900	236

Table 1 continued on next page

Table 1 (*continued*)

Star	α (J2000.0)	δ (J2000.0)	V	A_V	π (mas)	μ_α (mas yr $^{-1}$)	μ_δ (mas yr $^{-1}$)	RV	S/N
HD 187460	297.26244145	+29.88285283	8.350 \pm 0.013	0.303 \pm 0.112	5.66 \pm 0.90	-3.62	-1.13	-6.100	161
HD 188386	298.69910343	+05.70285399	8.180 \pm 0.012	0.238 \pm 0.057	6.97 \pm 1.04	14.84	3.86	-73.744	231
HD 192153	303.49872720	-17.67615463	8.286 \pm 0.016	0.327 \pm 0.150	9.03 \pm 0.94	105.82	-9.15	-37.994	244
HD 192699	304.02502117	+04.58079271	6.454 \pm 0.011	0.040 \pm 0.009	15.24 \pm 0.57	-39.24	-52.15	13.050	259
HD 193342	304.25226885	+56.90458900	8.086 \pm 0.013	0.683 \pm 0.355	5.69 \pm 0.46	-36.19	-54.81	-24.246	213
HD 193391	304.90545561	+13.01077579	8.232 \pm 0.015	0.091 \pm 0.002	7.59 \pm 1.15	10.75	-12.86	-41.912	196
HD 194541	306.26683336	+32.46851434	7.514 \pm 0.011	0.250 \pm 0.090	8.65 \pm 0.57	30.38	-6.64	-20.453	191
HD 195787	307.64394878	+58.28723746	7.630 \pm 0.012	0.484 \pm 0.252	8.36 \pm 0.77	-29.14	-112.57	-10.278	235
HD 195824	308.40476843	+01.26925199	8.048 \pm 0.014	0.072 \pm 0.016	8.47 \pm 1.03	33.24	1.88	7.740	236
HD 196645	309.58717207	+13.33140947	7.805 \pm 0.014	0.058 \pm 0.013	10.61 \pm 0.77	117.79	90.93	-33.297	251
HD 197162	310.15383860	+37.39745221	8.019 \pm 0.012	0.335 \pm 0.120	6.40 \pm 0.60	85.80	-2.42	-139.688	233
HD 198599	312.94706285	-10.31726086	7.492 \pm 0.012	0.149 \pm 0.024	2.09 \pm 0.89	0.53	-1.85	20.713	220
HD 200081	315.34339842	-02.51400509	7.966 \pm 0.013	0.159 \pm 0.035	3.93 \pm 0.65	0.82	-11.03	7.670	224
HD 200491	315.73292717	+28.98485993	7.735 \pm 0.012	0.186 \pm 0.084	6.46 \pm 0.75	7.05	-6.96	-7.484	188
HD 200964	316.66600997	+03.80311890	6.494 \pm 0.011	0.044 \pm 0.010	13.85 \pm 0.52	94.99	50.47	-71.884	212
HD 202696	319.22480389	+27.25812220	8.225 \pm 0.014	0.082 \pm 0.018	7.52 \pm 0.99	45.98	36.04	-34.433	200
HD 202867	319.68879093	-02.13688563	8.129 \pm 0.016	0.128 \pm 0.021	8.06 \pm 0.96	-21.57	-18.81	14.212	235
HD 203471	320.39329902	+28.56467913	8.347 \pm 0.015	0.184 \pm 0.083	6.52 \pm 0.96	-39.31	-69.50	23.620	222
HD 205163	323.41424732	-06.37384661	8.218 \pm 0.016	0.149 \pm 0.024	4.35 \pm 1.05	-7.88	-25.04	50.098	197
HD 206610	325.85375016	-07.40825239	8.352 \pm 0.015	0.149 \pm 0.024	5.16 \pm 0.95	2.35	2.34	-18.658	158
HD 206635	325.85558305	+01.80091007	8.306 \pm 0.015	0.126 \pm 0.020	8.34 \pm 0.79	147.42	-27.12	-40.357	225
HD 207077	326.68352806	-08.00718390	8.278 \pm 0.015	0.135 \pm 0.022	7.33 \pm 0.93	18.56	-40.75	-20.370	220
HD 208585	329.22168900	+17.43978357	8.004 \pm 0.013	0.089 \pm 0.020	6.88 \pm 0.92	-15.04	-2.33	-26.979	223
HD 210011	331.30785945	+63.57841729	6.944 \pm 0.011	0.459 \pm 0.124	5.23 \pm 0.48	22.81	1.31	-10.319	235
HD 210521	332.84335013	-22.20867611	8.113 \pm 0.014	0.171 \pm 0.010	6.07 \pm 0.69	-7.44	-3.91	-13.818	252
HD 210702	332.96387858	+16.04055286	5.937 \pm 0.010	0.046 \pm 0.033	18.20 \pm 0.39	-3.15	-18.02	16.340	231
HD 212771	336.76279598	-17.26365469	7.603 \pm 0.015	0.161 \pm 0.010	7.63 \pm 0.80	-87.59	-103.17	14.863	246
HD 213278	337.61609827	-04.81656969	8.081 \pm 0.013	0.070 \pm 0.018	7.44 \pm 1.04	96.87	50.88	-53.476	240
HD 215049	340.71769137	-27.88689167	8.280 \pm 0.015	0.099 \pm 0.013	8.90 \pm 0.89	72.47	-60.74	-29.844	232

Table 1 continued on next page

Table 1 (*continued*)

Star	α (J2000.0)	δ (J2000.0)	V	A_V	π (mas)	μ_α (mas yr $^{-1}$)	μ_δ (mas yr $^{-1}$)	RV (km s $^{-1}$)	S/N
HD 215549	341.39361744	+30.44255608	6.397 \pm 0.011	0.034 \pm 0.018	16.67 \pm 0.60	-251.54	-349.76	-1.590	233
HD 215908	341.95126700	+49.17859778	8.031 \pm 0.013	0.275 \pm 0.096	6.26 \pm 0.72	0.86	5.22	6.348	247
HD 216834	344.08517871	-06.54583717	8.133 \pm 0.013	0.070 \pm 0.018	6.09 \pm 0.95	-1.13	-18.21	-32.615	239
HD 217496	345.28274861	-09.55391710	7.863 \pm 0.012	0.070 \pm 0.018	8.76 \pm 1.06	-24.68	-90.42	-2.206	234
HD 217591	345.47622512	-05.96628891	7.875 \pm 0.014	0.070 \pm 0.018	8.04 \pm 0.75	23.11	-32.88	-9.106	194
HD 217681	345.63288706	-11.26569736	7.760 \pm 0.012	0.147 \pm 0.009	9.21 \pm 1.03	-65.92	-16.46	-0.257	191
HD 219553	349.20710502	-21.20309181	7.261 \pm 0.011	0.099 \pm 0.040	11.35 \pm 0.93	20.90	-49.30	3.458	170
HD 220122	350.30717859	-12.82986877	8.406 \pm 0.020	0.100 \pm 0.015	3.76 \pm 1.35	-14.59	-4.80	-46.327	227
HD 220952	351.99218978	+23.58672686	7.853 \pm 0.013	0.145 \pm 0.026	7.99 \pm 0.52	80.12	27.95	-15.604	233
HD 221504	353.21108334	-21.68768845	8.086 \pm 0.014	0.099 \pm 0.040	10.49 \pm 0.75	23.56	-8.99	-1.391	219
HD 222112	354.47039864	-05.97836440	8.400 \pm 0.017	0.100 \pm 0.015	6.07 \pm 1.18	43.82	-54.34	-12.685	143
HD 223627	357.79449152	+44.54770122	8.215 \pm 0.013	0.213 \pm 0.128	6.29 \pm 0.96	23.74	-39.09	-52.620	198
HD 224032	358.65154469	+05.05659038	8.232 \pm 0.014	0.070 \pm 0.018	9.12 \pm 0.96	116.64	-55.58	0.000	224
HD 224679	359.95462711	-02.11260592	8.360 \pm 0.014	0.099 \pm 0.035	4.76 \pm 0.82	79.47	-21.95	-17.394	236
HD 225021	000.66702757	+51.47240100	7.707 \pm 0.011	0.146 \pm 0.020	6.96 \pm 0.78	42.11	-4.88	-6.225	201
HD 236427	007.47524003	+59.25486282	8.253 \pm 0.012	0.305 \pm 0.098	9.16 \pm 0.75	-1.16	-71.28	-12.479	216
HIP 43212	132.04376862	+15.11066823	8.352 \pm 0.015	0.169 \pm 0.132	3.83 \pm 1.18	-8.59	-3.84	2.819	211
HIP 87123	267.00448087	+32.65584898	8.359 \pm 0.014	0.150 \pm 0.007	7.09 \pm 0.62	-27.79	20.17	-66.098	193

Table 2. List of Fe I and Fe II lines.

λ	Ion ^a	χ	$\log gf$	$\log \Gamma_w^b$	EW_{\odot}
(Å)		(eV)		$(4\pi s N_H)^{-1}$	(mÅ)
5023.185	26.0	4.283	-1.524	-7.135	37.9
5025.303	26.0	4.284	-1.919	-7.140	20.6
5044.211	26.0	2.851	-2.206	-7.280	72.3
5054.642	26.0	3.640	-2.087	-7.599	38.3
5058.496	26.0	3.642	-2.809	-7.599	12.1
5067.149	26.0	4.220	-1.068	-7.187	65.3
5109.651	26.0	4.301	-0.853	-7.150	74.2
5159.057	26.0	4.283	-0.932	-7.175	70.1
5196.059	26.0	4.256	-0.732	-7.510	74.8
5197.935	26.0	4.301	-1.608	-7.175	33.2
5213.806	26.0	3.943	-2.802	-7.253	7.0
5225.526	26.0	0.110	-4.845	-7.820	72.1
5228.375	26.0	4.220	-1.169	-7.233	59.0
5243.777	26.0	4.256	-1.095	-7.215	62.0

Table 2 continued on next page

Table 2 (*continued*)

λ	Ion ^a	χ	$\log gf$	$\log \Gamma_w^b$	EW_{\odot}
(Å)		(eV)		$(4\pi s N_H)^{-1}$	(mÅ)
5247.050	26.0	0.087	-4.994	-7.822	66.9
5250.209	26.0	0.121	-4.959	-7.820	67.0
5253.020	26.0	2.279	-3.975	-7.570	16.6
5288.525	26.0	3.695	-1.452	-7.596	65.4
5294.547	26.0	3.640	-2.694	-7.538	15.4
5295.312	26.0	4.415	-1.595	-7.135	29.2
5322.040	26.0	2.279	-2.956	-7.600	60.7
5373.708	26.0	4.473	-0.952	-7.123	60.2
5376.830	26.0	4.295	-2.094	-7.529	14.8
5379.573	26.0	3.695	-1.555	-7.575	61.3
5386.333	26.0	4.154	-1.797	-7.172	31.4
5386.960	26.0	3.642	-2.504	-7.780	21.5
5389.478	26.0	4.415	-0.619	-7.159	83.9
5398.279	26.0	4.446	-0.788	-7.144	71.7
5401.266	26.0	4.320	-1.823	-7.219	23.5
5406.774	26.0	4.371	-1.496	-7.189	35.7
5417.033	26.0	4.415	-1.478	-7.166	34.8

Table 2 continued on next page

Table 2 (*continued*)

λ (Å)	Ion ^a	χ	$\log gf$	$\log \Gamma_w^b$ $(4\pi s N_H)^{-1}$	EW $_{\odot}$ (mÅ)
5432.948	26.0	4.446	-0.808	-7.153	70.4
5441.339	26.0	4.312	-1.683	-7.234	29.7
5464.279	26.0	4.143	-1.629	-7.770	37.7
5466.396	26.0	4.371	-0.721	-7.204	79.0
5466.987	26.0	3.573	-2.237	-7.820	35.2
5473.162	26.0	4.191	-2.072	-7.173	18.9
5491.832	26.0	4.186	-2.258	-7.700	13.3
5522.446	26.0	4.209	-1.488	-7.257	43.5
5539.280	26.0	3.642	-2.612	-7.554	18.2
5543.935	26.0	4.218	-1.237	-7.263	56.7
5546.505	26.0	4.371	-1.210	-7.224	50.7
5546.990	26.0	4.218	-1.812	-7.263	28.1
5560.211	26.0	4.435	-1.126	-7.189	52.1
5587.574	26.0	4.143	-1.684	-7.800	35.5
5618.632	26.0	4.209	-1.359	-7.264	50.4
5619.595	26.0	4.386	-1.503	-7.233	34.9
5633.946	26.0	4.991	-0.225	-7.337	73.2

Table 2 continued on next page

Table 2 (*continued*)

λ	Ion ^a	χ	$\log gf$	$\log \Gamma_w^b$	EW_\odot
(Å)		(eV)		$(4\pi s N_H)^{-1}$	(mÅ)
5636.695	26.0	3.640	-2.570	-7.581	19.8
5638.262	26.0	4.220	-0.869	-7.269	77.6
5641.434	26.0	4.256	-1.039	-7.264	65.8
5646.684	26.0	4.261	-2.482	-7.480	7.5
5651.468	26.0	4.473	-1.819	-7.187	18.6
5652.317	26.0	4.261	-1.829	-7.251	25.6
5661.344	26.0	4.284	-1.906	-7.244	21.8
5667.518	26.0	4.178	-1.407	-7.530	47.6
5677.684	26.0	4.103	-2.676	-7.268	6.9
5679.023	26.0	4.652	-0.827	-7.099	59.5
5680.240	26.0	4.186	-2.379	-7.660	10.7
5696.088	26.0	4.549	-1.937	-7.156	13.1
5701.543	26.0	2.559	-2.243	-7.576	84.3
5705.464	26.0	4.301	-1.502	-7.260	39.0
5731.761	26.0	4.256	-1.194	-7.271	57.2
5738.227	26.0	4.220	-2.231	-7.220	13.6
5741.847	26.0	4.256	-1.690	-7.272	32.1

Table 2 continued on next page

Table 2 (*continued*)

λ	Ion ^a	χ	$\log gf$	$\log \Gamma_w^b$	EW_{\odot}
(Å)		(eV)		$(4\pi s N_H)^{-1}$	(mÅ)
5752.031	26.0	4.549	-0.913	-7.510	54.5
5760.344	26.0	3.642	-2.549	-7.549	20.7
5775.080	26.0	4.220	-1.171	-7.530	57.0
5778.453	26.0	2.588	-3.535	-7.576	22.2
5784.658	26.0	3.397	-2.634	-7.234	27.1
5793.914	26.0	4.220	-1.677	-7.278	34.5
5806.725	26.0	4.608	-0.944	-7.148	54.4
5809.217	26.0	3.884	-1.712	-7.154	50.0
5811.914	26.0	4.143	-2.398	-7.800	11.2
5814.807	26.0	4.283	-1.881	-7.272	23.0
5815.217	26.0	4.154	-2.441	-7.271	10.2
5827.877	26.0	3.283	-3.266	-7.261	10.5
5848.126	26.0	4.608	-1.158	-7.520	40.1
5849.683	26.0	3.695	-3.015	-7.567	7.7
5852.218	26.0	4.549	-1.248	-7.188	40.6
5853.148	26.0	1.485	-5.157	-7.790	8.1
5855.075	26.0	4.608	-1.595	-7.158	22.4

Table 2 continued on next page

Table 2 (*continued*)

λ	Ion ^a	χ	$\log gf$	$\log \Gamma_w^b$	EW_{\odot}
(Å)		(eV)		$(4\pi s N_H)^{-1}$	(mÅ)
5856.088	26.0	4.295	-1.598	-7.532	33.8
5859.586	26.0	4.549	-0.578	-7.510	71.3
5862.356	26.0	4.549	-0.304	-7.520	86.2
5905.671	26.0	4.652	-0.841	-7.144	58.3
5916.247	26.0	2.454	-2.960	-7.601	54.9
5927.788	26.0	4.652	-1.128	-7.148	42.4
5929.677	26.0	4.549	-1.262	-7.204	40.1
5930.180	26.0	4.652	-0.386	-7.149	88.3
5934.654	26.0	3.929	-1.244	-7.153	75.8
5956.693	26.0	0.859	-4.639	-7.780	50.8
5983.680	26.0	4.549	-0.648	-7.510	68.3
5984.815	26.0	4.733	-0.262	-7.420	82.0
5987.065	26.0	4.795	-0.465	-7.420	66.8
6003.011	26.0	3.882	-1.195	-7.181	81.2
6005.541	26.0	2.588	-3.522	-7.750	23.0
6008.556	26.0	3.884	-0.918	-7.540	87.9
6012.209	26.0	2.223	-3.862	-7.649	23.9

Table 2 continued on next page

Table 2 (*continued*)

λ	Ion ^a	χ	$\log gf$	$\log \Gamma_w^b$	EW_{\odot}
(Å)		(eV)		$(4\pi s N_H)^{-1}$	(mÅ)
6034.035	26.0	4.312	-2.369	-7.279	8.8
6035.337	26.0	4.295	-2.551	-7.502	6.2
6054.073	26.0	4.371	-2.263	-7.270	9.8
6056.004	26.0	4.733	-0.558	-7.130	72.2
6078.491	26.0	4.795	-0.292	-7.410	77.0
6079.009	26.0	4.652	-1.064	-7.177	45.7
6082.710	26.0	2.223	-3.622	-7.654	34.3
6085.257	26.0	2.759	-2.908	-7.601	43.2
6093.642	26.0	4.608	-1.402	-7.202	30.8
6096.664	26.0	3.984	-1.861	-7.152	37.8
6098.243	26.0	4.559	-1.825	-7.238	16.3
6127.906	26.0	4.143	-1.503	-7.790	44.4
6136.993	26.0	2.198	-3.037	-7.691	64.1
6151.617	26.0	2.176	-3.357	-7.696	49.8
6157.727	26.0	4.076	-1.257	-7.790	58.9
6159.378	26.0	4.608	-1.910	-7.216	12.7
6165.359	26.0	4.143	-1.487	-7.780	45.3

Table 2 continued on next page

Table 2 (*continued*)

λ	Ion ^a	χ	$\log gf$	$\log \Gamma_w^b$	EW_{\odot}
(Å)		(eV)		$(4\pi s N_H)^{-1}$	(mÅ)
6173.334	26.0	2.223	-2.938	-7.690	67.9
6187.989	26.0	3.943	-1.724	-7.179	47.3
6200.312	26.0	2.608	-2.457	-7.589	73.1
6213.429	26.0	2.223	-2.650	-7.691	82.4
6219.280	26.0	2.198	-2.549	-7.694	89.1
6220.779	26.0	3.882	-2.390	-7.208	19.2
6226.734	26.0	3.884	-2.143	-7.208	29.0
6232.640	26.0	3.654	-1.232	-7.540	83.7
6240.646	26.0	2.223	-3.337	-7.661	48.4
6265.132	26.0	2.176	-2.633	-7.700	85.8
6335.329	26.0	2.198	-2.423	-7.698	96.8
6380.743	26.0	4.186	-1.312	-7.790	51.8
6385.718	26.0	4.733	-1.887	-7.187	10.7
6392.537	26.0	2.279	-4.007	-7.643	17.5
6574.226	26.0	0.990	-5.019	-7.830	28.3
6591.312	26.0	4.593	-2.065	-7.697	9.8
6593.869	26.0	2.433	-2.461	-7.629	83.7

Table 2 continued on next page

Table 2 (*continued*)

λ	Ion ^a	χ	$\log gf$	$\log \Gamma_w^b$	EW_{\odot}
(Å)		(eV)		$(4\pi s N_H)^{-1}$	(mÅ)
6597.561	26.0	4.795	-0.984	-7.190	44.0
6608.025	26.0	2.279	-4.017	-7.648	17.5
6609.109	26.0	2.559	-2.708	-7.610	64.5
6625.021	26.0	1.011	-5.374	-7.830	14.9
6627.543	26.0	4.549	-1.542	-7.250	27.8
6646.930	26.0	2.608	-3.988	-7.604	9.9
6653.851	26.0	4.154	-2.475	-7.153	10.2
6699.141	26.0	4.593	-2.167	-7.667	8.0
6703.565	26.0	2.759	-3.078	-7.633	36.6
6710.318	26.0	1.485	-4.876	-7.733	15.6
6713.742	26.0	4.795	-1.485	-7.207	20.9
6725.355	26.0	4.103	-2.257	-7.181	17.3
6726.666	26.0	4.607	-1.062	-7.500	46.9
6732.064	26.0	4.584	-2.208	-7.700	7.5
6733.150	26.0	4.638	-1.490	-7.247	26.5
6739.520	26.0	1.557	-4.955	-7.726	11.7
6745.100	26.0	4.580	-2.164	-7.726	8.3

Table 2 continued on next page

Table 2 (*continued*)

λ	Ion ^a	χ	$\log gf$	$\log \Gamma_w^b$	EW_{\odot}
(Å)		(eV)		$(4\pi s N_H)^{-1}$	(mÅ)
6745.955	26.0	4.076	-2.709	-7.820	7.3
6750.151	26.0	2.424	-2.672	-7.609	73.6
6752.707	26.0	4.638	-1.285	-7.249	36.1
6806.842	26.0	2.728	-3.153	-7.643	34.7
6839.830	26.0	2.559	-3.433	-7.617	29.7
6842.685	26.0	4.638	-1.245	-7.189	38.5
6857.249	26.0	4.076	-2.125	-7.820	22.2
6861.937	26.0	2.424	-3.852	-7.637	18.7
5100.655	26.1	2.807	-4.212	-7.892	20.4
5132.661	26.1	2.807	-4.088	-7.894	24.8
5197.568	26.1	3.231	-2.497	-7.880	80.0
5234.623	26.1	3.221	-2.357	-7.880	82.8
5264.802	26.1	3.231	-3.185	-7.875	45.5
5284.103	26.1	2.891	-3.237	-7.887	57.3
5325.552	26.1	3.221	-3.246	-7.883	43.1
5414.070	26.1	3.221	-3.647	-7.878	27.0
5425.248	26.1	3.200	-3.304	-7.886	41.7

Table 2 continued on next page

Table 2 (*continued*)

λ (Å)	Ion ^a (eV)	χ	$\log gf$	$\log \Gamma_w^b$ ($4\pi s N_H$) $^{-1}$	EW $_{\odot}$ (mÅ)
5534.838	26.1	3.245	-2.986	-7.883	57.9
5991.371	26.1	3.153	-3.609	-7.895	31.3
6084.102	26.1	3.199	-3.840	-7.892	21.3
6113.319	26.1	3.221	-4.155	-7.893	11.9
6149.246	26.1	3.889	-2.789	-7.870	36.4
6238.386	26.1	3.889	-2.634	-7.870	43.0
6247.557	26.1	3.892	-2.427	-7.870	52.1
6369.459	26.1	2.891	-4.203	-7.899	19.0
6416.919	26.1	3.892	-2.754	-7.873	39.8

^aFe I and Fe II ions are represented by the notations 26.0 and 26.1, following the format used by MOOG.

^b $\log \Gamma_w$ is the logarithm of the van der Waals damping constant.

Table 3. Atmospheric Parameters.

Star	T_{eff}	$\log g$	[Fe/H]	ξ	σ	N	σ	N
	(K)			(km s $^{-1}$)	(Fe I)	(Fe II)	(Fe I)	(Fe II)
HD 1100	4808 ± 29	2.89 ± 0.17	-0.06 ± 0.02	1.165 ± 0.030	0.05	133	0.11	17
HD 1293	5160 ± 21	3.27 ± 0.06	-0.44 ± 0.01	0.990 ± 0.030	0.04	133	0.06	14
HD 1384	4875 ± 50	3.39 ± 0.18	0.31 ± 0.02	1.093 ± 0.060	0.10	136	0.10	11
HD 1502	4988 ± 22	3.21 ± 0.07	-0.00 ± 0.01	1.123 ± 0.030	0.05	137	0.05	15
HD 2946	5488 ± 15	3.64 ± 0.06	-0.23 ± 0.01	1.171 ± 0.020	0.03	138	0.06	15
HD 3458	5168 ± 25	2.90 ± 0.09	-0.04 ± 0.02	1.420 ± 0.030	0.05	140	0.06	14
HD 4313	4943 ± 29	3.26 ± 0.06	0.09 ± 0.02	1.104 ± 0.030	0.06	139	0.06	14
HD 4395	5610 ± 18	3.75 ± 0.07	-0.15 ± 0.01	1.218 ± 0.030	0.04	145	0.06	16
HD 4917	4794 ± 50	2.85 ± 0.17	0.08 ± 0.03	1.252 ± 0.040	0.08	137	0.10	16
HD 5891	4795 ± 22	2.50 ± 0.03	-0.35 ± 0.01	1.465 ± 0.030	0.05	133	0.06	16
HD 6019	5071 ± 21	3.09 ± 0.06	-0.48 ± 0.01	1.210 ± 0.030	0.04	146	0.05	16
HD 6030	4972 ± 25	3.27 ± 0.09	-0.02 ± 0.01	1.079 ± 0.030	0.05	136	0.08	17
HD 7530	5033 ± 18	3.24 ± 0.05	-0.33 ± 0.01	1.116 ± 0.020	0.04	138	0.03	12
HD 7931	4814 ± 29	3.07 ± 0.08	0.06 ± 0.02	1.100 ± 0.030	0.06	131	0.12	17
HD 7980	4750 ± 46	2.87 ± 0.20	0.06 ± 0.03	1.206 ± 0.040	0.08	139	0.13	17
HD 8375	5240 ± 11	3.60 ± 0.03	-0.03 ± 0.01	1.033 ± 0.020	0.03	134	0.05	16
HD 8407	4977 ± 18	3.05 ± 0.03	-0.25 ± 0.01	1.150 ± 0.020	0.04	138	0.07	16
HD 8508	4816 ± 26	2.57 ± 0.06	-0.28 ± 0.02	1.427 ± 0.030	0.06	138	0.11	15
HD 9156	5036 ± 18	2.80 ± 0.09	-0.09 ± 0.01	1.385 ± 0.030	0.05	143	0.09	17
HD 9218	4830 ± 25	2.91 ± 0.16	-0.14 ± 0.02	1.135 ± 0.030	0.05	135	0.08	16
HD 9313	4934 ± 29	3.28 ± 0.08	0.00 ± 0.02	0.915 ± 0.040	0.06	134	0.10	16
HD 9554	4813 ± 29	2.43 ± 0.14	-0.35 ± 0.02	1.432 ± 0.030	0.05	137	0.08	14
HD 9625	4964 ± 29	2.75 ± 0.11	-0.03 ± 0.02	1.345 ± 0.030	0.06	138	0.07	16
HD 10011	5115 ± 18	3.43 ± 0.08	-0.12 ± 0.01	1.092 ± 0.020	0.04	136	0.04	14
HD 10212	4929 ± 22	3.08 ± 0.05	-0.14 ± 0.01	1.070 ± 0.020	0.05	136	0.06	15
HD 10245	4671 ± 57	3.03 ± 0.13	0.17 ± 0.03	0.823 ± 0.070	0.11	132	0.11	8

Table 3 continued on next page

Table 3 (*continued*)

Star	T_{eff}	$\log g$	[Fe/H]	ξ	σ	N	σ	N
	(K)			(km s $^{-1}$)	(Fe I)	(Fe II)	(Fe I)	(Fe II)
HD 10383	4838 ± 43	3.14 ± 0.09	0.18 ± 0.03	1.141 ± 0.050	0.09	139	0.10	16
HD 10479	4941 ± 25	2.54 ± 0.09	-0.29 ± 0.02	1.474 ± 0.030	0.05	140	0.08	17
HD 10823	5167 ± 18	3.46 ± 0.07	-0.17 ± 0.01	1.083 ± 0.020	0.04	138	0.07	17
HD 10909	4855 ± 25	3.11 ± 0.04	-0.45 ± 0.01	1.443 ± 0.030	0.05	135	0.11	15
HD 11288	5218 ± 15	3.35 ± 0.07	0.01 ± 0.01	1.300 ± 0.030	0.05	139	0.10	15
HD 11970	5154 ± 11	3.53 ± 0.03	-0.26 ± 0.01	1.037 ± 0.020	0.03	136	0.04	15
HD 12137	4947 ± 25	3.05 ± 0.04	0.02 ± 0.02	1.136 ± 0.030	0.05	135	0.09	17
HD 12164	5486 ± 15	3.60 ± 0.03	-0.11 ± 0.01	1.244 ± 0.020	0.03	138	0.05	16
HD 13167	5744 ± 25	3.78 ± 0.07	0.21 ± 0.01	1.358 ± 0.020	0.03	132	0.06	15
HD 14787	5004 ± 25	3.29 ± 0.15	-0.05 ± 0.02	1.071 ± 0.030	0.05	141	0.06	15
HD 15336	5122 ± 25	3.16 ± 0.06	-0.19 ± 0.01	0.910 ± 0.030	0.05	137	0.10	16
HD 15391	4930 ± 22	2.89 ± 0.16	-0.45 ± 0.02	1.256 ± 0.020	0.04	142	0.05	15
HD 15928	5389 ± 18	3.67 ± 0.07	-0.25 ± 0.01	1.134 ± 0.030	0.03	141	0.05	16
HD 16175	5960 ± 25	4.10 ± 0.06	0.31 ± 0.02	1.272 ± 0.030	0.04	134	0.06	15
HD 16178	4967 ± 29	2.72 ± 0.10	-0.09 ± 0.02	1.384 ± 0.030	0.06	137	0.05	15
HD 16984	4917 ± 22	3.12 ± 0.08	-0.16 ± 0.02	1.075 ± 0.030	0.05	135	0.07	16
HD 17311	5054 ± 22	3.41 ± 0.12	-0.09 ± 0.01	1.059 ± 0.030	0.05	139	0.04	15
HD 17620	5230 ± 18	3.51 ± 0.04	-0.16 ± 0.01	1.125 ± 0.020	0.04	139	0.07	16
HD 18015	5643 ± 15	3.63 ± 0.07	-0.14 ± 0.01	1.328 ± 0.030	0.04	137	0.06	16
HD 18645	5517 ± 30	3.50 ± 0.03	0.04 ± 0.02	1.468 ± 0.040	0.07	137	0.06	13
HD 18667	4928 ± 25	3.11 ± 0.06	-0.09 ± 0.01	1.126 ± 0.030	0.05	141	0.08	16
HD 18742	4997 ± 18	3.13 ± 0.03	-0.14 ± 0.01	1.150 ± 0.030	0.05	133	0.05	15
HD 19522	5570 ± 11	3.83 ± 0.07	-0.12 ± 0.01	1.137 ± 0.020	0.03	134	0.03	15
HD 19659	5745 ± 20	3.72 ± 0.08	0.09 ± 0.02	1.317 ± 0.030	0.04	139	0.07	15
HD 21340	4948 ± 25	3.07 ± 0.03	-0.09 ± 0.01	1.131 ± 0.030	0.05	137	0.08	17
HD 21449	4745 ± 42	2.54 ± 0.09	0.01 ± 0.03	1.400 ± 0.030	0.07	135	0.10	16
HD 21581	4918 ± 29	2.31 ± 0.13	-1.61 ± 0.03	1.596 ± 0.110	0.06	89	0.04	13
HD 22233	5174 ± 25	3.13 ± 0.07	-0.02 ± 0.01	1.244 ± 0.020	0.04	134	0.09	16
HD 22657	4828 ± 25	3.07 ± 0.06	-0.03 ± 0.01	1.121 ± 0.030	0.05	137	0.10	16

Table 3 continued on next page

Table 3 (*continued*)

Star	T_{eff}	$\log g$	[Fe/H]	ξ	σ	N	σ	N
	(K)			(km s $^{-1}$)	(Fe I)	(Fe II)	(Fe I)	(Fe II)
HD 22682	5055 ± 21	3.36 ± 0.13	-0.06 ± 0.01	1.059 ± 0.020	0.04	130	0.06	16
HD 22844	5265 ± 22	3.78 ± 0.06	0.21 ± 0.01	1.079 ± 0.030	0.05	137	0.07	16
HD 23134	4892 ± 26	3.17 ± 0.06	0.00 ± 0.02	1.041 ± 0.030	0.06	138	0.09	17
HD 23825	5640 ± 15	3.78 ± 0.06	0.13 ± 0.01	1.217 ± 0.030	0.04	141	0.06	15
HD 24148	4926 ± 25	3.10 ± 0.05	-0.10 ± 0.01	1.160 ± 0.030	0.05	135	0.06	15
HD 24316	4792 ± 26	2.87 ± 0.08	-0.12 ± 0.02	1.190 ± 0.030	0.06	138	0.11	17
HD 24365	5205 ± 15	3.62 ± 0.03	-0.25 ± 0.01	1.042 ± 0.020	0.03	137	0.03	17
HD 25622	5021 ± 25	3.12 ± 0.07	-0.06 ± 0.02	1.144 ± 0.030	0.05	140	0.07	16
HD 25975	4974 ± 39	3.37 ± 0.11	0.09 ± 0.02	1.034 ± 0.030	0.06	137	0.07	15
HD 26007	4830 ± 25	2.73 ± 0.06	-0.27 ± 0.01	1.239 ± 0.030	0.05	135	0.07	16
HD 26634	4943 ± 22	3.04 ± 0.05	-0.27 ± 0.01	1.158 ± 0.020	0.04	136	0.05	16
HD 27297	5174 ± 21	3.56 ± 0.06	-0.03 ± 0.01	1.021 ± 0.030	0.04	139	0.05	15
HD 27956	4885 ± 25	3.03 ± 0.05	-0.18 ± 0.01	1.131 ± 0.030	0.05	137	0.07	16
HD 28678	5091 ± 25	3.21 ± 0.13	-0.15 ± 0.02	1.188 ± 0.030	0.04	137	0.05	15
HD 28737	4736 ± 25	2.81 ± 0.14	-0.24 ± 0.02	1.121 ± 0.030	0.05	133	0.10	14
HD 30090	5365 ± 26	3.50 ± 0.05	-0.25 ± 0.02	0.788 ± 0.050	0.06	134	0.08	11
HD 30128	4981 ± 31	3.00 ± 0.06	0.15 ± 0.02	1.246 ± 0.030	0.07	136	0.11	17
HD 30166	4825 ± 36	2.86 ± 0.18	-0.10 ± 0.03	1.176 ± 0.030	0.06	135	0.10	17
HD 30856	4967 ± 25	3.17 ± 0.09	-0.11 ± 0.02	1.091 ± 0.030	0.05	138	0.07	16
HD 30882	4831 ± 33	2.91 ± 0.16	-0.14 ± 0.02	1.142 ± 0.030	0.05	134	0.09	17
HD 31018	5911 ± 22	3.91 ± 0.08	0.16 ± 0.01	1.428 ± 0.030	0.04	138	0.04	15
HD 31451	4975 ± 25	3.31 ± 0.06	-0.09 ± 0.01	1.053 ± 0.030	0.05	136	0.08	17
HD 31543	5637 ± 38	3.89 ± 0.16	0.06 ± 0.02	1.224 ± 0.060	0.08	128	0.11	9
HD 31693	4998 ± 29	3.28 ± 0.15	-0.05 ± 0.03	1.081 ± 0.030	0.06	141	0.07	15
HD 33142	5013 ± 22	3.37 ± 0.08	0.06 ± 0.01	1.018 ± 0.030	0.05	135	0.10	17
HD 33240	4785 ± 33	2.37 ± 0.08	-0.13 ± 0.02	1.468 ± 0.030	0.07	129	0.09	12
HD 33298	5413 ± 14	3.75 ± 0.04	-0.20 ± 0.01	1.138 ± 0.020	0.02	135	0.03	16
HD 33844	4833 ± 36	3.14 ± 0.07	0.18 ± 0.02	1.194 ± 0.040	0.08	135	0.11	15
HD 34538	4913 ± 20	3.08 ± 0.06	-0.28 ± 0.01	1.102 ± 0.020	0.04	138	0.06	14

Table 3 continued on next page

Table 3 (*continued*)

Star	T_{eff}	$\log g$	[Fe/H]	ξ	σ	N	σ	N
	(K)			(km s $^{-1}$)	(Fe I)	(Fe II)	(Fe I)	(Fe II)
HD 34909	5022 ± 22	3.13 ± 0.04	-0.02 ± 0.01	1.133 ± 0.020	0.04	133	0.08	17
HD 37445	4902 ± 29	2.62 ± 0.09	-0.14 ± 0.02	1.392 ± 0.030	0.06	140	0.08	15
HD 37601	4963 ± 22	3.24 ± 0.06	0.06 ± 0.01	1.098 ± 0.030	0.05	137	0.07	15
HD 38505	5001 ± 29	3.54 ± 0.06	0.12 ± 0.02	0.993 ± 0.040	0.06	132	0.08	14
HD 39142	4789 ± 26	2.50 ± 0.07	-0.16 ± 0.02	1.370 ± 0.030	0.06	138	0.09	16
HD 39731	5181 ± 25	3.03 ± 0.04	0.01 ± 0.01	1.354 ± 0.030	0.05	142	0.07	14
HD 39828	4931 ± 29	3.14 ± 0.06	0.04 ± 0.02	1.146 ± 0.030	0.06	133	0.09	17
HD 40537	5006 ± 18	3.49 ± 0.06	-0.16 ± 0.01	0.993 ± 0.030	0.04	136	0.09	16
HD 45210	5659 ± 26	3.59 ± 0.07	-0.09 ± 0.02	1.343 ± 0.040	0.05	140	0.06	13
HD 45410	4998 ± 18	3.22 ± 0.04	-0.08 ± 0.01	1.096 ± 0.020	0.04	134	0.07	16
HD 45506	5113 ± 18	3.31 ± 0.06	-0.01 ± 0.01	1.174 ± 0.020	0.04	135	0.07	16
HD 47562	5043 ± 25	3.12 ± 0.06	-0.30 ± 0.01	1.166 ± 0.030	0.04	136	0.07	16
HD 48122	5100 ± 21	3.20 ± 0.04	-0.49 ± 0.01	1.130 ± 0.030	0.04	136	0.04	17
HD 50275	4951 ± 29	3.21 ± 0.11	0.10 ± 0.03	1.128 ± 0.030	0.06	136	0.06	14
HD 51272	4872 ± 33	2.99 ± 0.06	0.03 ± 0.02	1.105 ± 0.030	0.06	139	0.10	17
HD 64413	4928 ± 20	2.51 ± 0.05	-0.41 ± 0.01	1.505 ± 0.020	0.04	133	0.07	15
HD 64730	5173 ± 29	3.48 ± 0.07	-0.07 ± 0.02	0.799 ± 0.050	0.08	137	0.13	14
HD 72003	4868 ± 29	3.02 ± 0.07	-0.03 ± 0.02	1.121 ± 0.030	0.06	138	0.10	17
HD 72440	5652 ± 25	3.75 ± 0.07	-0.05 ± 0.01	1.280 ± 0.030	0.04	145	0.06	16
HD 72490	5018 ± 25	3.23 ± 0.06	-0.20 ± 0.01	1.139 ± 0.030	0.05	141	0.07	17
HD 74390	4890 ± 32	3.15 ± 0.06	0.08 ± 0.02	1.140 ± 0.040	0.07	136	0.10	16
HD 76445	4858 ± 25	3.23 ± 0.07	-0.16 ± 0.01	1.008 ± 0.030	0.05	136	0.08	14
HD 77172	4887 ± 25	3.25 ± 0.07	-0.03 ± 0.01	1.053 ± 0.030	0.05	133	0.10	17
HD 77818	4821 ± 29	3.09 ± 0.06	-0.11 ± 0.02	1.097 ± 0.030	0.06	139	0.11	15
HD 80811	4997 ± 11	3.53 ± 0.04	-0.44 ± 0.01	0.924 ± 0.030	0.04	140	0.05	14
HD 82074	5175 ± 11	3.46 ± 0.07	-0.34 ± 0.01	1.116 ± 0.020	0.03	137	0.05	15
HD 82886	5099 ± 15	3.27 ± 0.06	-0.27 ± 0.01	1.157 ± 0.020	0.04	138	0.05	17
HD 83024	4794 ± 36	2.98 ± 0.06	0.09 ± 0.02	1.190 ± 0.040	0.08	133	0.11	17
HD 83394	4992 ± 14	3.20 ± 0.04	-0.26 ± 0.01	1.091 ± 0.030	0.04	141	0.06	16

Table 3 continued on next page

Table 3 (*continued*)

Star	T_{eff}	$\log g$	[Fe/H]	ξ	σ	N	σ	N
	(K)			(km s $^{-1}$)	(Fe I)	(Fe II)	(Fe I)	(Fe II)
HD 83752	6089 ± 63	3.93 ± 0.13	0.18 ± 0.02	1.396 ± 0.050	0.07	135	0.10	13
HD 85440	5192 ± 18	3.51 ± 0.04	-0.04 ± 0.01	1.071 ± 0.020	0.03	131	0.06	17
HD 85472	5351 ± 11	3.76 ± 0.03	-0.01 ± 0.01	1.059 ± 0.020	0.02	130	0.05	16
HD 87230	5026 ± 32	3.17 ± 0.09	0.09 ± 0.02	1.220 ± 0.030	0.06	138	0.10	17
HD 87669	4806 ± 31	2.99 ± 0.09	-0.07 ± 0.02	1.125 ± 0.030	0.06	134	0.11	14
HD 88134	4909 ± 33	3.10 ± 0.09	0.03 ± 0.03	1.115 ± 0.040	0.07	137	0.09	17
HD 88654	5275 ± 28	3.61 ± 0.06	0.11 ± 0.02	1.180 ± 0.030	0.05	140	0.08	17
HD 89391	4943 ± 25	3.30 ± 0.06	-0.18 ± 0.01	1.075 ± 0.030	0.05	138	0.09	17
HD 90043	5005 ± 22	3.26 ± 0.04	-0.02 ± 0.01	1.081 ± 0.030	0.05	140	0.06	15
HD 90792	4909 ± 29	2.51 ± 0.08	-0.06 ± 0.03	1.595 ± 0.030	0.06	135	0.10	16
HD 93396	5402 ± 18	3.83 ± 0.06	0.30 ± 0.01	1.122 ± 0.030	0.04	132	0.05	15
HD 93461	5113 ± 18	3.48 ± 0.04	-0.04 ± 0.01	1.055 ± 0.030	0.05	139	0.06	16
HD 93864	5029 ± 15	3.41 ± 0.04	-0.21 ± 0.01	1.023 ± 0.020	0.04	138	0.06	17
HD 94834	4856 ± 33	3.20 ± 0.13	0.08 ± 0.02	1.012 ± 0.030	0.05	128	0.12	16
HD 95089	4950 ± 29	3.22 ± 0.06	0.06 ± 0.02	1.110 ± 0.030	0.06	138	0.08	16
HD 95526	4911 ± 25	3.19 ± 0.06	-0.13 ± 0.01	1.033 ± 0.030	0.04	135	0.08	17
HD 96063	5120 ± 15	3.42 ± 0.06	-0.19 ± 0.01	1.078 ± 0.020	0.03	134	0.05	15
HD 96683	5107 ± 29	3.35 ± 0.18	0.17 ± 0.03	1.189 ± 0.030	0.06	140	0.08	14
HD 97601	5112 ± 25	3.20 ± 0.09	-0.08 ± 0.02	1.178 ± 0.030	0.05	138	0.05	14
HD 98219	4970 ± 25	3.32 ± 0.11	0.03 ± 0.02	1.011 ± 0.030	0.05	138	0.08	16
HD 99706	4912 ± 26	3.10 ± 0.06	0.05 ± 0.02	1.128 ± 0.030	0.06	138	0.09	17
HD 100337	4998 ± 25	3.17 ± 0.06	-0.14 ± 0.01	1.103 ± 0.030	0.04	135	0.08	17
HD 102329	4760 ± 38	2.77 ± 0.14	0.12 ± 0.03	1.190 ± 0.030	0.06	134	0.11	16
HD 102444	5304 ± 15	3.69 ± 0.03	-0.05 ± 0.01	1.109 ± 0.020	0.03	141	0.06	16
HD 102956	5025 ± 29	3.38 ± 0.16	0.16 ± 0.02	1.073 ± 0.040	0.06	136	0.10	17
HD 103616	5166 ± 25	3.76 ± 0.10	-0.06 ± 0.02	0.906 ± 0.040	0.06	135	0.12	15
HD 104017	4784 ± 40	3.03 ± 0.07	0.15 ± 0.03	1.115 ± 0.040	0.08	135	0.11	13
HD 106270	5567 ± 11	3.76 ± 0.03	0.06 ± 0.01	1.186 ± 0.020	0.03	140	0.04	15
HD 106279	4908 ± 22	2.52 ± 0.03	-0.34 ± 0.01	1.439 ± 0.020	0.05	134	0.05	16

Table 3 continued on next page

Table 3 (*continued*)

Star	T_{eff}	$\log g$	[Fe/H]	ξ	σ	N	σ	N
	(K)			(km s $^{-1}$)	(Fe I)	(Fe II)	(Fe I)	(Fe II)
HD 107990	4880 ± 29	2.63 ± 0.09	-0.07 ± 0.02	1.382 ± 0.030	0.05	136	0.08	16
HD 108189	5388 ± 15	3.52 ± 0.04	-0.06 ± 0.01	1.216 ± 0.030	0.05	140	0.09	16
HD 108863	4871 ± 26	3.02 ± 0.04	0.07 ± 0.02	1.151 ± 0.030	0.06	139	0.10	16
HD 109159	5219 ± 15	3.64 ± 0.04	-0.13 ± 0.01	1.033 ± 0.020	0.03	137	0.05	16
HD 109218	5320 ± 14	3.73 ± 0.04	-0.10 ± 0.01	1.078 ± 0.020	0.03	135	0.03	15
HD 109929	6128 ± 36	4.16 ± 0.04	0.36 ± 0.02	1.518 ± 0.040	0.05	132	0.05	14
HD 112115	4708 ± 58	2.55 ± 0.13	0.09 ± 0.03	1.266 ± 0.050	0.10	130	0.12	15
HD 112973	4941 ± 18	3.18 ± 0.03	-0.31 ± 0.01	1.085 ± 0.020	0.04	141	0.05	15
HD 112988	4906 ± 11	3.16 ± 0.03	-0.32 ± 0.01	1.050 ± 0.020	0.04	137	0.07	15
HD 114161	4856 ± 38	2.95 ± 0.10	0.09 ± 0.02	1.183 ± 0.030	0.07	134	0.09	17
HD 114659	4850 ± 36	3.07 ± 0.09	0.06 ± 0.03	1.144 ± 0.030	0.06	132	0.10	16
HD 116029	4874 ± 36	3.17 ± 0.09	0.12 ± 0.02	1.105 ± 0.040	0.08	139	0.11	17
HD 117623	4946 ± 29	2.92 ± 0.09	-0.07 ± 0.02	0.740 ± 0.040	0.07	141	0.08	17
HD 117762	5187 ± 15	3.46 ± 0.07	-0.33 ± 0.01	1.064 ± 0.020	0.03	133	0.05	15
HD 118082	4850 ± 29	3.07 ± 0.06	0.07 ± 0.02	1.111 ± 0.030	0.06	137	0.12	17
HD 118744	4819 ± 33	2.84 ± 0.19	-0.06 ± 0.03	1.219 ± 0.030	0.06	136	0.05	14
HD 120531	4963 ± 25	3.10 ± 0.06	-0.22 ± 0.01	1.164 ± 0.030	0.05	138	0.07	16
HD 122253	5078 ± 15	3.43 ± 0.08	-0.03 ± 0.01	1.010 ± 0.020	0.04	135	0.07	17
HD 123239	4850 ± 22	2.95 ± 0.06	-0.16 ± 0.01	1.161 ± 0.030	0.05	134	0.05	15
HD 124641	4731 ± 29	2.67 ± 0.10	-0.14 ± 0.02	1.202 ± 0.030	0.06	132	0.09	17
HD 125217	4887 ± 36	3.17 ± 0.09	0.15 ± 0.02	1.107 ± 0.040	0.08	131	0.11	15
HD 125390	4882 ± 29	3.04 ± 0.04	-0.11 ± 0.02	1.129 ± 0.030	0.06	140	0.10	17
HD 125607	5027 ± 32	3.33 ± 0.08	0.01 ± 0.02	1.056 ± 0.030	0.05	134	0.08	14
HD 126991	5175 ± 14	3.40 ± 0.07	-0.59 ± 0.01	1.118 ± 0.030	0.03	132	0.04	15
HD 127374	4908 ± 29	2.59 ± 0.09	-0.22 ± 0.02	1.392 ± 0.030	0.05	139	0.08	17
HD 128095	4987 ± 25	3.38 ± 0.06	-0.06 ± 0.01	1.028 ± 0.030	0.05	135	0.07	16
HD 128720	5048 ± 29	3.50 ± 0.04	0.14 ± 0.02	1.060 ± 0.040	0.06	143	0.07	15
HD 131496	4834 ± 33	3.06 ± 0.09	0.11 ± 0.02	1.121 ± 0.030	0.06	136	0.12	17
HD 136418	4973 ± 22	3.38 ± 0.08	-0.08 ± 0.01	1.024 ± 0.030	0.05	138	0.06	15

Table 3 continued on next page

Table 3 (*continued*)

Star	T_{eff}	$\log g$	[Fe/H]	ξ	σ	N	σ	N
	(K)			(km s $^{-1}$)	(Fe I)	(Fe II)	(Fe I)	(Fe II)
HD 136513	4887 ± 25	2.94 ± 0.10	-0.24 ± 0.01	1.191 ± 0.030	0.05	138	0.07	17
HD 140025	5564 ± 15	3.87 ± 0.08	0.18 ± 0.01	1.130 ± 0.020	0.04	138	0.09	17
HD 141712	5178 ± 22	3.51 ± 0.03	0.10 ± 0.01	1.155 ± 0.030	0.05	137	0.07	15
HD 142091	4863 ± 29	3.11 ± 0.07	0.13 ± 0.02	1.099 ± 0.030	0.07	135	0.11	16
HD 142245	4838 ± 36	3.27 ± 0.09	0.20 ± 0.02	1.055 ± 0.040	0.07	134	0.10	14
HD 144363	4975 ± 25	3.26 ± 0.06	-0.11 ± 0.01	1.028 ± 0.030	0.05	135	0.07	17
HD 145428	4836 ± 32	3.05 ± 0.07	-0.25 ± 0.02	1.071 ± 0.030	0.04	136	0.08	16
HD 146278	4785 ± 29	2.82 ± 0.13	-0.08 ± 0.02	1.182 ± 0.030	0.06	131	0.09	17
HD 150331	5726 ± 35	2.60 ± 0.09	-0.18 ± 0.02	2.156 ± 0.050	0.06	132	0.06	12
HD 152581	5156 ± 18	3.36 ± 0.06	-0.28 ± 0.01	1.146 ± 0.020	0.04	133	0.06	16
HD 152733	4842 ± 26	3.04 ± 0.06	0.04 ± 0.02	1.108 ± 0.030	0.06	135	0.09	17
HD 155413	5824 ± 25	3.81 ± 0.07	0.24 ± 0.01	1.412 ± 0.030	0.04	140	0.07	16
HD 158038	4871 ± 50	3.26 ± 0.18	0.20 ± 0.03	1.166 ± 0.050	0.10	139	0.10	15
HD 158449	5060 ± 11	3.27 ± 0.06	-0.21 ± 0.01	1.144 ± 0.020	0.04	141	0.06	15
HD 160215	4912 ± 25	3.34 ± 0.08	-0.01 ± 0.01	0.994 ± 0.030	0.05	138	0.09	15
HD 163528	4995 ± 29	3.18 ± 0.04	0.01 ± 0.02	1.105 ± 0.030	0.06	141	0.07	15
HD 166494	5705 ± 20	3.74 ± 0.08	0.21 ± 0.02	1.377 ± 0.030	0.05	141	0.07	15
HD 167042	4971 ± 22	3.26 ± 0.09	0.05 ± 0.01	1.075 ± 0.020	0.05	136	0.07	17
HD 171264	5272 ± 18	3.65 ± 0.04	-0.02 ± 0.01	1.115 ± 0.020	0.04	140	0.07	16
HD 175541	5101 ± 18	3.47 ± 0.07	-0.08 ± 0.01	1.068 ± 0.020	0.04	137	0.04	14
HD 178251	4798 ± 21	2.72 ± 0.06	-0.63 ± 0.01	1.279 ± 0.030	0.05	143	0.04	14
HD 180053	5107 ± 32	3.43 ± 0.11	0.14 ± 0.02	1.187 ± 0.040	0.07	140	0.10	15
HD 180902	5006 ± 25	3.34 ± 0.08	0.03 ± 0.01	1.058 ± 0.030	0.05	139	0.09	17
HD 181342	4934 ± 36	3.22 ± 0.09	0.20 ± 0.02	1.147 ± 0.040	0.07	138	0.11	15
HD 183473	5634 ± 11	3.89 ± 0.07	-0.09 ± 0.01	1.240 ± 0.020	0.03	135	0.03	14
HD 185269	5998 ± 35	3.96 ± 0.05	0.12 ± 0.01	1.447 ± 0.040	0.04	136	0.07	16
HD 185351	5040 ± 26	3.28 ± 0.11	0.09 ± 0.02	1.112 ± 0.030	0.06	139	0.07	16
HD 185351	5039 ± 29	3.30 ± 0.08	0.10 ± 0.02	1.099 ± 0.030	0.06	137	0.08	16
HD 185351	5041 ± 29	3.23 ± 0.13	0.09 ± 0.03	1.118 ± 0.030	0.06	139	0.09	17

Table 3 continued on next page

Table 3 (*continued*)

Star	T_{eff}	$\log g$	[Fe/H]	ξ	σ	N	σ	N
	(K)			(km s $^{-1}$)	(Fe I)	(Fe II)	(Fe I)	(Fe II)
HD 187460	4662 ± 51	2.65 ± 0.14	-0.24 ± 0.03	1.271 ± 0.050	0.11	131	0.14	11
HD 188386	4965 ± 20	3.15 ± 0.06	-0.02 ± 0.01	1.098 ± 0.020	0.05	135	0.07	15
HD 192153	5206 ± 18	3.66 ± 0.08	-0.24 ± 0.01	1.014 ± 0.030	0.03	136	0.04	15
HD 192699	5140 ± 15	3.39 ± 0.07	-0.19 ± 0.01	1.127 ± 0.020	0.04	136	0.03	15
HD 193342	4940 ± 29	3.18 ± 0.07	0.05 ± 0.02	1.121 ± 0.030	0.06	139	0.09	16
HD 193391	4997 ± 26	3.02 ± 0.04	0.09 ± 0.02	1.230 ± 0.030	0.06	140	0.08	15
HD 194541	4803 ± 33	3.01 ± 0.04	0.09 ± 0.02	1.165 ± 0.030	0.07	137	0.10	17
HD 195787	5014 ± 11	3.30 ± 0.07	-0.12 ± 0.01	1.046 ± 0.020	0.04	133	0.05	15
HD 195824	5104 ± 18	3.42 ± 0.07	-0.08 ± 0.01	1.077 ± 0.030	0.04	135	0.08	17
HD 196645	5106 ± 18	3.47 ± 0.06	-0.11 ± 0.01	1.023 ± 0.020	0.03	133	0.06	16
HD 197162	4925 ± 25	3.19 ± 0.10	-0.34 ± 0.01	1.141 ± 0.030	0.04	137	0.09	17
HD 198599	4937 ± 43	2.87 ± 0.16	-0.06 ± 0.03	0.439 ± 0.060	0.08	138	0.11	15
HD 200081	4933 ± 25	2.73 ± 0.07	-0.10 ± 0.02	0.838 ± 0.030	0.06	137	0.10	16
HD 200491	5119 ± 15	3.03 ± 0.04	0.01 ± 0.01	1.281 ± 0.030	0.05	140	0.05	14
HD 200964	5064 ± 18	3.25 ± 0.06	-0.17 ± 0.01	1.122 ± 0.020	0.04	136	0.06	16
HD 202696	4857 ± 33	2.97 ± 0.07	0.05 ± 0.02	1.166 ± 0.030	0.07	138	0.10	17
HD 202867	5146 ± 21	3.56 ± 0.04	-0.10 ± 0.01	1.051 ± 0.030	0.04	136	0.06	15
HD 203471	5507 ± 18	3.80 ± 0.04	-0.03 ± 0.01	1.152 ± 0.020	0.03	137	0.06	14
HD 205163	5033 ± 43	2.89 ± 0.14	0.10 ± 0.02	1.371 ± 0.040	0.08	137	0.11	15
HD 206610	4836 ± 32	3.10 ± 0.07	0.10 ± 0.02	1.122 ± 0.040	0.07	132	0.11	16
HD 206635	5032 ± 18	3.64 ± 0.04	-0.22 ± 0.01	0.903 ± 0.030	0.04	135	0.07	16
HD 207077	5138 ± 11	3.32 ± 0.04	-0.40 ± 0.01	1.111 ± 0.020	0.03	138	0.03	13
HD 208585	5006 ± 35	3.21 ± 0.12	-0.04 ± 0.02	1.093 ± 0.030	0.05	136	0.08	17
HD 210011	5093 ± 29	2.79 ± 0.07	0.08 ± 0.02	1.194 ± 0.030	0.07	137	0.08	11
HD 210521	5100 ± 11	3.33 ± 0.06	-0.07 ± 0.01	1.117 ± 0.030	0.04	135	0.07	17
HD 210702	4974 ± 25	3.21 ± 0.06	0.07 ± 0.01	1.073 ± 0.030	0.05	136	0.08	17
HD 212771	5104 ± 15	3.44 ± 0.11	-0.09 ± 0.01	1.085 ± 0.020	0.04	140	0.06	16
HD 213278	5193 ± 11	3.52 ± 0.04	-0.26 ± 0.01	1.050 ± 0.020	0.03	139	0.04	15
HD 215049	5174 ± 18	3.72 ± 0.04	0.03 ± 0.01	1.007 ± 0.030	0.04	138	0.07	16

Table 3 continued on next page

Table 3 (*continued*)

Star	T_{eff}	$\log g$	[Fe/H]	ξ	σ	N	σ	N
	(K)			(km s $^{-1}$)	(Fe I)	(Fe II)	(Fe I)	(Fe II)
HD 215549	4921 ± 25	3.26 ± 0.10	-0.28 ± 0.01	1.029 ± 0.030	0.05	144	0.08	16
HD 215908	5131 ± 18	3.35 ± 0.07	-0.28 ± 0.01	1.157 ± 0.020	0.04	137	0.05	16
HD 216834	5123 ± 18	3.48 ± 0.04	-0.31 ± 0.01	1.053 ± 0.020	0.03	136	0.04	15
HD 217496	5074 ± 15	3.44 ± 0.07	-0.08 ± 0.01	1.073 ± 0.020	0.04	129	0.05	13
HD 217591	5108 ± 25	3.44 ± 0.10	-0.13 ± 0.01	1.139 ± 0.030	0.04	137	0.04	15
HD 217681	4977 ± 26	3.46 ± 0.08	0.16 ± 0.02	1.029 ± 0.030	0.06	135	0.12	17
HD 219553	4846 ± 36	3.13 ± 0.07	0.17 ± 0.02	1.147 ± 0.040	0.08	132	0.12	16
HD 220122	4865 ± 29	2.49 ± 0.07	-0.29 ± 0.02	1.471 ± 0.030	0.06	141	0.07	16
HD 220952	4976 ± 25	3.29 ± 0.07	0.03 ± 0.01	1.084 ± 0.030	0.05	137	0.06	15
HD 221504	5397 ± 22	3.80 ± 0.09	0.29 ± 0.01	1.130 ± 0.030	0.05	138	0.07	14
HD 222112	4817 ± 43	3.07 ± 0.09	0.17 ± 0.03	1.145 ± 0.050	0.09	137	0.13	16
HD 223627	4792 ± 29	2.94 ± 0.11	-0.04 ± 0.02	1.133 ± 0.030	0.06	138	0.11	17
HD 224032	5806 ± 31	4.03 ± 0.07	0.41 ± 0.02	1.369 ± 0.040	0.06	135	0.09	15
HD 224679	5757 ± 29	3.67 ± 0.06	0.08 ± 0.02	1.345 ± 0.040	0.05	137	0.07	14
HD 225021	4979 ± 29	2.95 ± 0.08	0.19 ± 0.02	1.308 ± 0.030	0.06	132	0.09	14
HD 236427	5162 ± 18	3.68 ± 0.04	0.02 ± 0.01	1.004 ± 0.020	0.04	137	0.05	16
HIP 43212	4937 ± 31	2.92 ± 0.12	0.08 ± 0.02	1.306 ± 0.030	0.06	139	0.08	16
HIP 87123	4806 ± 39	3.02 ± 0.08	-0.20 ± 0.03	1.058 ± 0.030	0.06	139	0.08	15

Table 4. Atmospheric Parameters Sensitivities.

Parameter	ΔT_{eff}	$\Delta \log g$	$\Delta [\text{Fe}/\text{H}]$	$\Delta \xi$
	(± 100 K)	(± 0.20 dex)	(± 0.20 dex)	(± 0.200 km s $^{-1}$)
T_{eff} (K)	...	-79 $+29$	$+29$ -30	$+72$ -37
$\log g$ (dex)	$+0.27$ -0.22	...	-0.05 $+0.02$	$+0.20$ -0.09
[Fe/H] (dex)	$+0.08$ -0.07	$+0.01$ -0.01	...	-0.02 $+0.05$
ξ (km s $^{-1}$)	-0.044 -0.009	-0.098 $+0.043$	$+0.020$ -0.024	...

Table 5. Broadening Parameters.

Star	FWHM_{inst}	V_{macro}	$v \sin i$
	(Å)	(km s $^{-1}$)	(km s $^{-1}$)
HD 1100	0.112	4.00	0.6 ± 0.8
HD 1293	0.112	3.51	2.2 ± 0.6
HD 1384	0.112	3.39	2.4 ± 0.4
HD 1502	0.112	3.43	1.2 ± 1.0
HD 2946	0.112	3.82	3.4 ± 0.8
HD 3458	0.112	4.00	3.2 ± 0.6
HD 4313	0.112	3.41	2.2 ± 0.4
HD 4395	0.112	4.03	1.2 ± 1.0
HD 4917	0.112	4.00	2.2 ± 0.6
HD 5891	0.096	4.00	3.2 ± 0.4
HD 6019	0.112	3.46	1.0 ± 0.8
HD 6030	0.112	3.42	1.2 ± 0.6
HD 7530	0.112	3.45	1.6 ± 0.8
HD 7931	0.112	3.38	1.8 ± 0.6

Table 5 continued on next page

Table 5 (*continued*)

Star	FWHM_{inst}	V_{macro}	$v \sin i$
	(Å)	(km s $^{-1}$)	(km s $^{-1}$)
HD 7980	0.112	4.00	1.0 ± 0.8
HD 8375	0.096	3.56	0.6 ± 0.8
HD 8407	0.112	3.42	2.2 ± 0.4
HD 8508	0.112	4.00	3.6 ± 0.4
HD 9156	0.112	4.00	2.6 ± 0.6
HD 9218	0.096	4.00	0.0 ± 0.8
HD 9313	0.112	3.41	1.6 ± 0.8
HD 9554	0.112	4.00	3.2 ± 0.6
HD 9625	0.112	4.00	2.2 ± 0.6
HD 10011	0.112	3.48	2.0 ± 0.6
HD 10212	0.112	3.41	2.2 ± 0.4
HD 10245	0.112	3.35	2.6 ± 0.8
HD 10383	0.112	3.38	1.8 ± 0.8
HD 10479	0.112	4.00	2.2 ± 0.4
HD 10823	0.112	3.51	0.4 ± 1.0
HD 10909	0.112	3.39	3.8 ± 0.4
HD 11288	0.112	3.54	5.0 ± 0.4

Table 5 continued on next page

Table 5 (*continued*)

Star	FWHM_{inst}	V_{macro}	$v \sin i$
	(Å)	(km s $^{-1}$)	(km s $^{-1}$)
HD 11970	0.112	3.50	0.8 ± 0.8
HD 12137	0.112	3.41	2.4 ± 0.4
HD 12164	0.112	3.82	0.4 ± 1.2
HD 13167	0.112	4.36	2.8 ± 0.6
HD 14787	0.112	3.43	1.6 ± 0.8
HD 15336	0.112	3.49	2.6 ± 0.4
HD 15391	0.112	4.00	1.2 ± 1.0
HD 15928	0.112	3.69	2.2 ± 0.6
HD 16175	0.096	4.42	4.2 ± 0.6
HD 16178	0.112	4.00	1.6 ± 0.8
HD 16984	0.112	3.40	1.4 ± 0.8
HD 17311	0.112	3.45	1.2 ± 0.6
HD 17620	0.112	3.55	2.8 ± 0.6
HD 18015	0.112	4.10	3.4 ± 0.8
HD 18645	0.112	3.86	8.8 ± 0.6
HD 18667	0.112	3.41	1.8 ± 0.6
HD 18742	0.112	3.43	1.6 ± 0.6

Table 5 continued on next page

Table 5 (*continued*)

Star	FWHM_{inst}	V_{macro}	$v \sin i$
	(Å)	(km s $^{-1}$)	(km s $^{-1}$)
HD 19522	0.096	3.95	0.0 ± 1.2
HD 19659	0.096	4.37	4.2 ± 0.4
HD 21340	0.096	3.41	1.6 ± 0.6
HD 21449	0.112	4.00	2.6 ± 0.4
HD 21581	0.112	4.00	0.0 ± 3.4
HD 22233	0.112	3.52	3.0 ± 0.4
HD 22657	0.112	3.38	1.6 ± 0.6
HD 22682	0.112	3.45	0.4 ± 0.8
HD 22844	0.112	3.58	2.0 ± 0.6
HD 23134	0.112	3.40	1.6 ± 0.6
HD 23825	0.112	4.09	3.2 ± 0.8
HD 24148	0.112	3.41	1.8 ± 0.6
HD 24316	0.112	4.00	1.0 ± 0.8
HD 24365	0.096	3.54	0.0 ± 0.8
HD 25622	0.112	3.44	2.4 ± 0.4
HD 25975	0.112	3.42	0.0 ± 1.2
HD 26007	0.112	4.00	1.2 ± 0.8

Table 5 continued on next page

Table 5 (*continued*)

Star	FWHM_{inst}	V_{macro}	$v \sin i$
	(Å)	(km s ⁻¹)	(km s ⁻¹)
HD 26634	0.112	3.41	1.4 ± 0.8
HD 27297	0.112	3.52	1.2 ± 0.8
HD 27956	0.112	3.40	2.2 ± 0.4
HD 28678	0.112	3.47	1.0 ± 0.8
HD 28737	0.112	4.00	0.0 ± 1.0
HD 30090	0.065	3.67	3.0 ± 0.2
HD 30128	0.112	3.43	2.8 ± 0.4
HD 30166	0.112	4.00	1.2 ± 0.6
HD 30856	0.112	3.42	1.0 ± 0.6
HD 30882	0.096	4.00	0.6 ± 0.8
HD 31018	0.112	5.00	3.4 ± 0.6
HD 31451	0.096	3.42	0.8 ± 0.6
HD 31543	0.112	4.09	2.6 ± 0.6
HD 31693	0.112	3.43	2.0 ± 0.6
HD 33142	0.112	3.44	1.2 ± 0.8
HD 33240	0.112	4.00	4.8 ± 0.2
HD 33298	0.096	3.72	0.0 ± 1.0

Table 5 continued on next page

Table 5 (*continued*)

Star	FWHM_{inst}	V_{macro}	$v \sin i$
	(Å)	(km s $^{-1}$)	(km s $^{-1}$)
HD 33844	0.112	3.38	2.0 ± 0.6
HD 34538	0.112	3.40	1.4 ± 0.6
HD 34909	0.112	3.44	2.2 ± 0.4
HD 37445	0.096	4.00	1.0 ± 0.8
HD 37601	0.112	3.42	1.8 ± 0.6
HD 38505	0.112	3.43	1.6 ± 0.8
HD 39142	0.112	4.00	2.2 ± 0.4
HD 39731	0.112	3.52	2.6 ± 0.6
HD 39828	0.112	3.41	2.4 ± 0.4
HD 40537	0.112	3.43	1.8 ± 0.6
HD 45210	0.096	4.14	6.8 ± 0.4
HD 45410	0.096	3.43	1.4 ± 0.4
HD 45506	0.112	3.48	1.2 ± 0.6
HD 47562	0.112	3.45	2.6 ± 0.4
HD 48122	0.096	3.48	1.2 ± 0.6
HD 50275	0.096	3.42	1.6 ± 0.6
HD 51272	0.096	4.00	1.2 ± 0.6

Table 5 continued on next page

Table 5 (*continued*)

Star	FWHM_{inst}	V_{macro}	$v \sin i$
	(Å)	(km s $^{-1}$)	(km s $^{-1}$)
HD 64413	0.112	4.00	3.2 ± 0.4
HD 64730	0.112	3.51	2.8 ± 0.6
HD 72003	0.112	3.39	2.2 ± 0.4
HD 72440	0.112	4.12	4.4 ± 0.6
HD 72490	0.112	3.44	2.4 ± 0.4
HD 74390	0.112	3.40	1.8 ± 0.6
HD 76445	0.112	3.39	1.8 ± 0.6
HD 77172	0.112	3.40	1.4 ± 0.8
HD 77818	0.112	3.38	1.0 ± 0.6
HD 80811	0.112	3.43	1.4 ± 0.8
HD 82074	0.112	3.52	0.8 ± 0.8
HD 82886	0.096	3.47	0.0 ± 1.2
HD 83024	0.112	4.00	1.6 ± 0.6
HD 83394	0.096	3.43	1.0 ± 0.6
HD 83752	0.112	6.09	4.2 ± 1.0
HD 85440	0.096	3.53	2.0 ± 0.6
HD 85472	0.096	3.65	1.2 ± 0.6

Table 5 continued on next page

Table 5 (*continued*)

Star	FWHM_{inst}	V_{macro}	$v \sin i$
	(Å)	(km s $^{-1}$)	(km s $^{-1}$)
HD 87230	0.112	3.44	3.4 ± 0.6
HD 87669	0.112	4.00	1.0 ± 0.8
HD 88134	0.096	3.40	1.2 ± 0.4
HD 88654	0.112	3.59	1.4 ± 0.8
HD 89391	0.112	3.41	2.0 ± 0.4
HD 90043	0.096	3.43	1.4 ± 0.4
HD 90792	0.112	4.00	2.8 ± 0.4
HD 93396	0.112	3.71	1.6 ± 0.8
HD 93461	0.112	3.48	2.0 ± 0.4
HD 93864	0.096	3.44	0.0 ± 0.8
HD 94834	0.096	3.39	0.6 ± 0.8
HD 95089	0.112	3.42	2.0 ± 0.6
HD 95526	0.096	3.40	1.0 ± 0.6
HD 96063	0.096	3.49	0.0 ± 1.0
HD 96683	0.096	3.48	1.2 ± 0.6
HD 97601	0.096	3.48	2.4 ± 0.4
HD 98219	0.096	3.42	0.4 ± 0.8

Table 5 continued on next page

Table 5 (*continued*)

Star	FWHM_{inst}	V_{macro}	$v \sin i$
	(Å)	(km s $^{-1}$)	(km s $^{-1}$)
HD 99706	0.096	3.40	1.8 ± 0.6
HD 100337	0.096	3.43	2.2 ± 0.4
HD 102329	0.096	4.00	1.2 ± 0.6
HD 102444	0.096	3.61	1.6 ± 0.6
HD 102956	0.096	3.44	1.6 ± 0.6
HD 103616	0.096	3.51	1.8 ± 0.6
HD 104017	0.096	3.37	1.4 ± 0.8
HD 106270	0.096	3.95	2.6 ± 0.4
HD 106279	0.096	4.00	2.0 ± 0.4
HD 107990	0.096	4.00	1.8 ± 0.6
HD 108189	0.096	3.69	6.4 ± 0.4
HD 108863	0.096	3.39	1.6 ± 0.6
HD 109159	0.096	3.54	0.0 ± 1.0
HD 109218	0.096	3.62	0.0 ± 1.0
HD 109929	0.112	5.59	7.2 ± 0.6
HD 112115	0.096	4.00	1.4 ± 0.8
HD 112973	0.096	3.41	0.8 ± 0.8

Table 5 continued on next page

Table 5 (*continued*)

Star	FWHM_{inst}	V_{macro}	$v \sin i$
	(Å)	(km s $^{-1}$)	(km s $^{-1}$)
HD 112988	0.096	3.40	0.0 ± 1.0
HD 114161	0.096	4.00	0.4 ± 1.0
HD 114659	0.096	3.39	1.0 ± 0.6
HD 116029	0.096	3.39	1.0 ± 0.6
HD 117623	0.096	4.00	2.6 ± 0.4
HD 117762	0.112	3.52	0.0 ± 1.4
HD 118082	0.112	3.39	2.6 ± 0.4
HD 118744	0.096	4.00	0.0 ± 0.8
HD 120531	0.112	3.42	2.6 ± 0.4
HD 122253	0.096	3.46	0.6 ± 0.8
HD 123239	0.096	4.00	0.0 ± 0.8
HD 124641	0.096	4.00	0.0 ± 0.8
HD 125217	0.112	3.40	2.8 ± 0.4
HD 125390	0.112	3.40	2.2 ± 0.4
HD 125607	0.096	3.44	0.4 ± 0.8
HD 126991	0.096	3.52	0.0 ± 1.2
HD 127374	0.112	4.00	1.0 ± 0.8

Table 5 continued on next page

Table 5 (*continued*)

Star	FWHM_{inst}	V_{macro}	$v \sin i$
	(Å)	(km s $^{-1}$)	(km s $^{-1}$)
HD 128095	0.096	3.43	0.0 ± 1.2
HD 128720	0.112	3.45	1.8 ± 0.6
HD 131496	0.096	3.38	1.6 ± 0.6
HD 136418	0.096	3.42	0.8 ± 0.8
HD 136513	0.096	4.00	0.0 ± 0.6
HD 140025	0.096	3.94	0.0 ± 1.0
HD 141712	0.112	3.52	1.6 ± 0.8
HD 142091	0.096	3.39	1.8 ± 0.6
HD 142245	0.112	3.38	1.4 ± 0.8
HD 144363	0.096	3.42	0.0 ± 1.2
HD 145428	0.096	3.38	1.0 ± 0.6
HD 146278	0.096	4.00	0.0 ± 0.8
HD 150331	0.112	4.00	6.0 ± 0.6
HD 152581	0.096	3.50	0.0 ± 1.2
HD 152733	0.096	3.39	1.6 ± 0.6
HD 155413	0.096	4.63	4.0 ± 0.4
HD 158038	0.096	3.39	0.8 ± 0.8

Table 5 continued on next page

Table 5 (*continued*)

Star	FWHM_{inst}	V_{macro}	$v \sin i$
	(Å)	(km s $^{-1}$)	(km s $^{-1}$)
HD 158449	0.096	3.46	0.0 ± 1.2
HD 160215	0.096	3.40	1.0 ± 0.6
HD 163528	0.112	3.43	1.2 ± 0.6
HD 166494	0.096	4.25	5.8 ± 0.6
HD 167042	0.096	3.42	1.0 ± 0.6
HD 171264	0.112	3.58	1.4 ± 0.8
HD 175541	0.096	3.48	0.8 ± 0.6
HD 178251	0.112	4.00	0.0 ± 1.4
HD 180053	0.096	3.48	2.2 ± 0.4
HD 180902	0.112	3.43	2.2 ± 0.4
HD 181342	0.112	3.41	2.4 ± 0.6
HD 183473	0.112	4.08	0.0 ± 1.2
HD 185269	0.096	5.46	4.0 ± 0.8
HD 185351	0.096	3.45	1.6 ± 0.6
HD 185351	0.096	3.45	1.6 ± 0.6
HD 185351	0.096	3.45	1.8 ± 0.6
HD 187460	0.112	4.00	4.2 ± 0.6

Table 5 continued on next page

Table 5 (*continued*)

Star	FWHM_{inst}	V_{macro}	$v \sin i$
	(Å)	(km s $^{-1}$)	(km s $^{-1}$)
HD 188386	0.096	3.42	1.2 ± 0.4
HD 192153	0.112	3.54	1.0 ± 0.8
HD 192699	0.096	3.50	1.0 ± 0.6
HD 193342	0.112	3.41	0.0 ± 0.8
HD 193391	0.112	3.43	3.4 ± 0.4
HD 194541	0.112	3.38	1.2 ± 0.6
HD 195787	0.112	3.44	0.0 ± 0.6
HD 195824	0.112	3.48	1.2 ± 0.6
HD 196645	0.112	3.48	0.0 ± 1.2
HD 197162	0.112	3.41	0.8 ± 0.8
HD 198599	0.112	4.00	3.4 ± 0.4
HD 200081	0.112	4.00	3.4 ± 0.6
HD 200491	0.112	3.48	2.6 ± 0.4
HD 200964	0.112	3.46	1.6 ± 0.6
HD 202696	0.112	4.00	1.8 ± 0.6
HD 202867	0.112	3.50	2.0 ± 0.6
HD 203471	0.112	3.85	5.2 ± 0.6

Table 5 continued on next page

Table 5 (*continued*)

Star	FWHM_{inst}	V_{macro}	$v \sin i$
	(Å)	(km s $^{-1}$)	(km s $^{-1}$)
HD 205163	0.096	4.00	4.8 ± 0.4
HD 206610	0.112	3.38	1.6 ± 0.8
HD 206635	0.112	3.44	0.0 ± 1.4
HD 207077	0.112	3.49	1.8 ± 0.8
HD 208585	0.112	3.43	2.0 ± 0.4
HD 210011	0.112	4.00	4.2 ± 0.4
HD 210521	0.112	3.48	1.8 ± 0.6
HD 210702	0.096	3.42	1.6 ± 0.6
HD 212771	0.112	3.48	1.6 ± 0.6
HD 213278	0.112	3.53	1.2 ± 0.8
HD 215049	0.112	3.52	0.6 ± 0.8
HD 215549	0.112	3.41	1.6 ± 0.8
HD 215908	0.112	3.49	1.8 ± 0.6
HD 216834	0.112	3.49	1.0 ± 0.8
HD 217496	0.112	3.46	1.6 ± 0.6
HD 217591	0.112	3.48	1.6 ± 0.8
HD 217681	0.112	3.42	2.0 ± 0.6

Table 5 continued on next page

Table 5 (*continued*)

Star	FWHM_{inst}	V_{macro}	$v \sin i$
	(Å)	(km s $^{-1}$)	(km s $^{-1}$)
HD 219553	0.112	3.39	2.6 ± 0.4
HD 220122	0.112	4.00	2.4 ± 0.4
HD 220952	0.112	3.42	0.0 ± 1.2
HD 221504	0.112	3.70	2.2 ± 0.4
HD 222112	0.112	3.38	2.6 ± 0.4
HD 223627	0.112	4.00	1.0 ± 0.6
HD 224032	0.096	3.63	4.6 ± 0.4
HD 224679	0.112	4.40	7.6 ± 0.6
HD 225021	0.112	4.00	2.8 ± 0.4
HD 236427	0.112	3.51	1.0 ± 0.6
HIP 43212	0.096	4.00	2.4 ± 0.4
HIP 87123	0.096	3.38	0.8 ± 0.8

Table 6. Evolutionary Parameters.

Star	M	R	$\log g$	Age
	(M_{\odot})	(R_{\odot})		(Gyr)
HD 1100	1.284 ± 0.112	5.627 ± 0.648	3.018 ± 0.075	4.449 ± 1.303
HD 1293	1.250 ± 0.099	3.674 ± 0.502	3.377 ± 0.088	3.672 ± 0.929
HD 1384	1.381 ± 0.105	3.581 ± 0.449	3.443 ± 0.092	4.067 ± 0.935
HD 1502	1.540 ± 0.097	4.355 ± 0.532	3.319 ± 0.081	2.617 ± 0.479
HD 2946	1.452 ± 0.111	3.221 ± 0.471	3.556 ± 0.092	2.638 ± 0.566
HD 3458	2.102 ± 0.257	6.393 ± 1.469	3.121 ± 0.147	1.019 ± 0.356
HD 4313	1.658 ± 0.109	5.068 ± 0.533	3.220 ± 0.069	2.188 ± 0.430
HD 4395	1.358 ± 0.047	2.681 ± 0.191	3.681 ± 0.050	3.298 ± 0.408
HD 4917	1.268 ± 0.108	4.902 ± 0.549	3.133 ± 0.089	5.010 ± 1.471
HD 5891	1.143 ± 0.202	9.773 ± 1.933	2.488 ± 0.167	5.694 ± 3.296
HD 6019	1.219 ± 0.086	4.781 ± 0.480	3.138 ± 0.064	3.959 ± 0.919
HD 6030	1.394 ± 0.078	3.796 ± 0.399	3.396 ± 0.072	3.451 ± 0.574
HD 7530	1.194 ± 0.115	3.985 ± 0.651	3.287 ± 0.104	4.647 ± 1.514
HD 7931	1.298 ± 0.083	4.754 ± 0.425	3.170 ± 0.065	4.556 ± 0.987
HD 7980	1.340 ± 0.110	6.214 ± 0.596	2.951 ± 0.075	4.151 ± 1.110
HD 8375	1.604 ± 0.022	3.707 ± 0.096	3.475 ± 0.015	2.276 ± 0.086
HD 8407	1.127 ± 0.065	3.711 ± 0.335	3.324 ± 0.060	6.027 ± 1.248
HD 8508	1.212 ± 0.130	7.405 ± 1.158	2.755 ± 0.137	4.705 ± 1.726
HD 9156	2.128 ± 0.252	8.573 ± 2.001	2.872 ± 0.153	1.025 ± 0.334
HD 9218	1.236 ± 0.093	5.601 ± 0.510	3.006 ± 0.060	4.822 ± 1.242
HD 9313	1.389 ± 0.074	4.152 ± 0.341	3.317 ± 0.060	3.533 ± 0.564
HD 9554	1.032 ± 0.087	6.229 ± 0.720	2.835 ± 0.078	7.884 ± 2.359
HD 9625	2.158 ± 0.239	9.389 ± 1.585	2.799 ± 0.104	1.054 ± 0.337
HD 10011	1.540 ± 0.093	4.026 ± 0.463	3.388 ± 0.075	2.416 ± 0.425
HD 10212	1.247 ± 0.080	4.223 ± 0.431	3.255 ± 0.069	4.605 ± 1.006
HD 10245	1.194 ± 0.115	5.370 ± 0.824	3.028 ± 0.119	6.552 ± 2.217

Table 6 continued on next page

Table 6 (*continued*)

Star	M	R	$\log g$	Age
	(M_\odot)	(R_\odot)		(Gyr)
HD 10383	1.539 ± 0.209	5.380 ± 1.168	3.136 ± 0.140	2.881 ± 1.144
HD 10479	1.327 ± 0.242	6.249 ± 2.345	2.942 ± 0.253	3.557 ± 1.992
HD 10823	1.513 ± 0.083	3.839 ± 0.409	3.422 ± 0.069	2.464 ± 0.394
HD 10909	0.945 ± 0.038	5.571 ± 0.442	2.894 ± 0.061	10.074 ± 1.418
HD 11288	1.545 ± 0.206	3.417 ± 0.830	3.532 ± 0.153	2.571 ± 1.017
HD 11970	1.345 ± 0.085	3.321 ± 0.417	3.496 ± 0.083	3.223 ± 0.585
HD 12137	1.690 ± 0.123	5.590 ± 0.711	3.144 ± 0.084	2.003 ± 0.422
HD 12164	1.535 ± 0.101	3.399 ± 0.415	3.533 ± 0.078	2.440 ± 0.450
HD 13167	1.297 ± 0.092	2.046 ± 0.246	3.901 ± 0.080	4.333 ± 2.320
HD 14787	1.533 ± 0.126	4.491 ± 0.696	3.291 ± 0.102	2.550 ± 0.597
HD 15336	1.262 ± 0.158	2.957 ± 0.639	3.570 ± 0.135	4.205 ± 1.722
HD 15391	1.118 ± 0.152	8.416 ± 2.418	2.609 ± 0.245	5.668 ± 2.594
HD 15928	1.371 ± 0.070	2.930 ± 0.281	3.610 ± 0.065	3.042 ± 0.405
HD 16175	1.339 ± 0.026	1.709 ± 0.072	4.073 ± 0.030	3.172 ± 0.807
HD 16178	1.985 ± 0.121	8.565 ± 0.762	2.843 ± 0.063	1.291 ± 0.231
HD 16984	1.177 ± 0.086	4.112 ± 0.455	3.253 ± 0.074	5.570 ± 1.431
HD 17311	1.568 ± 0.089	4.463 ± 0.465	3.307 ± 0.068	2.335 ± 0.390
HD 17620	1.790 ± 0.186	4.917 ± 0.931	3.280 ± 0.119	1.512 ± 0.455
HD 18015	1.449 ± 0.073	3.075 ± 0.317	3.595 ± 0.066	2.816 ± 0.415
HD 18645	1.500 ± 0.072	3.089 ± 0.305	3.608 ± 0.065	2.835 ± 0.475
HD 18667	1.198 ± 0.102	3.586 ± 0.559	3.380 ± 0.105	5.449 ± 1.643
HD 18742	1.474 ± 0.097	4.759 ± 0.552	3.223 ± 0.075	2.729 ± 0.521
HD 19522	1.391 ± 0.104	2.820 ± 0.407	3.652 ± 0.093	3.159 ± 0.832
HD 19659	1.617 ± 0.043	3.492 ± 0.181	3.533 ± 0.034	2.331 ± 0.193
HD 21340	1.813 ± 0.144	7.221 ± 0.992	2.952 ± 0.089	1.570 ± 0.335
HD 21449	1.518 ± 0.209	10.597 ± 0.692	2.544 ± 0.090	2.924 ± 1.239
HD 21581	0.864 ± 0.058	15.119 ± 1.160	1.988 ± 0.052	9.140 ± 2.095
HD 22233	1.856 ± 0.169	4.987 ± 0.839	3.284 ± 0.107	1.478 ± 0.395
HD 22657	1.281 ± 0.094	5.016 ± 0.495	3.117 ± 0.065	4.602 ± 1.160

Table 6 continued on next page

Table 6 (*continued*)

Star	M	R	$\log g$	Age
	(M_\odot)	(R_\odot)		(Gyr)
HD 22682	1.553 ± 0.041	4.246 ± 0.189	3.346 ± 0.031	2.446 ± 0.186
HD 22844	1.516 ± 0.062	3.077 ± 0.231	3.616 ± 0.047	3.016 ± 0.364
HD 23134	1.421 ± 0.207	4.785 ± 1.226	3.203 ± 0.164	3.386 ± 1.451
HD 23825	1.403 ± 0.087	2.574 ± 0.237	3.729 ± 0.066	3.232 ± 2.645
HD 24148	1.630 ± 0.248	6.498 ± 1.755	2.997 ± 0.174	2.146 ± 0.903
HD 24316	1.433 ± 0.156	9.543 ± 1.826	2.608 ± 0.161	3.156 ± 1.065
HD 24365	1.343 ± 0.072	3.093 ± 0.317	3.557 ± 0.067	3.236 ± 0.488
HD 25622	1.975 ± 0.177	7.630 ± 1.514	2.941 ± 0.138	1.268 ± 0.310
HD 25975	1.520 ± 0.048	4.135 ± 0.128	3.360 ± 0.035	2.842 ± 0.252
HD 26007	1.156 ± 0.137	6.924 ± 1.725	2.793 ± 0.202	5.607 ± 2.290
HD 26634	1.333 ± 0.103	5.640 ± 0.638	3.033 ± 0.071	3.393 ± 0.818
HD 27297	1.424 ± 0.142	3.033 ± 0.546	3.599 ± 0.114	3.192 ± 0.949
HD 27956	1.244 ± 0.102	5.154 ± 0.596	3.081 ± 0.074	4.573 ± 1.279
HD 28678	2.083 ± 0.223	8.339 ± 1.856	2.887 ± 0.150	1.047 ± 0.306
HD 28737	1.066 ± 0.105	6.877 ± 1.035	2.763 ± 0.105	7.650 ± 2.661
HD 30090	1.559 ± 0.039	3.803 ± 0.169	3.442 ± 0.028	2.134 ± 0.150
HD 30128	2.034 ± 0.255	6.381 ± 1.389	3.109 ± 0.136	1.218 ± 0.449
HD 30166	1.386 ± 0.106	6.546 ± 0.574	2.920 ± 0.064	3.386 ± 0.789
HD 30856	1.366 ± 0.073	4.353 ± 0.372	3.268 ± 0.060	3.461 ± 0.534
HD 30882	1.244 ± 0.116	5.681 ± 0.691	2.997 ± 0.081	4.729 ± 1.490
HD 31018	1.552 ± 0.051	2.636 ± 0.146	3.760 ± 0.037	2.612 ± 0.927
HD 31451	1.407 ± 0.094	4.335 ± 0.520	3.285 ± 0.080	3.200 ± 0.617
HD 31543	1.637 ± 0.171	3.625 ± 0.742	3.505 ± 0.134	2.194 ± 0.822
HD 31693	1.872 ± 0.195	7.071 ± 1.592	2.984 ± 0.155	1.478 ± 0.416
HD 33142	1.609 ± 0.081	4.302 ± 0.388	3.349 ± 0.059	2.359 ± 0.352
HD 33240	1.147 ± 0.114	5.601 ± 0.778	2.974 ± 0.093	6.354 ± 2.225
HD 33298	1.103 ± 0.164	2.014 ± 0.629	3.844 ± 0.215	5.847 ± 3.973
HD 33844	1.531 ± 0.093	5.259 ± 0.365	3.154 ± 0.053	2.912 ± 0.531
HD 34538	1.239 ± 0.046	5.525 ± 0.144	3.019 ± 0.028	4.264 ± 0.528

Table 6 continued on next page

Table 6 (*continued*)

Star	M	R	$\log g$	Age
	(M_\odot)	(R_\odot)		(Gyr)
HD 34909	1.514 ± 0.119	4.009 ± 0.646	3.384 ± 0.107	2.700 ± 0.616
HD 37445	1.595 ± 0.262	7.649 ± 2.510	2.845 ± 0.222	2.283 ± 1.055
HD 37601	1.706 ± 0.039	5.234 ± 0.150	3.205 ± 0.024	1.979 ± 0.130
HD 38505	1.625 ± 0.114	4.264 ± 0.551	3.362 ± 0.084	2.350 ± 0.495
HD 39142	1.315 ± 0.175	10.009 ± 1.791	2.530 ± 0.152	4.075 ± 1.743
HD 39731	1.390 ± 0.179	2.880 ± 0.630	3.635 ± 0.135	3.520 ± 1.452
HD 39828	1.529 ± 0.206	4.796 ± 1.242	3.233 ± 0.170	2.723 ± 1.030
HD 40537	1.273 ± 0.043	3.565 ± 0.185	3.411 ± 0.038	4.139 ± 0.468
HD 45210	1.586 ± 0.090	3.598 ± 0.388	3.499 ± 0.069	2.238 ± 0.369
HD 45410	1.581 ± 0.039	4.992 ± 0.154	3.212 ± 0.024	2.303 ± 0.157
HD 45506	1.808 ± 0.036	4.945 ± 0.180	3.280 ± 0.024	1.598 ± 0.088
HD 47562	1.627 ± 0.228	6.454 ± 1.585	3.001 ± 0.158	1.893 ± 0.723
HD 48122	1.295 ± 0.091	4.958 ± 0.532	3.132 ± 0.069	3.240 ± 0.691
HD 50275	1.588 ± 0.161	4.577 ± 0.857	3.290 ± 0.123	2.490 ± 0.735
HD 51272	1.923 ± 0.145	8.249 ± 1.002	2.862 ± 0.083	1.470 ± 0.307
HD 64413	1.178 ± 0.172	8.114 ± 2.638	2.663 ± 0.260	4.879 ± 2.357
HD 64730	1.764 ± 0.160	4.705 ± 0.783	3.312 ± 0.106	1.664 ± 0.441
HD 72003	1.387 ± 0.171	5.163 ± 1.036	3.127 ± 0.129	3.562 ± 1.324
HD 72440	1.391 ± 0.139	2.733 ± 0.522	3.685 ± 0.123	3.202 ± 1.541
HD 72490	1.339 ± 0.086	4.174 ± 0.483	3.296 ± 0.079	3.466 ± 0.672
HD 74390	1.518 ± 0.180	5.024 ± 1.031	3.190 ± 0.132	2.841 ± 0.967
HD 76445	1.016 ± 0.040	3.776 ± 0.239	3.263 ± 0.051	9.554 ± 1.336
HD 77172	1.294 ± 0.094	4.272 ± 0.496	3.261 ± 0.078	4.404 ± 1.083
HD 77818	1.210 ± 0.091	5.330 ± 0.460	3.040 ± 0.061	5.288 ± 1.396
HD 80811	0.947 ± 0.039	3.634 ± 0.308	3.266 ± 0.059	9.948 ± 1.432
HD 82074	1.386 ± 0.019	3.763 ± 0.116	3.402 ± 0.022	2.800 ± 0.088
HD 82886	1.507 ± 0.082	4.735 ± 0.460	3.239 ± 0.062	2.326 ± 0.363
HD 83024	1.272 ± 0.084	4.722 ± 0.362	3.167 ± 0.062	4.956 ± 1.120
HD 83394	1.277 ± 0.056	4.460 ± 0.296	3.218 ± 0.043	3.863 ± 0.557

Table 6 continued on next page

Table 6 (*continued*)

Star	M	R	$\log g$	Age
	(M_\odot)	(R_\odot)		(Gyr)
HD 83752	1.664 ± 0.054	2.854 ± 0.188	3.720 ± 0.047	2.043 ± 0.598
HD 85440	1.563 ± 0.076	3.629 ± 0.354	3.485 ± 0.063	2.437 ± 0.348
HD 85472	1.329 ± 0.043	2.516 ± 0.131	3.733 ± 0.031	3.883 ± 0.401
HD 87230	1.700 ± 0.080	4.590 ± 0.371	3.317 ± 0.054	2.023 ± 0.282
HD 87669	1.185 ± 0.110	5.065 ± 0.639	3.075 ± 0.084	5.855 ± 1.923
HD 88134	1.394 ± 0.101	4.394 ± 0.514	3.269 ± 0.082	3.549 ± 0.780
HD 88654	1.526 ± 0.060	3.200 ± 0.233	3.584 ± 0.045	2.818 ± 0.321
HD 89391	1.185 ± 0.072	3.974 ± 0.340	3.286 ± 0.061	5.326 ± 1.158
HD 90043	1.708 ± 0.042	5.267 ± 0.184	3.200 ± 0.026	1.891 ± 0.137
HD 90792	1.600 ± 0.238	6.183 ± 1.431	3.032 ± 0.142	2.293 ± 0.941
HD 93396	1.431 ± 0.074	2.687 ± 0.253	3.705 ± 0.066	3.476 ± 1.735
HD 93461	1.443 ± 0.106	3.251 ± 0.480	3.545 ± 0.097	3.037 ± 0.617
HD 93864	1.266 ± 0.055	3.602 ± 0.268	3.400 ± 0.050	4.065 ± 0.582
HD 94834	1.282 ± 0.068	3.997 ± 0.250	3.315 ± 0.053	4.743 ± 0.869
HD 95089	1.552 ± 0.111	4.591 ± 0.557	3.278 ± 0.080	2.620 ± 0.542
HD 95526	1.228 ± 0.095	4.283 ± 0.537	3.236 ± 0.084	4.907 ± 1.314
HD 96063	1.489 ± 0.107	4.009 ± 0.575	3.377 ± 0.094	2.544 ± 0.524
HD 96683	1.816 ± 0.139	4.547 ± 0.639	3.354 ± 0.089	1.714 ± 0.393
HD 97601	1.632 ± 0.078	4.375 ± 0.369	3.341 ± 0.055	2.080 ± 0.290
HD 98219	1.558 ± 0.083	4.549 ± 0.416	3.287 ± 0.061	2.559 ± 0.394
HD 99706	1.594 ± 0.097	5.293 ± 0.480	3.166 ± 0.060	2.413 ± 0.434
HD 100337	1.556 ± 0.151	5.290 ± 0.898	3.156 ± 0.108	2.335 ± 0.644
HD 102329	1.412 ± 0.163	5.996 ± 0.930	3.005 ± 0.099	3.639 ± 1.268
HD 102444	1.431 ± 0.086	2.924 ± 0.345	3.634 ± 0.075	3.076 ± 0.491
HD 102956	1.670 ± 0.097	4.213 ± 0.442	3.384 ± 0.068	2.201 ± 0.386
HD 103616	1.583 ± 0.069	3.855 ± 0.306	3.438 ± 0.051	2.309 ± 0.290
HD 104017	1.257 ± 0.091	4.441 ± 0.423	3.215 ± 0.075	5.324 ± 1.332
HD 106270	1.351 ± 0.074	2.475 ± 0.194	3.759 ± 0.050	3.475 ± 2.491
HD 106279	1.189 ± 0.137	5.915 ± 1.115	2.942 ± 0.128	4.802 ± 1.868

Table 6 continued on next page

Table 6 (*continued*)

Star	M	R	$\log g$	Age
	(M_\odot)	(R_\odot)		(Gyr)
HD 107990	1.896 ± 0.225	10.097 ± 1.367	2.680 ± 0.087	1.508 ± 0.465
HD 108189	1.847 ± 0.100	4.724 ± 0.488	3.326 ± 0.067	1.457 ± 0.230
HD 108863	1.545 ± 0.134	5.417 ± 0.732	3.132 ± 0.085	2.679 ± 0.673
HD 109159	1.421 ± 0.050	3.189 ± 0.242	3.556 ± 0.050	2.997 ± 0.271
HD 109218	1.279 ± 0.056	2.474 ± 0.142	3.731 ± 0.030	4.072 ± 0.593
HD 109929	1.411 ± 0.026	1.789 ± 0.085	4.055 ± 0.034	2.457 ± 0.597
HD 112115	1.586 ± 0.304	10.807 ± 1.283	2.545 ± 0.107	2.698 ± 1.513
HD 112973	1.145 ± 0.076	4.783 ± 0.420	3.110 ± 0.055	5.507 ± 1.287
HD 112988	1.079 ± 0.073	4.946 ± 0.470	3.055 ± 0.056	6.792 ± 1.638
HD 114161	1.948 ± 0.166	8.342 ± 1.120	2.858 ± 0.089	1.457 ± 0.349
HD 114659	1.821 ± 0.289	7.738 ± 1.981	2.894 ± 0.162	1.749 ± 0.768
HD 116029	1.445 ± 0.094	4.655 ± 0.395	3.234 ± 0.062	3.345 ± 0.633
HD 117623	2.160 ± 0.198	10.068 ± 1.059	2.739 ± 0.066	1.079 ± 0.301
HD 117762	1.542 ± 0.088	4.522 ± 0.467	3.288 ± 0.066	2.099 ± 0.342
HD 118082	1.443 ± 0.109	5.145 ± 0.570	3.147 ± 0.073	3.277 ± 0.732
HD 118744	1.448 ± 0.163	6.785 ± 1.275	2.908 ± 0.128	3.058 ± 1.011
HD 120531	1.257 ± 0.071	4.469 ± 0.353	3.209 ± 0.056	4.219 ± 0.800
HD 122253	1.494 ± 0.038	3.582 ± 0.227	3.476 ± 0.044	2.806 ± 0.188
HD 123239	1.319 ± 0.141	6.071 ± 1.110	2.964 ± 0.120	3.865 ± 1.315
HD 124641	1.143 ± 0.110	6.592 ± 0.822	2.830 ± 0.083	6.433 ± 2.182
HD 125217	1.702 ± 0.231	5.848 ± 1.546	3.107 ± 0.176	2.116 ± 0.817
HD 125390	1.410 ± 0.174	5.832 ± 1.241	3.028 ± 0.139	3.224 ± 1.178
HD 125607	1.535 ± 0.094	4.044 ± 0.482	3.383 ± 0.080	2.639 ± 0.468
HD 126991	1.038 ± 0.049	3.265 ± 0.238	3.399 ± 0.047	6.402 ± 1.062
HD 127374	1.175 ± 0.105	4.722 ± 0.596	3.132 ± 0.084	5.389 ± 1.684
HD 128095	1.347 ± 0.066	3.639 ± 0.344	3.418 ± 0.068	3.653 ± 0.543
HD 128720	1.483 ± 0.150	3.308 ± 0.647	3.543 ± 0.127	3.096 ± 0.918
HD 131496	1.317 ± 0.077	4.367 ± 0.372	3.250 ± 0.065	4.428 ± 0.842
HD 136418	1.307 ± 0.048	3.627 ± 0.208	3.408 ± 0.044	3.983 ± 0.490

Table 6 continued on next page

Table 6 (*continued*)

Star	M	R	$\log g$	Age
	(M_\odot)	(R_\odot)		(Gyr)
HD 136513	1.172 ± 0.111	5.161 ± 0.670	3.054 ± 0.081	5.378 ± 1.772
HD 140025	1.426 ± 0.076	2.666 ± 0.189	3.712 ± 0.051	3.273 ± 2.521
HD 141712	1.812 ± 0.116	4.487 ± 0.532	3.364 ± 0.075	1.679 ± 0.317
HD 142091	1.487 ± 0.052	4.860 ± 0.117	3.208 ± 0.031	3.104 ± 0.302
HD 142245	1.546 ± 0.092	5.151 ± 0.373	3.176 ± 0.055	2.855 ± 0.514
HD 144363	1.370 ± 0.106	4.221 ± 0.599	3.296 ± 0.095	3.450 ± 0.794
HD 145428	1.247 ± 0.110	6.636 ± 0.691	2.863 ± 0.073	4.324 ± 1.276
HD 146278	1.308 ± 0.098	6.332 ± 0.568	2.924 ± 0.061	4.131 ± 1.017
HD 150331	2.052 ± 0.043	6.110 ± 0.238	3.150 ± 0.028	1.007 ± 0.055
HD 152581	1.481 ± 0.159	4.137 ± 0.858	3.347 ± 0.134	2.423 ± 0.739
HD 152733	1.383 ± 0.072	5.051 ± 0.366	3.144 ± 0.052	3.660 ± 0.586
HD 155413	1.548 ± 0.050	2.616 ± 0.119	3.766 ± 0.035	2.709 ± 1.281
HD 158038	1.533 ± 0.114	4.890 ± 0.404	3.217 ± 0.068	2.918 ± 0.655
HD 158449	1.946 ± 0.122	7.965 ± 0.962	2.897 ± 0.082	1.237 ± 0.215
HD 160215	1.269 ± 0.060	3.681 ± 0.248	3.382 ± 0.051	4.751 ± 0.797
HD 163528	1.713 ± 0.115	5.262 ± 0.601	3.202 ± 0.075	1.906 ± 0.381
HD 166494	1.549 ± 0.076	3.076 ± 0.167	3.623 ± 0.042	2.586 ± 2.076
HD 167042	1.533 ± 0.031	4.310 ± 0.100	3.328 ± 0.022	2.727 ± 0.157
HD 171264	1.636 ± 0.080	3.790 ± 0.350	3.467 ± 0.059	2.151 ± 0.312
HD 175541	1.616 ± 0.103	4.330 ± 0.513	3.346 ± 0.076	2.141 ± 0.401
HD 178251	0.923 ± 0.047	8.313 ± 0.594	2.536 ± 0.049	9.774 ± 1.714
HD 180053	1.719 ± 0.067	4.171 ± 0.299	3.405 ± 0.046	1.997 ± 0.228
HD 180902	1.576 ± 0.079	4.320 ± 0.406	3.337 ± 0.063	2.470 ± 0.372
HD 181342	1.753 ± 0.084	5.153 ± 0.370	3.230 ± 0.051	1.932 ± 0.277
HD 183473	1.391 ± 0.037	2.789 ± 0.160	3.663 ± 0.041	3.134 ± 0.357
HD 185269	1.359 ± 0.047	1.988 ± 0.066	3.947 ± 0.027	3.451 ± 0.902
HD 185351	1.781 ± 0.020	4.867 ± 0.108	3.285 ± 0.014	1.746 ± 0.045
HD 187460	1.050 ± 0.094	7.788 ± 1.134	2.649 ± 0.114	8.088 ± 2.542
HD 188386	1.482 ± 0.128	4.331 ± 0.741	3.308 ± 0.113	2.896 ± 0.720

Table 6 continued on next page

Table 6 (*continued*)

Star	M	R	$\log g$	Age
	(M_\odot)	(R_\odot)		(Gyr)
HD 192153	1.334 ± 0.078	3.036 ± 0.327	3.570 ± 0.069	3.328 ± 0.559
HD 192699	1.532 ± 0.034	4.143 ± 0.166	3.361 ± 0.027	2.347 ± 0.152
HD 193342	2.044 ± 0.095	8.602 ± 0.412	2.852 ± 0.032	1.249 ± 0.193
HD 193391	1.480 ± 0.124	3.634 ± 0.626	3.460 ± 0.115	3.041 ± 0.728
HD 194541	1.467 ± 0.094	5.884 ± 0.417	3.037 ± 0.052	3.170 ± 0.593
HD 195787	1.690 ± 0.107	5.650 ± 0.644	3.134 ± 0.073	1.849 ± 0.335
HD 195824	1.443 ± 0.099	3.425 ± 0.493	3.500 ± 0.095	2.964 ± 0.565
HD 196645	1.377 ± 0.052	3.155 ± 0.256	3.550 ± 0.055	3.340 ± 0.322
HD 197162	1.257 ± 0.091	6.004 ± 0.528	2.953 ± 0.057	3.931 ± 0.948
HD 198599	2.428 ± 0.427	12.023 ± 3.260	2.636 ± 0.166	0.762 ± 0.386
HD 200081	1.952 ± 0.149	9.393 ± 1.020	2.755 ± 0.079	1.398 ± 0.283
HD 200491	1.954 ± 0.123	5.570 ± 0.637	3.210 ± 0.072	1.291 ± 0.236
HD 200964	1.542 ± 0.041	4.679 ± 0.190	3.259 ± 0.028	2.336 ± 0.181
HD 202696	1.281 ± 0.093	4.146 ± 0.490	3.283 ± 0.085	4.720 ± 1.173
HD 202867	1.481 ± 0.101	3.528 ± 0.488	3.486 ± 0.091	2.732 ± 0.527
HD 203471	1.513 ± 0.128	3.197 ± 0.532	3.581 ± 0.108	2.647 ± 0.679
HD 205163	1.928 ± 0.259	5.740 ± 1.454	3.178 ± 0.165	1.403 ± 0.550
HD 206610	1.766 ± 0.300	7.221 ± 2.031	2.941 ± 0.175	1.925 ± 0.914
HD 206635	1.234 ± 0.064	3.478 ± 0.298	3.419 ± 0.057	4.404 ± 0.777
HD 207077	1.252 ± 0.076	3.607 ± 0.365	3.394 ± 0.063	3.699 ± 0.731
HD 208585	1.541 ± 0.132	4.545 ± 0.693	3.283 ± 0.102	2.530 ± 0.620
HD 210011	2.885 ± 0.127	11.634 ± 1.092	2.741 ± 0.061	0.438 ± 0.053
HD 210521	1.759 ± 0.110	4.997 ± 0.563	3.259 ± 0.071	1.681 ± 0.308
HD 210702	1.659 ± 0.038	4.861 ± 0.143	3.257 ± 0.025	2.154 ± 0.145
HD 212771	1.752 ± 0.104	5.036 ± 0.527	3.250 ± 0.066	1.676 ± 0.287
HD 213278	1.416 ± 0.117	3.536 ± 0.576	3.466 ± 0.106	2.776 ± 0.650
HD 215049	1.415 ± 0.086	2.903 ± 0.338	3.637 ± 0.076	3.313 ± 0.542
HD 215549	1.075 ± 0.051	4.401 ± 0.180	3.155 ± 0.038	7.045 ± 1.220
HD 215908	1.639 ± 0.119	5.249 ± 0.703	3.185 ± 0.086	1.815 ± 0.378

Table 6 continued on next page

Table 6 (*continued*)

Star	M	R	$\log g$	Age
	(M_\odot)	(R_\odot)		(Gyr)
HD 216834	1.445 ± 0.163	4.369 ± 0.984	3.290 ± 0.148	2.568 ± 0.803
HD 217496	1.467 ± 0.094	3.679 ± 0.511	3.445 ± 0.093	2.842 ± 0.505
HD 217591	1.533 ± 0.079	4.101 ± 0.387	3.370 ± 0.062	2.435 ± 0.365
HD 217681	1.599 ± 0.097	4.149 ± 0.462	3.379 ± 0.073	2.517 ± 0.461
HD 219553	1.412 ± 0.091	4.528 ± 0.390	3.249 ± 0.063	3.691 ± 0.709
HD 220122	1.241 ± 0.194	8.801 ± 2.718	2.616 ± 0.242	4.468 ± 2.250
HD 220952	1.599 ± 0.066	4.713 ± 0.317	3.268 ± 0.046	2.370 ± 0.293
HD 221504	1.371 ± 0.072	2.451 ± 0.174	3.769 ± 0.052	3.790 ± 2.561
HD 222112	1.362 ± 0.198	4.584 ± 1.125	3.222 ± 0.161	4.186 ± 1.843
HD 223627	1.249 ± 0.123	5.465 ± 0.729	3.032 ± 0.086	5.000 ± 1.685
HD 224032	1.461 ± 0.074	2.210 ± 0.238	3.886 ± 0.073	2.980 ± 0.844
HD 224679	1.669 ± 0.158	3.712 ± 0.705	3.494 ± 0.124	2.070 ± 0.898
HD 225021	1.910 ± 0.125	5.565 ± 0.626	3.201 ± 0.071	1.484 ± 0.288
HD 236427	1.495 ± 0.060	3.279 ± 0.266	3.555 ± 0.054	2.844 ± 0.313
HIP 43212	2.158 ± 0.238	9.148 ± 1.740	2.822 ± 0.122	1.087 ± 0.345
HIP 87123	1.029 ± 0.061	4.784 ± 0.421	3.063 ± 0.073	8.921 ± 1.870

Table 7. Galactic UVW space velocities.

Star	U (km s $^{-1}$)	V (km s $^{-1}$)	W (km s $^{-1}$)
HD 1100	36.132	-6.115	-29.551
HD 1293	-25.861	17.024	-39.147
HD 1384	28.312	-29.649	-20.650
HD 1502	-40.350	-41.970	-8.545
HD 2946	-24.045	-0.934	-10.325
HD 3458	7.253	-2.470	4.137
HD 4313	-3.335	11.923	-9.298
HD 4395	49.210	11.520	-3.237
HD 4917	-4.942	-17.733	8.737
HD 5891	56.833	-88.163	28.657
HD 6019	18.923	-4.990	18.268
HD 6030	-7.004	-1.722	28.430
HD 7530	-36.505	-17.887	-51.427
HD 7931	-38.315	-24.418	-6.597

Table 7 continued on next page

Table 7 (*continued*)

Star	<i>U</i>	<i>V</i>	<i>W</i>
	(km s ⁻¹)	(km s ⁻¹)	(km s ⁻¹)
HD 7980	67.684	-14.982	-6.755
HD 8375	-58.681	-19.825	33.245
HD 8407	-49.757	-2.384	17.434
HD 8508	-24.558	-45.446	-58.222
HD 9156	-21.986	7.281	-19.994
HD 9218	-19.819	-23.693	-6.565
HD 9313	34.168	-57.701	-42.035
HD 9554	-17.982	-51.131	24.821
HD 9625	41.199	-30.414	7.471
HD 10011	-53.946	-12.498	-34.803
HD 10212	41.319	-10.967	-26.873
HD 10245
HD 10383	8.799	-18.468	-27.685
HD 10479	-42.243	-1.762	15.234
HD 10823	11.344	-5.773	-34.919
HD 10909	-113.306	-12.656	16.038
HD 11288	-30.806	-42.203	1.147

Table 7 continued on next page

Table 7 (*continued*)

Star	<i>U</i>	<i>V</i>	<i>W</i>
	(km s ⁻¹)	(km s ⁻¹)	(km s ⁻¹)
HD 11970	-40.040	-54.905	17.353
HD 12137	-7.063	-26.119	0.767
HD 12164	28.179	-3.656	-0.104
HD 13167	-7.680	-33.043	-9.375
HD 14787	7.419	7.138	7.625
HD 15336	27.477	-2.773	20.246
HD 15391	-25.139	22.191	-19.992
HD 15928	-1.925	23.475	-13.470
HD 16175	-10.405	14.252	-20.172
HD 16178	32.075	-35.906	-12.923
HD 16984	-71.268	-5.193	-31.094
HD 17311	18.997	13.763	-35.101
HD 17620	4.963	2.558	-4.260
HD 18015	-30.676	-27.173	-0.273
HD 18645	10.517	-7.585	-5.774
HD 18667	-16.329	-20.887	8.402
HD 18742	23.743	1.012	3.575

Table 7 continued on next page

Table 7 (*continued*)

Star	<i>U</i>	<i>V</i>	<i>W</i>
	(km s ⁻¹)	(km s ⁻¹)	(km s ⁻¹)
HD 19522	-94.429	-43.612	2.288
HD 19659	46.477	-24.004	-5.099
HD 21340	-30.978	-37.347	6.116
HD 21449	-6.369	-16.817	14.543
HD 21581	-103.792	-129.639	-102.860
HD 22233	-11.734	-7.616	-13.809
HD 22657	-63.697	-17.308	-28.814
HD 22682	29.448	-31.098	-4.555
HD 22844	5.968	-38.834	8.540
HD 23134	8.793	-7.227	-26.963
HD 23825	39.050	-38.928	-32.247
HD 24148	-46.702	-41.401	-11.445
HD 24316	30.720	-17.901	-87.763
HD 24365	-36.351	-29.534	19.458
HD 25622	-14.653	10.905	7.658
HD 25975	44.323	-29.419	-35.459
HD 26007	-29.023	-8.051	13.866

Table 7 continued on next page

Table 7 (*continued*)

Star	<i>U</i>	<i>V</i>	<i>W</i>
	(km s ⁻¹)	(km s ⁻¹)	(km s ⁻¹)
HD 26634	-15.370	-42.342	24.692
HD 27297	-39.334	-47.890	-4.496
HD 27956	0.941	-38.768	-48.431
HD 28678	-50.468	-20.110	-30.581
HD 28737	11.598	-21.361	2.743
HD 30090	-17.219	24.259	12.829
HD 30128	-20.357	-28.463	10.246
HD 30166	12.192	-34.685	-31.537
HD 30856	-14.198	-32.257	-15.472
HD 30882	19.827	-58.967	7.919
HD 31018	3.881	-10.904	-0.687
HD 31451	-1.877	-6.103	-9.751
HD 31543	27.932	-29.259	-8.210
HD 31693	-18.052	-28.139	-10.046
HD 33142	-37.832	-0.233	-12.592
HD 33240	0.494	-11.219	-6.246
HD 33298	7.018	-0.320	18.116

Table 7 continued on next page

Table 7 (*continued*)

Star	<i>U</i>	<i>V</i>	<i>W</i>
	(km s ⁻¹)	(km s ⁻¹)	(km s ⁻¹)
HD 33844	-37.794	-18.898	0.710
HD 34538	-47.198	-44.885	-39.515
HD 34909	11.299	-10.080	-11.565
HD 37445	-31.556	-7.609	-30.093
HD 37601	31.829	-8.756	0.001
HD 38505	-62.419	-60.707	-0.933
HD 39142	-8.966	1.299	-6.958
HD 39731	-27.889	-13.132	-13.757
HD 39828	-26.216	-18.607	10.823
HD 40537	-43.685	-47.814	18.848
HD 45210	-56.739	-0.759	-27.061
HD 45410	-77.919	-55.967	-21.088
HD 45506	-40.632	-11.743	-32.316
HD 47562	4.303	-22.640	-11.038
HD 48122	3.067	-9.084	37.864
HD 50275	-80.920	-36.272	-8.617
HD 51272	-25.341	-7.551	-35.054

Table 7 continued on next page

Table 7 (*continued*)

Star	<i>U</i>	<i>V</i>	<i>W</i>
	(km s ⁻¹)	(km s ⁻¹)	(km s ⁻¹)
HD 64413	2.936	-28.289	1.814
HD 64730	-7.065	-38.805	-20.078
HD 72003	-14.359	-39.196	-14.351
HD 72440	21.392	-11.803	-24.371
HD 72490	-11.191	-25.136	24.063
HD 74390	51.105	-53.156	-27.664
HD 76445	22.843	-1.735	-1.693
HD 77172	-33.269	-86.388	-36.903
HD 77818	25.800	-64.533	-10.565
HD 80811	-28.348	-111.984	-65.966
HD 82074	7.015	-0.852	-19.274
HD 82886	0.661	-21.379	14.167
HD 83024	-40.939	-1.415	-27.216
HD 83394	-35.500	-57.009	39.847
HD 83752	-24.924	-34.259	-5.332
HD 85440	4.899	-6.597	-3.636
HD 85472	13.267	-32.020	10.199

Table 7 continued on next page

Table 7 (*continued*)

Star	<i>U</i>	<i>V</i>	<i>W</i>
	(km s ⁻¹)	(km s ⁻¹)	(km s ⁻¹)
HD 87230	-27.388	-49.038	-11.217
HD 87669	74.016	-37.545	26.092
HD 88134	15.080	-34.911	18.824
HD 88654	17.263	-1.753	-5.890
HD 89391	25.672	-31.163	7.990
HD 90043	24.068	-9.059	12.016
HD 90792	-25.103	-35.838	0.193
HD 93396	-17.729	-59.457	-15.490
HD 93461	6.137	-15.714	5.942
HD 93864	-60.503	-46.238	-35.769
HD 94834	-34.276	4.788	-9.516
HD 95089	-6.597	-35.397	-16.796
HD 95526	-66.936	-92.772	0.067
HD 96063	24.505	-2.138	0.758
HD 96683	-19.548	-23.622	-0.931
HD 97601	46.690	-24.120	-40.540
HD 98219	-68.247	-25.184	-43.401

Table 7 continued on next page

Table 7 (*continued*)

Star	<i>U</i>	<i>V</i>	<i>W</i>
	(km s ⁻¹)	(km s ⁻¹)	(km s ⁻¹)
HD 99706	51.958	-42.142	-5.681
HD 100337	35.745	8.217	-19.876
HD 102329	-23.425	-31.759	-1.154
HD 102444	-1.127	-33.049	4.710
HD 102956	7.511	-20.594	-18.546
HD 103616	15.260	-46.341	-46.765
HD 104017	-6.620	10.651	-7.253
HD 106270	-22.601	-44.307	3.348
HD 106279	16.700	-13.983	-44.073
HD 107990	49.430	-1.110	-13.614
HD 108189	-61.768	-13.415	-0.122
HD 108863	-29.936	-40.065	-33.777
HD 109159	-45.234	-28.989	7.492
HD 109218	-23.394	-48.090	2.968
HD 109929	-11.553	-7.539	-11.757
HD 112115	-36.403	-50.748	3.559
HD 112973	-34.668	-28.006	-33.301

Table 7 continued on next page

Table 7 (*continued*)

Star	<i>U</i>	<i>V</i>	<i>W</i>
	(km s ⁻¹)	(km s ⁻¹)	(km s ⁻¹)
HD 112988	-38.711	-30.084	-31.050
HD 114161	-27.205	-18.061	-6.596
HD 114659	-0.225	-8.917	-2.801
HD 116029	10.941	-29.540	-7.410
HD 117623	-27.148	-31.497	4.213
HD 117762	-60.346	31.319	0.387
HD 118082	-5.970	10.819	-25.005
HD 118744	4.122	4.434	-0.840
HD 120531	-11.301	4.159	26.186
HD 122253	-7.799	7.747	-13.239
HD 123239	22.955	5.263	42.413
HD 124641	-6.259	2.639	12.256
HD 125217	-10.315	-16.450	-9.380
HD 125390	-6.616	-44.780	-64.903
HD 125607	-10.673	-47.075	-23.312
HD 126991	-142.931	-48.216	-42.798
HD 127374	-34.761	-11.794	-22.964

Table 7 continued on next page

Table 7 (*continued*)

Star	<i>U</i>	<i>V</i>	<i>W</i>
	(km s ⁻¹)	(km s ⁻¹)	(km s ⁻¹)
HD 128095	69.335	-17.441	14.847
HD 128720	41.564	-24.804	-1.394
HD 131496	26.444	2.285	-13.003
HD 136418	58.460	-69.784	-12.521
HD 136513	-51.594	-41.024	-28.461
HD 140025	35.171	2.120	27.845
HD 141712	9.959	-32.101	-4.682
HD 142091	33.256	-41.301	-18.913
HD 142245	-0.537	-24.229	20.182
HD 144363	0.502	12.525	10.053
HD 145428	-25.843	-78.742	30.229
HD 146278	65.944	-41.205	23.422
HD 150331	-13.531	-31.617	1.857
HD 152581	13.759	-1.634	-10.815
HD 152733	-53.506	-7.941	-11.521
HD 155413	-19.294	-19.086	-8.971
HD 158038	36.720	11.917	-17.330

Table 7 continued on next page

Table 7 (*continued*)

Star	<i>U</i>	<i>V</i>	<i>W</i>
	(km s ⁻¹)	(km s ⁻¹)	(km s ⁻¹)
HD 158449	-32.891	-8.012	9.839
HD 160215	-45.805	-55.667	-3.056
HD 163528	-38.861	-51.348	-28.469
HD 166494	-37.829	-19.943	-21.244
HD 167042	-62.765	-0.477	-22.798
HD 171264	8.451	9.500	-9.543
HD 175541	46.017	-27.470	-20.507
HD 178251	78.696	-28.841	-75.709
HD 180053	-15.512	-2.246	11.428
HD 180902	-9.011	-5.482	-17.902
HD 181342	9.706	-22.399	15.508
HD 183473	-97.380	-21.625	-7.492
HD 185269	18.771	-8.569	-2.685
HD 185351	24.171	-12.668	5.840
HD 187460	-0.391	-6.592	1.920
HD 188386	-56.915	-47.510	7.097
HD 192153	-58.978	-9.789	-31.280

Table 7 continued on next page

Table 7 (*continued*)

Star	<i>U</i>	<i>V</i>	<i>W</i>
	(km s ⁻¹)	(km s ⁻¹)	(km s ⁻¹)
HD 192699	23.755	-4.032	-1.364
HD 193342	55.369	-22.408	-3.768
HD 193391	-22.036	-37.155	-0.372
HD 194541	-12.821	-18.204	-14.594
HD 195787	62.177	-1.591	-24.179
HD 195824	-6.469	8.034	-17.341
HD 196645	-73.584	1.447	-10.590
HD 197162	-66.192	-131.037	-44.752
HD 198599	14.843	7.213	-13.257
HD 200081	10.011	-5.448	-10.340
HD 200491	-1.840	-8.615	-5.591
HD 200964	-68.683	-38.616	17.727
HD 202696	-44.044	-24.367	2.889
HD 202867	21.720	0.758	-3.602
HD 203471	59.348	5.907	-19.264
HD 205163	44.397	7.075	-36.152
HD 206610	-11.930	-8.810	11.725

Table 7 continued on next page

Table 7 (*continued*)

Star	<i>U</i>	<i>V</i>	<i>W</i>
	(km s ⁻¹)	(km s ⁻¹)	(km s ⁻¹)
HD 206635	-72.813	-46.314	-37.961
HD 207077	-8.214	-34.249	-3.620
HD 208585	2.622	-22.315	18.248
HD 210011	-14.269	-13.330	-12.411
HD 210521	-1.377	-6.184	13.924
HD 210702	6.575	11.064	-11.138
HD 212771	75.184	-40.424	2.084
HD 213278	-83.193	-17.956	21.833
HD 215049	-35.264	-46.300	6.331
HD 215549	113.456	-15.861	-43.452
HD 215908	-3.873	6.047	2.187
HD 216834	-0.586	-27.799	22.188
HD 217496	32.899	-37.785	-8.210
HD 217591	-4.675	-24.406	-5.188
HD 217681	32.854	3.168	11.559
HD 219553	1.851	-20.682	-8.998
HD 220122	9.560	-16.327	46.510

Table 7 continued on next page

Table 7 (*continued*)

Star	<i>U</i>	<i>V</i>	<i>W</i>
	(km s ⁻¹)	(km s ⁻¹)	(km s ⁻¹)
HD 220952	-47.219	-22.520	6.424
HD 221504	-7.862	-8.035	-2.331
HD 222112	-10.654	-53.172	-13.864
HD 223627	12.722	-59.469	-16.077
HD 224032	-39.182	-46.468	-28.563
HD 224679	-57.886	-60.007	-9.621
HD 225021	-21.590	-18.731	-7.444
HD 236427	10.573	-10.854	-35.878
HIP 43212	-7.211	-4.763	-8.300
HIP 87123	-43.135	-54.089	-10.479

Table 8. K magnitudes and Photometric
Effective Temperatures.

Star	K_S	T_{eff}^{Phot}
		(K)
HD 1100	5.319	4801 \pm 32
HD 1293	6.354	5247 \pm 46
HD 1384	5.785	4947 \pm 37
HD 1502	6.120	5027 \pm 44
HD 2946	6.275	5508 \pm 45
HD 3458	6.180	5156 \pm 31
HD 4313	5.595	5015 \pm 40
HD 4395	5.972	5620 \pm 43
HD 4917	5.610	4801 \pm 31
HD 5891	5.621	4994 \pm 31
HD 6019	5.579	5100 \pm 43
HD 6030	5.553	4930 \pm 40
HD 7530	6.087	5018 \pm 38
HD 7931	5.512	4844 \pm 37

Table 8 continued on next page

Table 8 (*continued*)

Star	K_S	T_{eff}^{Phot}
		(K)
HD 7980	5.202	4837 ± 29
HD 8375	4.290	5231 ± 42
HD 8407	5.479	4962 ± 39
HD 8508	5.352	4784 ± 31
HD 9156	5.938	4775 ± 32
HD 9218	5.562	4847 ± 29
HD 9313	5.483	4908 ± 37
HD 9554	5.914	4808 ± 38
HD 9625	6.092	4934 ± 34
HD 10011	5.880	5136 ± 41
HD 10212	5.818	4954 ± 39
HD 10245	5.836	4868 ± 39
HD 10383	5.931	4896 ± 39
HD 10479	6.441	4911 ± 34
HD 10823	6.023	5174 ± 51
HD 10909	5.544	4706 ± 41
HD 11288	6.387	5176 ± 45

Table 8 continued on next page

Table 8 (*continued*)

Star	K_S	T_{eff}^{Phot}
		(K)
HD 11970	6.139	5188 \pm 39
HD 12137	5.398	5007 \pm 41
HD 12164	6.212	5527 \pm 49
HD 13167	6.711	5734 \pm 47
HD 14787	5.388	4985 \pm 40
HD 15336	6.848	5177 \pm 49
HD 15391	6.334	4946 \pm 35
HD 15928	5.950	5434 \pm 46
HD 16175	5.853	5915 \pm 47
HD 16178	5.762	4850 \pm 31
HD 16984	5.804	4807 \pm 42
HD 17311	6.056	5168 \pm 40
HD 17620	6.118	5174 \pm 41
HD 18015	6.204	5689 \pm 46
HD 18645	5.999	5413 \pm 46
HD 18667	6.019	4954 \pm 42
HD 18742	5.554	4982 \pm 42

Table 8 continued on next page

Table 8 (*continued*)

Star	K_S	T_{eff}^{Phot}
		(K)
HD 19522	6.414	5694 \pm 47
HD 19659	5.459	5754 \pm 43
HD 21340	5.137	5043 \pm 40
HD 21449	4.814	4857 \pm 33
HD 21581	6.414	5101 \pm 35
HD 22233	5.687	5084 \pm 39
HD 22657	5.417	4886 \pm 39
HD 22682	4.531	5030 \pm 37
HD 22844	6.129	5472 \pm 42
HD 23134	6.022	5006 \pm 40
HD 23825	6.185	5504 \pm 47
HD 24148	5.809	5013 \pm 39
HD 24316	5.294	4911 \pm 36
HD 24365	5.821	5278 \pm 40
HD 25622	5.407	5085 \pm 44
HD 25975
HD 26007	5.892	4796 \pm 33

Table 8 continued on next page

Table 8 (*continued*)

Star	K_S	T_{eff}^{Phot}
		(K)
HD 26634	5.701	5079 ± 41
HD 27297	6.110	5087 ± 42
HD 27956	5.732	5025 ± 42
HD 28678	5.775	4837 ± 42
HD 28737	5.677	4716 ± 36
HD 30090	4.707	5518 ± 42
HD 30128	5.998	5105 ± 41
HD 30166	5.152	4924 ± 30
HD 30856	5.657	5105 ± 43
HD 30882	5.832	5073 ± 36
HD 31018	6.084	6493 ± 55
HD 31451	5.811	5133 ± 40
HD 31543	6.381	5593 ± 53
HD 31693	5.429	5037 ± 39
HD 33142	5.792	5098 ± 39
HD 33240	5.797	4922 ± 34
HD 33298	6.385	5554 ± 46

Table 8 continued on next page

Table 8 (*continued*)

Star	K_S	T_{eff}^{Phot}
		(K)
HD 33844	4.945	4905 \pm 37
HD 34538
HD 34909	5.775	5045 \pm 42
HD 37445	5.913	4907 \pm 30
HD 37601
HD 38505	5.401	5002 \pm 38
HD 39142	5.510	4879 \pm 34
HD 39731	6.088	5093 \pm 40
HD 39828	5.380	4929 \pm 44
HD 40537	5.094	5010 \pm 41
HD 45210	5.964	5608 \pm 43
HD 45410
HD 45506
HD 47562	6.030	5005 \pm 46
HD 48122	5.890	5232 \pm 44
HD 50275	5.978	4980 \pm 40
HD 51272	5.482	4906 \pm 36

Table 8 continued on next page

Table 8 (*continued*)

Star	K_S	T_{eff}^{Phot}
		(K)
HD 64413	5.917	4879 \pm 33
HD 64730	5.970	5168 \pm 40
HD 72003	5.313	4868 \pm 37
HD 72440	6.585	5587 \pm 42
HD 72490	5.614	4940 \pm 39
HD 74390	5.892	4916 \pm 37
HD 76445	5.284	4808 \pm 40
HD 77172	5.726	4866 \pm 38
HD 77818	5.202	4747 \pm 36
HD 80811	6.159	4967 \pm 39
HD 82074
HD 82886	5.452	5094 \pm 39
HD 83024	5.490	4767 \pm 35
HD 83394	5.217	4932 \pm 39
HD 83752	6.154	5960 \pm 57
HD 85440	5.763	5169 \pm 43
HD 85472	5.547	5267 \pm 71

Table 8 continued on next page

Table 8 (*continued*)

Star	K_S	T_{eff}^{Phot}
		(K)
HD 87230	5.568	5062 \pm 39
HD 87669	5.704	4700 \pm 31
HD 88134	5.927	4876 \pm 40
HD 88654	5.698	5284 \pm 44
HD 89391	5.608	4960 \pm 40
HD 90043
HD 90792	5.698	4812 \pm 33
HD 93396	6.122	5359 \pm 41
HD 93461	6.108	5016 \pm 39
HD 93864	5.791	5051 \pm 40
HD 94834	5.200	4802 \pm 37
HD 95089	5.626	4859 \pm 38
HD 95526	6.008	4915 \pm 41
HD 96063	6.050	4967 \pm 47
HD 96683	5.865	4949 \pm 38
HD 97601	5.363	5074 \pm 38
HD 98219	5.813	5057 \pm 41

Table 8 continued on next page

Table 8 (*continued*)

Star	K_S	T_{eff}^{Phot}
		(K)
HD 99706	5.335	4927 ± 37
HD 100337	5.656	4953 ± 46
HD 102329	5.402	4731 ± 30
HD 102444	5.999	5230 ± 46
HD 102956	5.663	4968 ± 38
HD 103616	5.593	5266 ± 42
HD 104017	5.375	4782 ± 36
HD 106270	5.862	5508 ± 46
HD 106279	6.095	4927 ± 33
HD 107990	5.591	4872 ± 31
HD 108189	5.814	5364 ± 45
HD 108863	5.392	4866 ± 40
HD 109159	5.963	5329 ± 43
HD 109218	6.155	5257 ± 44
HD 109929	6.320	6014 ± 48
HD 112115	5.566	4681 ± 30
HD 112973	5.350	4907 ± 39

Table 8 continued on next page

Table 8 (*continued*)

Star	K_S	T_{eff}^{Phot}
		(K)
HD 112988	5.436	4856 ± 40
HD 114161	5.631	4882 ± 34
HD 114659	5.922	4866 ± 41
HD 116029	5.534	4894 ± 36
HD 117623	5.037	5138 ± 31
HD 117762	5.805	5121 ± 41
HD 118082	5.677	4954 ± 43
HD 118744	5.430	4764 ± 31
HD 120531	5.701	4983 ± 37
HD 122253	5.626	5064 ± 39
HD 123239	5.856	4894 ± 31
HD 124641	5.490	4703 ± 28
HD 125217	5.886	5006 ± 39
HD 125390	5.875	4913 ± 38
HD 125607	5.899	5048 ± 38
HD 126991	5.838	5159 ± 45
HD 127374	5.808	4827 ± 36

Table 8 continued on next page

Table 8 (*continued*)

Star	K_S	T_{eff}^{Phot}
		(K)
HD 128095	5.869	4979 ± 37
HD 128720	6.107	5027 ± 41
HD 131496	5.437	4864 ± 37
HD 136418
HD 136513	5.848	4803 ± 30
HD 140025	6.453	5557 ± 45
HD 141712	6.312	5219 ± 40
HD 142091
HD 142245	5.110	4867 ± 44
HD 144363	5.842	5006 ± 39
HD 145428	5.203	5111 ± 43
HD 146278	5.540	4824 ± 29
HD 150331
HD 152581	6.173	5042 ± 38
HD 152733	5.754	4904 ± 38
HD 155413	5.627	5849 ± 49
HD 158038	5.156	4948 ± 42

Table 8 continued on next page

Table 8 (*continued*)

Star	K_S	T_{eff}^{Phot}
		(K)
HD 158449	5.762	5387 \pm 41
HD 160215	5.804	4898 \pm 37
HD 163528	6.143	5041 \pm 41
HD 166494	5.991	5545 \pm 43
HD 167042
HD 171264	6.026	5479 \pm 49
HD 175541	5.829	5277 \pm 43
HD 178251	5.364	4804 \pm 29
HD 180053	5.840	5164 \pm 39
HD 180902	5.543	5143 \pm 41
HD 181342	5.251	5076 \pm 40
HD 183473
HD 185269	5.260	6015 \pm 45
HD 185351
HD 187460	5.734	4808 \pm 30
HD 188386	5.850	5040 \pm 37
HD 192153	6.224	5434 \pm 44

Table 8 continued on next page

Table 8 (*continued*)

Star	K_S	T_{eff}^{Phot}
		(K)
HD 192699	4.366	5113 \pm 43
HD 193342	5.794	5521 \pm 41
HD 193391	5.947	4957 \pm 43
HD 194541	5.132	4997 \pm 37
HD 195787	5.379	5366 \pm 47
HD 195824	5.887	5065 \pm 39
HD 196645	5.672	5082 \pm 42
HD 197162	5.625	5062 \pm 38
HD 198599	5.561	5369 \pm 35
HD 200081	5.870	5193 \pm 35
HD 200491	5.496	5087 \pm 43
HD 200964
HD 202696	5.877	4872 \pm 32
HD 202867	5.996	5147 \pm 46
HD 203471	6.478	5511 \pm 47
HD 205163	6.014	5066 \pm 34
HD 206610	5.952	4896 \pm 42

Table 8 continued on next page

Table 8 (*continued*)

Star	K_S	T_{eff}^{Phot}
		(K)
HD 206635	6.122	5091 \pm 48
HD 207077	6.150	5162 \pm 41
HD 208585	5.704	4941 \pm 37
HD 210011	4.865	5513 \pm 35
HD 210521	5.955	5160 \pm 39
HD 210702
HD 212771	5.496	5206 \pm 41
HD 213278	6.010	5160 \pm 43
HD 215049	6.233	5210 \pm 46
HD 215549
HD 215908	5.867	5258 \pm 44
HD 216834	5.975	5068 \pm 39
HD 217496	5.718	5080 \pm 40
HD 217591	5.601	4950 \pm 37
HD 217681	5.538	5068 \pm 37
HD 219553	4.907	4899 \pm 36
HD 220122	6.025	4861 \pm 33

Table 8 continued on next page

Table 8 (*continued*)

Star	K_S	T_{eff}^{Phot}
		(K)
HD 220952	5.587	5022 \pm 41
HD 221504	6.198	5381 \pm 41
HD 222112	5.937	4801 \pm 41
HD 223627	5.737	4859 \pm 30
HD 224032	6.657	5733 \pm 49
HD 224679	6.669	5640 \pm 49
HD 225021	5.436	4994 \pm 29
HD 236427	6.129	5326 \pm 40
HIP 43212	6.083	5019 \pm 39
HIP 87123	5.912	4851 \pm 38

Table 9. Results for the Giant Plant Occurrence given by Equation 2.

Retired A Stars	$\Delta[Fe/H]$	ΔM	FGK Dwarfs	M Dwarfs	α	Confidence	β	Confidence	C	Confidence
	(dex)	(M $_{\odot}$)				Interval		Interval		Interval
J10	0.00	0.00	J10	J10	0.99	(0.79,1.29)	1.19	(0.95,1.25)	0.072	(0.064,0.081)
This work	0.00	0.00	J10	J10	1.10	(0.92,1.40)	1.00	(0.81,1.12)	0.085	(0.073,0.091)
This work	0.00	0.00	J10,B16	M14	1.05	(0.81,1.33)	1.05	(0.88,1.26)	0.085	(0.075,0.093)
This work	-0.05	0.00	J10,B16	M14	1.10	(0.87,1.39)	0.95	(0.81,1.17)	0.090	(0.078,0.095)
This work	-0.10	0.00	J10,B16	M14	1.25	(0.97,1.49)	0.90	(0.74,1.08)	0.090	(0.079,0.098)
This work	0.00	-0.12	J10,B16	M14	1.05	(0.79,1.33)	1.05	(0.86,1.24)	0.085	(0.077,0.095)
This work	-0.05	-0.12	J10,B16	M14	1.15	(0.88,1.42)	0.95	(0.78,1.14)	0.090	(0.080,0.098)
This work	-0.10	-0.12	J10,B16	M14	1.15	(0.92,1.46)	0.85	(0.71,1.06)	0.095	(0.082,0.100)

References—J10: Johnson et al. (2010a); M14: Montet et al. (2014); B16: Brewer et al. (2016).

Table 10. Results for the Giant Plant Occurrence given by Equation 4.

Retired A Stars	$\Delta[Fe/H]$	ΔM	FGK Dwarfs	M Dwarfs	γ	Confidence	C	Confidence
	(dex)	(M $_{\odot}$)				Interval		Interval
This work	0.00	0.00	J10,B16	M14	1.04	(0.88,1.16)	0.086	(0.076,0.094)
This work	-0.05	0.00	J10,B16	M14	1.04	(0.87,1.16)	0.088	(0.079,0.097)
This work	-0.10	0.00	J10,B16	M14	1.00	(0.84,1.12)	0.092	(0.082,0.100)
This work	0.00	-0.12	J10,B16	M14	1.04	(0.87,1.15)	0.088	(0.078,0.096)
This work	-0.05	-0.12	J10,B16	M14	1.02	(0.84,1.13)	0.090	(0.081,0.099)
This work	-0.10	-0.12	J10,B16	M14	0.96	(0.81,1.09)	0.094	(0.084,0.102)

References—J10: Johnson et al. (2010a); M14: Montet et al. (2014); B16: Brewer et al. (2016).